Direct Measurement and Analysis of Cyclohexadienyl Oxidation

by

James Wagner Taylor

Submitted to the Department of Chemical Engineering
in partial fulfillment of the requirements for the degree of
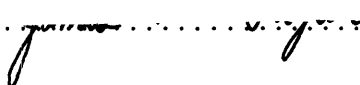
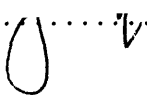Doctor of Philosophy in Chemical Engineering
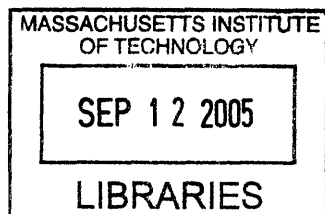
at the

MASSACHUSETTS INSTITUTE OF TECHNOLOGY

August 2005
[September 2005]

Author . . . .
Department of Chemical Engineering
August 30, 2005

Certified by . . . .
William H. Green
Associate Professor
Thesis Supervisor

Accepted by . . . .
Daniel Blankschtein
Professor of Chemical Engineering
Chairman, Committee for Graduate Students

Direct Measurement and Analysis of Cyclohexadienyl Oxidation

by

James Wagner Taylor

Submitted to the Department of Chemical Engineering
on August 30, 2005, in partial fulfillment of the
requirements for the degree of
Doctor of Philosophy in Chemical Engineering

Abstract

The oxidation of cyclohexadienyl radical (c-C_6H_7) and similar resonantly stabilized radicals are important in an astonishing array of processes in nature. Cyclohexadienyl radical has been postulated to be significant in a variety of processes that involve the atmospheric formation of benzene. In biology, there are specific enzymes that promote the formation of benzene-like intermediates from cyclohexadienyl radicals, called cyclohexadienyl dehydratases. In combustion processes, cyclohexadienyl radical is a possible link to the formation of soot and other large polyaromatic hydrocarbons (PAH's). Thus, the cyclohexadienyl radical moiety is important in many chemical processes, and its detailed study is of interest in many areas.

In this work, cyclohexadienyl radical is studied both computationally and experimentally in the liquid and gas phases. The cyclohexadienyl radical is created using laser-flash photolysis. The UV absorption bands of the radical are probed and it's relative concentration over time measured in non-polar solvents in both the presence and absence of oxygen. Several analytical and numerical models of the chemistry were constructed to explain a puzzling discrepancy in the reported liquid and gas phase reaction rates. The models and data developed were then used in testing new software for finding the global optimum of dynamic systems. Optimized parameters for several key reaction pathways are reported, as well as a detailed description of the procedure. Finally, c-C_6H_7 was studied in the gas phase using an ultra-fast laser system. Preliminary results from those experiments are reported, as well as recommendations for future work.

Thesis Supervisor: William H. Green
Title: Associate Professor

3

For my parents,
Harvey and Randi Taylor

SOLI DEO GLORIA

Acknowledgments

I would like to thank many kind souls who have helped me through my time at MIT, but before that I would like to make it clear that the mistakes found in this work are my own, and I did not need any help to make them.

First, I would like to thank my advisor William H. Green for his support throughout this project. I joined his group under difficult circumstances and I had to learn a lot very quickly. I appreciate the help he has given me and the patience he has shown me over many years. I will always treasure his advice and friendship. One degree of freedom below that is my committee, who has given me excellent advice and comments. Indeed, I remember one meeting where Bob Field and Herb Sawin solved a month's worth of problems in about 30 minutes. I am very grateful to them and to Jack Howard for their time and expertise in nearly four years worth of committee meetings.

Second, I would like to thank the many colleagues and friends who have helped me with this work. Of those, Huzeifa Ismail deserves the highest rank for all of his help and motivation through the last year of the old MIT Spectroscopy Lab. Without his help the gas phase research would have stalled, moving the equipment would have been a chore, and I would have learned a lot less. To him, many thanks.

Adam Singer deserves a tremendous thanks for his collaboration on the last part of his (and my) thesis. Together we found a good application for his spiffy GDOC program, which gave me the ability to finally solve a sticky optimization problem. I would also like to thank Benoît Chachuat for his help in packaging the code for distribution and for creating the multistart algorithm to go along with GDOC. I will be sad that this may be my last collaboration with both of them, but who knows what the future may tell.

Hans Carstensen deserves a great deal of praise for giving up hiking one weekend and showing me how to do experiments in the liquid phase. His attention to detail impressed me and writing a paper with him was no chore. I would also like to thank Koli Taghizadeh for her help with the GC/MS studies of the liquid phase products. Her ability to assign peaks is almost like magic. Some of her handiwork can be observed in Appendix C.

Contents

List of Figures

List of Tables

Chapter 1

Introduction

"A radical is a prodigal son. For him, the world is a strange place whose contours have to be explored according to one's destiny. He may eventually return to the house of his elders, but the return is by choice, and not, as of those who stayed behind, of unblinking filial obedience." – Daniel Bell, with an unusually clear and serendipitous metaphor for Variational Transition State Theory.

1.1   What are radicals?

What are radicals in the chemical sense? *Radicals* are atoms or molecules that have an unpaired electron in the outer or valence shell of electrons. Radicals react readily with other chemicals, because of the instability caused by this unbalanced electron. An example of a radical is methyl radical, formed by heating methane until it ejects a complete hydrogen atom.

Organic chemicals can often form radicals through thermal, photochemical, or spontaneous processes. For example, OH radical can be formed when hydrogen peroxide absorbs an ultraviolet photon. The resulting radicals in this reaction have no net charge, and are thus classified as free radicals. Peroxides can also form radicals when heated, however, if the heating is uncontrolled radical formation can occur fast enough to create explosions. The

same radical can often be created in several different ways.

The organic nomenclature of radicals is as follows: if an organic molecule becomes a radical, the name loses an e and adds a yl to the end.[54] Thus, 1,4-cyclohexadiene becomes cyclohexadienyl radical. The 1,4 part is dropped, since for this particular species losing the hydrogen removes the need for specifying the diene position. Several specialized names exist for common radicals, such as the vinyl radical, C_2H_3.

1.2   The lifetime of a radical

If the time over which a radical exists were likened to a human being's lifespan, then eons would pass in experiments. A typical radical species exists only a few microseconds in liquids and milliseconds in low pressure gases. Thus, to a radical, a second would be somewhere between a 1000 to a million years to a human being. Needless to say, the lifetime of a radical is short.

However, in its short lifespan, radicals can still undergo chemical reactions, making them faster than other mechanisms for transforming chemicals, and therefore dominant in many situations. There are several different types of reactions radicals can undergo, and they are generally grouped as follows:

initiation reactions: chemical reactions that generate more radicals than they consume

termination reactions: reactions that consume more radicals than are produced

propagation reactions: Reactions that have no net loss or gain of radicals, although the concentrations and types of radicals change.

There are many specialized sub-classes of radical reactions, such as disproportionation, H-abstraction, etc. that will be discussed in later sections when that type of reaction is relevant.

1.3 The importance of radicals and radical oxidation

Radical chemistry is the basis for many of the fundamental processes in the world around us. Biology has many processes which are affected by organic free radicals. For example, the 1998 Nobel prize was given for discovery of the use of nitric oxide (NO) in the body.[49]

One particular type of radical reaction that is industrially significant is radical oxidation. Oxygen is one of the most plentiful molecules available that react readily with radicals. When oxygen attacks an aliphatic radical it can form peroxyl radicals, which can subsequently dissociate to form alkenes.

$$R\text{-}CH_2\text{-}CH_2 + O_2 \rightleftharpoons R\text{-}CH_2\text{-}CH_2OO \rightarrow R\text{-}CH_2=CH_2 + HO_2 \qquad (1.1)$$
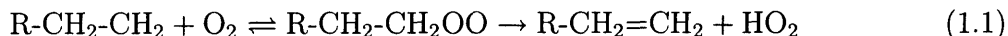
The rate of oxidation in many materials, such as foods, pharmaceuticals, and polymers, determines their useful life. However, since oxygen is also the cheapest oxidant, many commercial processes rely on hydrocarbon oxidation. Consequently, a large industry is devoted to both inhibiting and enhancing these reactions.

In addition to the commercial relevance, the details of hydrocarbon radical oxidation kinetics are critical in academic fields ranging from biology to atmospheric chemistry. Specifically, in combustion processes, the reversibility of oxygen addition is thought to be responsible for the Negative Temperature Coefficient (NTC) region, where oxidation rates are not a monotonic function of temperature.

Although many hydrocarbon radical oxidation reactions, including the title reaction, have been studied for decades, there are still many mysteries to be solved. For example, the decomposition pathway with the smallest barrier for the reaction of ethyl radical with oxygen was not conclusively identified until recently,[57] and systems as apparently simple as butyl + O_2 are still challenging areas of research.[15]

Under cool flame conditions, radical oxidation (R + O_2) reactions are now thought to rapidly form alkenes and other unsaturated species. As these unsaturated species accumulate, the combustion reactions become dominated by the reactions of resonantly stabilized

radicals with oxygen. Due to their late appearance in most combustion processes, these radicals are difficult to study using flame techniques. Thus, despite their importance in the latter stages of ignition, relatively little is known about the reactions of resonantly stabilized radicals with oxygen.

1.4   The cyclohexadienyl radical

An important radical intermediate in many processes is the cyclohexadienyl radical, shown in Figure 1-1. Cyclohexadienyl radical is formed when either 1,3 or 1,4-cyclohexadiene loses a hydrogen atom. Alternatively, H atom can add to benzene to form the radical as well. Cyclohexadienyl radical is unique, because of the ring's resonance structure, which helps to stabilize the SOMO level of the radical. However, loss of another hydrogen atom yields the stable molecule benzene. Thus, although the radical is stabilized there is still a strong thermodynamic impetus for reaction to benzene.

Cyclohexadienyl radical has been postulated to be significant in a variety of processes that involve the atmospheric formation of benzene.[14] In biology, there are specific enzymes that promote the formation of benzene-like intermediates from cyclohexadienyl radicals, called cyclohexadienyl dehydratases.[79] In combustion processes, cyclohexadienyl radical is a possible link to the formation of soot and other large polyaromatic hydrocarbons (PAH's). Thus, the cyclohexadienyl radical moiety is important in many chemical processes and its detailed study is of interest in many areas.

1.5   The cyclohexadienyl radical controversy

This thesis focuses on the reactions of resonantly stabilized cyclohexadienyl radicals, particularly those reactions involving molecular oxygen to form the isomeric cyclohexadienylperoxyl radicals:

$$c\text{-}C_6H_7 + O_2 \rightarrow o\text{-}C_6H_7OO \tag{1.2a}$$

Figure 1-1: 3D Structure of the cyclohexadienyl radical. The dots represent the space the actual structure would fill.

$$c\text{-}C_6H_7 + O_2 \rightarrow p\text{-}C_6H_7OO \tag{1.2b}$$
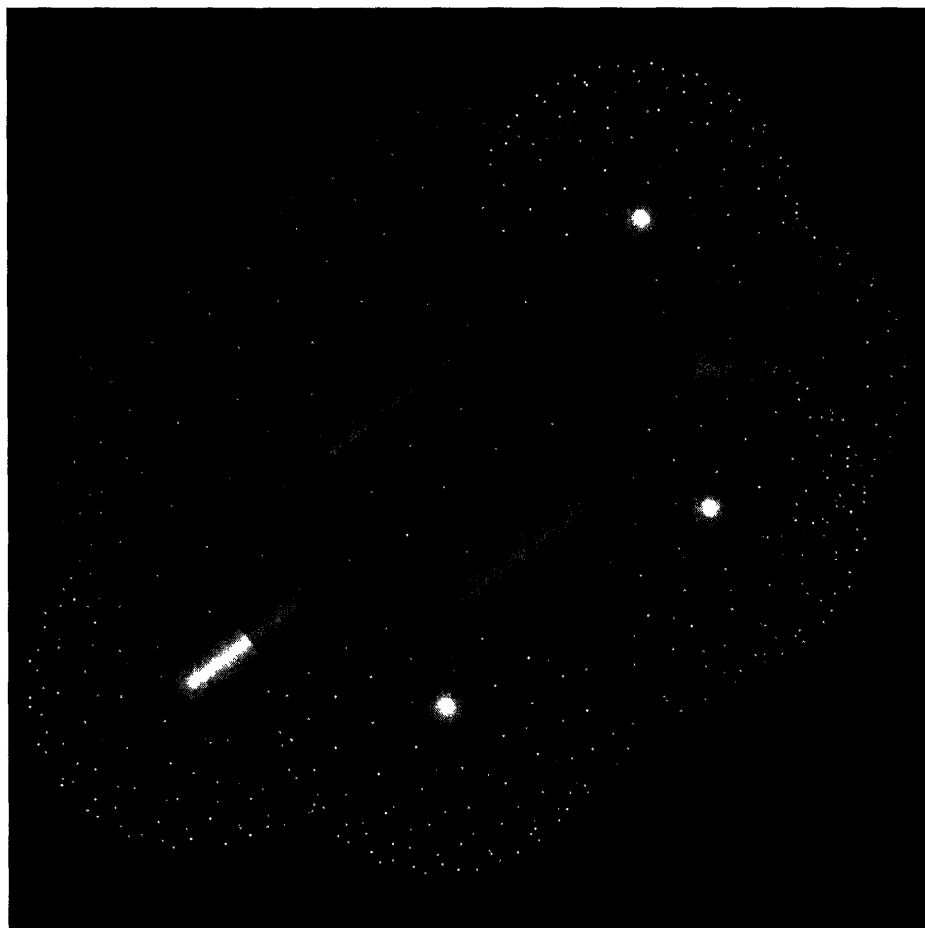
where *ortho* means the CH_2 group is adjacent to the CHOO group and *para* means they are on opposite sides of the six-membered ring, as shown in Figure 1-2. The *ortho* isomer contains a chiral carbon and exists as two enantiomers.

Figure 1-2: Structures of the cyclohexadienylperoxyl radicals. Note: the *ortho* isomer contains a chiral center (labeled with an asterisk) and exists as two enantiomers. In the preferred conformation, the O-O-C-H dihedral angle is 180°.

$$o\text{-}C_6H_7OO \qquad\qquad p\text{-}C_6H_7OO$$
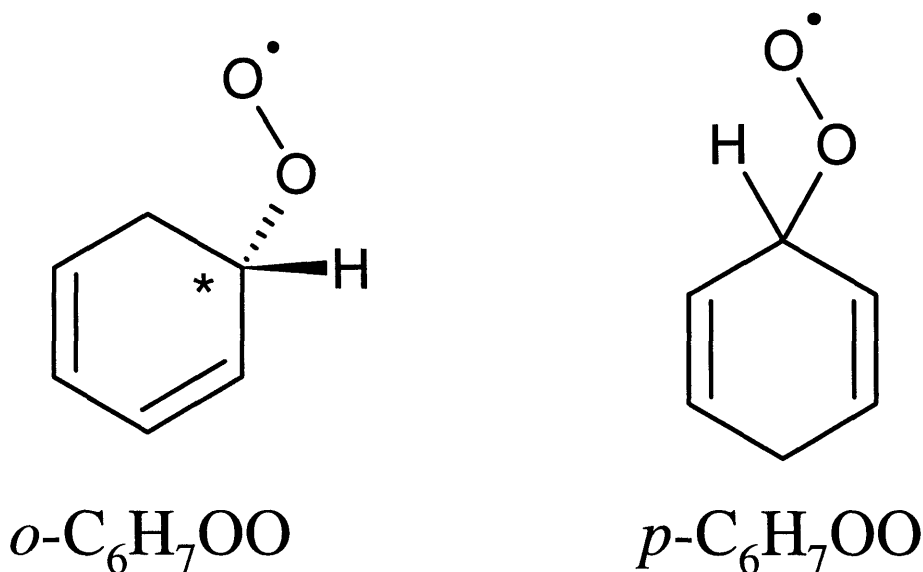
Recently published experimental investigations of the reaction of cyclohexadienyl with O_2 by Berho et al.[8] and Estupiñán et al.[17] indicate that cyclohexadienyl radicals react slowly with molecular oxygen in the gas phase ($k_{1.2} = k_{1.2a} + k_{1.2b} = 2.4 \times 10^7$ $M^{-1}s^{-1}$). However, earlier measurements of this reaction in water[51] and in a peroxide / benzene solution[43] came to different conclusions: the measured rates are fast and appear to be diffusion limited ($k_{1.2} \sim 10^9$ $M^{-1}s^{-1}$). The reaction rate in solution appears to be 50 times faster than that in the gas phase. There are similar differences in the literature regarding the analogous reaction

$$HOC_6H_6 + O_2 \rightleftharpoons o\text{-}HOC_6H_6OO \tag{1.3a}$$

$$HOC_6H_6 + O_2 \rightleftharpoons p\text{-}HOC_6H_6OO \qquad (1.3b)$$
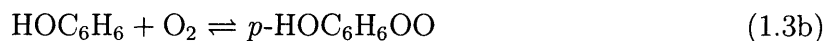
which has been extensively studied in both the gas phase[11,12,9,34,56,27] and in aqueous solution.[51,52,19,75]

Several published reports[2,25,27] suggest that reactions 1.2 and 1.3 and similar reactions of other resonantly stabilized radicals[80] have significant activation barriers in the gas phase, which might explain the slow rate reported by Estupiñán et al. However, all solution phase measurements indicate that these reactions are diffusion-limited,[51,43] suggesting that no significant barriers exist. The reason for the large differences between the recent gas phase measurements and the liquid phase results was unknown.

In addition to the kinetics, the thermochemistry of reaction 1.2 was uncertain: theoretical calculations predict that this and similar reactions are only slightly exothermic,[2,25,39] while the only direct experimental measurements find $\Delta H^o = -12$ kcal/mol for reaction 1.2 in organic solvents.[39] In aqueous solution, reaction 1.3 is known to be reversible, and rapidly equilibrates at room temperature.[19] The measured equilibrium constant corresponds to $\Delta G^o = -23.8$ kJ/mol for reaction 1.3 in aqueous solution (1M standard state). Curiously, under similar conditions, a corresponding equilibrium for reaction 1.2 was not found in aqueous solution.[51]

Hendry and Schuetzle found that in chlorobenzene, 1,4-cyclohexadiene and oxygen were quantitatively converted to benzene and H_2O_2. Based on this finding, the authors suggested that the dominant reaction is the direct abstraction of hydrogen.[28]

$$c\text{-}C_6H_7 + O_2 \rightarrow HO_2 + C_6H_6 \qquad (1.4)$$
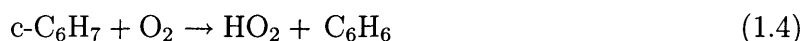
Although Hendry and Schuetzle gave arguments against it, their data do not conclusively rule out a sequential reaction, with reaction 1.2 followed rapidly by

$$o\text{-}C_6H_7OO \rightarrow HO_2 + C_6H_6 \qquad (1.5a)$$

25

$$p\text{-}C_6H_7OO \rightarrow HO_2 + C_6H_6 \tag{1.5b}$$

Recently, Estupiñán et al. have also argued that reaction 1.4 is the dominant reaction channel.[17] Note that both reactions 1.4 and 1.5 are highly exothermic because of the stability of the product, benzene. Concerted HO_2 elimination from adjacent carbons as in reaction 1.5a is known to be one of the primary channels for the decay of ethylperoxyl and other simple alkylperoxyls with β hydrogens in the gas phase at temperatures greater than 400 K.[57,36,70] Reaction 1.5b, where the oxygen removes a hydrogen from across the ring, is expected to have a considerably higher barrier than reaction 1.5a, though little is known regarding this reaction.[51,41]

Pan et al. found evidence that in an aqueous alkaline solution about 60% of the C_6H_7OO formed decomposes on a microsecond timescale to form HO_2 and benzene. They interpreted the 60% yield as meaning that $o\text{-}C_6H_7OO$ decomposes rapidly by reaction 1.5a ($k_{1.5} > 8 \times 10^5$ s^{-1}), but that the $p\text{-}C_6H_7OO$ decays by another pathway, i.e. reaction 1.5b is slow. It is unclear from their product data exactly what happened to the remaining 40% of the C_6H_7OO. Note that the data of Pan et al. does not conclusively rule out reaction 1.4, but the difference between the rate of $c\text{-}C_6H_7$ disappearance and the rate of HO_2 appearance indicates that $k_{1.2} > k_{1.4}$. Also, the high value for $k_{1.5}$ reported by Pan et al. is surprisingly two orders of magnitude faster than the rates for the analogous reactions of several hydroxylated cyclohexadienylperoxyls[19] measured by the same group using the same technique; no one has explained why reaction 4 should be so much faster in unsubstituted cyclohexadienylperoxyls. The photo-acoustic calorimetry of Kranenburg et al.[39] conclusively shows that in organic solvents at room temperature, reaction 1.2 is faster than 1.4, and also sets an upper bound of about 2×10^9 s^{-1} on reactions 1.5.

Cyclohexadienylperoxyl radicals have many other potential decay pathways in addition to reaction 1.5a; several of these have been studied theoretically by Lay et al.[41] and by Raoult et. al.[56] The most obvious decay channel is to lose O_2 by the reverse of reaction 1.2. The reverse of reaction 1.3 is known to occur on a 100 μs timescale in aqueous solution;

however the corresponding reverse of reaction 1.2 has not been detected. The fact that a significant amount of heat was evolved in the photo-acoustic calorimetry experiments of Kranenburg indicates that $k_{-1.2} < 2 \times 10^9\,\mathrm{s}^{-1}$ in organic solvents. Pan et al. proposed that para-cyclohexadienylperoxyl decays primarily via intramolecular addition of oxygen to one of the double bonds. However, both ab initio[41] and empirical[7] calculations indicate that, in contrast to the *ortho* isomer, this process is significantly endothermic for the *para* isomer. Lay, et al. also predicted that this process would have a high barrier, at least for hydroxylated cyclohexadienylperoxyls.

Most of the previous work on reaction 1.2 was done in the gas phase or in aqueous solution, so one might wonder if the 50 fold rate discrepancy is due to solvent effects or chemical activation effects. In this work, we performed experiments in the liquid and gas phases to determine the solvent effect on cyclohexadienyl reactions. In addition, we analyzed the reaction networks involved with both traditional and novel numerical techniques to resolve the discrepancy between the gas and liquid phases. The results yield insight into an important reaction intermediate and suggest new paths for exploring combustion radical reactions.

1.6 Structural outline of the thesis

First, in Chapter 1 discussed the motivations for studying radical chemistry and, specifically, cyclohexadienyl radical chemistry. Also, several literature sources are given for prior studies on the cyclohexadienyl radical. In Chapter 2, the method and results of experiments performed in organic solvents are presented. Spectroscopic evidence for the assignment of peaks to cyclohexadienyl radical are shown. In Chapter 3 a theoretical description of the reactions involving cyclohexadienyl radical is provided. Heats of reaction and equilibrium constants are calculated from photoacoustic calorimetry data in the literature. Rate constants are estimated using physically reasonable values based on other similar reactions. Analytical models are used to describe the qualitative features of the reaction network in both gas and liquid phases. Simulations of the reaction network are shown to be consistent

with the experimental data. In Chapter 4 we go one step further in analyzing the reaction network by performing optimization, not just simulation, on the chemical system to obtain rate parameters. A new method is presented which provides a way for determining if a model is inconsistent with experimental data. In addition, new methods of analysis provide a means for determining the limits to the number of parameters that can be extracted from experimental data. In Chapter 5, we discuss the results of gas phase experiments on the cyclohexadienyl radical and what lessons were learned. Finally, in Chapter 6 conclusions are drawn and future directions for the research are discussed.

Chapter 2

Liquid phase experiments

"Argument is conclusive, but it does not remove doubt, so that the mind may rest in the sure knowledge of the truth, unless it finds it by the method of experiment."
– Roger Bacon

2.1 Experimental approach

Reaction rates of cyclohexadienyl radicals with oxygen in different solvents were measured by laser flash photolysis using the experimental setup shown in Figure 2-1. An excimer laser pulse photolyzed di-tert-butyl peroxide to produce tert-butoxyl radicals (Reaction 2.1). These radicals reacted rapidly with excess amounts of 1,4-cyclohexadiene to rapidly generate cyclohexadienyl radicals (Reaction 2.2). The transient absorptions of the cyclohexadienyl radicals were recorded using light from a pulsed Xe flash lamp, passing through a monochromator to a photomultiplier.

$$(CH_3)_3COOC(CH_3)_3 + h\nu_{248} \rightarrow 2(CH_3)_3CO \qquad (2.1)$$

$$(CH_3)_3CO + 1,4\text{-}C_6H_8 \rightarrow (CH_3)_3COH + c\text{-}C_6H_7 \qquad (2.2)$$
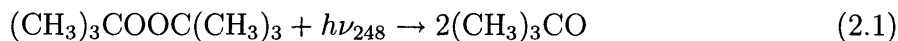
The solutions prepared typically contained between 0.1 and 1M 1,4-cyclohexadiene

Figure 2-1: Diagram of the experimental setup used to measure cyclohexadienyl radical kinetics in the liquid phase. The sequence of the experiment works as follows: (1) The pulsed Xe lamp flashes creating a stable base level of probe light. (2) The excimer laser fires initiating the chemistry. (3) The change in the probe light over the timescale of the experiment is recorded by the digital oscilloscope. (4) The final trace is transferred from the oscilloscope to computer and stored.

E = 200 mJ / pulse
λ= 248 nm
n = E / (hc / λ)
  = 2.5 $\times$ 10^{17} photons

2

1 Pulsed
   Xenon
   Lamp

$\diamond$ Photodiode

4   3
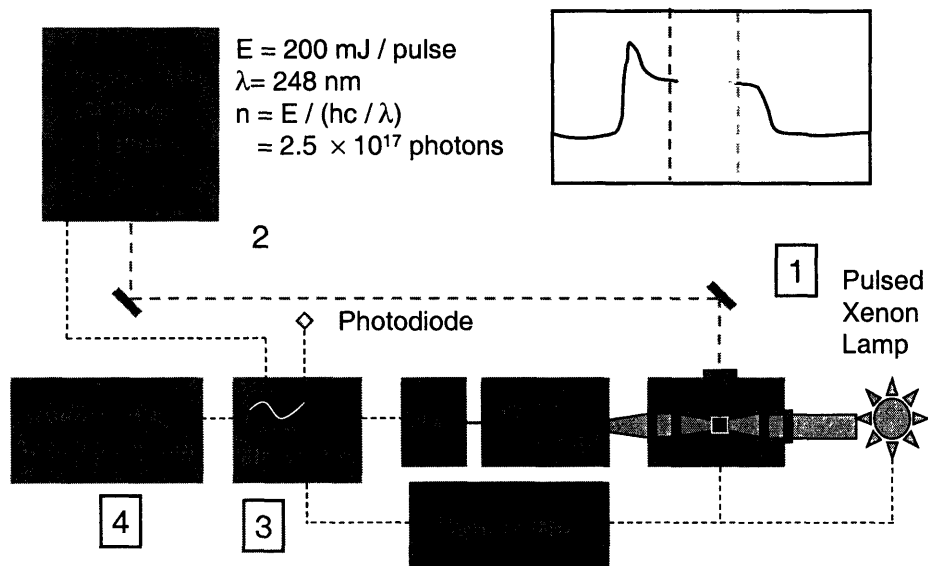
(Aldrich, 97%) and 0.1 M DTBP (di-tert-butyl peroxide, Aldrich, 98%) in one of four solvents: cyclohexane (Baker, HPLC Grade), dichloromethane (EM Science, 99.9%), perfluorohexane (Aldrich, 99%), and 1,1,2-trichlorotrifluoroethane (Aldrich, 99%). The chemicals were used as received. Oxygen was added to the liquid system by bubbling an O_2 / Ar mixture prepared using Sierra mass-flow controllers (accurate to $\pm$ 0.1%). A splitter was used to divert $\sim$ 20% of the 500 ml/min flow to the liquid sample. The partial pressures of the gases used in the experiment were corrected to take into account the vapor pressure of the solvent at the experimental temperature and atmospheric pressure. The O_2 solubilities were taken from literature.[77,69] The reagent solution was then circulated through a 1 cm x 4 mm flow cuvette (Spectrocell Corp.) at a constant flow rate of 15 ml/min to avoid accumulation of photolysis and reaction products.

A Lambda Physik Compex 102 Excimer Laser containing a KrF gas mixture generated 25 ns photolysis pulses at a wavelength of 248 nm. About 30 mJ of this light was directed onto the cuvette through an iris. The amount of photolysis light entering and leaving the sample cuvette was measured using a calibrated power meter from Ophir Optronics. The photolysis fluence was approximately 1 MW/cm^2.

Transient spectra were recorded using a Flash Kinetic Spectrometer (Applied Photophysics LKS.50). The probe beam was generated by a Xenon short arc flash lamp (OSRAM, XBO 150 W/CR OFR) mounted in a convection-cooled housing. The duration of the pulsed probe light was about 1.5 ms, and the intensity of the central portion of the pulse was flat within 0.5% for 100 μs. Since the 100 μs plateau is much longer than the reaction times measured, the lamp output was essentially constant during each recorded transient absorption period.

The probe beam was focused through the sample cuvette using a standard crossed beam arrangement. The probe beam was approximately 1 mm in diameter and was set to pass close to the face of the cuvette exposed to the laser pulse, where the highest concentration of the transient species is formed.

After exiting the cuvette the probe beam passed through a Schott WG 305 filter to

suppress scattered light from the photolysis beam. The beam was then focused onto the entrance slit of an f/3.4 holographic diffraction grating monochromator, having a symmetrical Czerny-Turner configuration. The light passing through the monochromator was detected by a Hamamatsu 1P28 side window photomultiplier (200-650 nm wavelength range). The signal output from the photomultiplier was digitized by a Hewlett Packard HP54510 Digitizing Oscilloscope. The collected data were stored and analyzed on the spectrometer workstation. The monochromator wavelength was adjusted with a stepper motor drive controlled by a microprocessor, which is interfaced to the spectrometer workstation. The spectra were typically recorded by averaging 30-100 transient absorption traces containing 500 temporal data points for each transient absorption. The data were collected so that 10% of the acquisition period provides pre-trigger information.

Each spectrum was normalized to the probe light intensity immediately before the photolysis pulse, thus reducing signal artifacts due to electronic pickup of the excimer discharge or to pulse-to-pulse variations in the flash-lamp intensity. The signal was further corrected by subtracting the baseline measured by blocking the photolysis beam with a shutter. The transient absorption data from the spectrometer was analyzed using the singular value decomposition and multivariate least-squares regression as implemented in the Pro-Kineticist[38] package. Non-linear least-squares regression and numerical integration of ODE's were performed with MATLAB.

2.2 Frequency-domain results

The transient absorption of c-C_6H_7 was measured in several non-polar solvents: cyclohexane, dichloromethane, perfluorohexane, and 1,1,2-trichlorotrifluoroethane. The observed band positions in these solvents are listed in Table 2.1 and the UV spectra are shown in Figure 2-2.

In all cases, the UV band displays a characteristic two-hump structure. In some experiments, this band is overlapped by a weaker broad band with a peak around 280 nm, which has a different time-dependence from those in Table 1.

32

Figure 2-2: UV absorption spectra of cyclohexadienyl radical in various solvents at room temperature (298 K) and pressure (1 atm). 1,4-C_6H_8 and DTBP concentration for each solvent was 0.1M. The relative heights of the spectral peaks probably correspond to slightly different concentrations of cyclohexadienyl in solution, as opposed to a solvent effect changing the absorption coefficient.
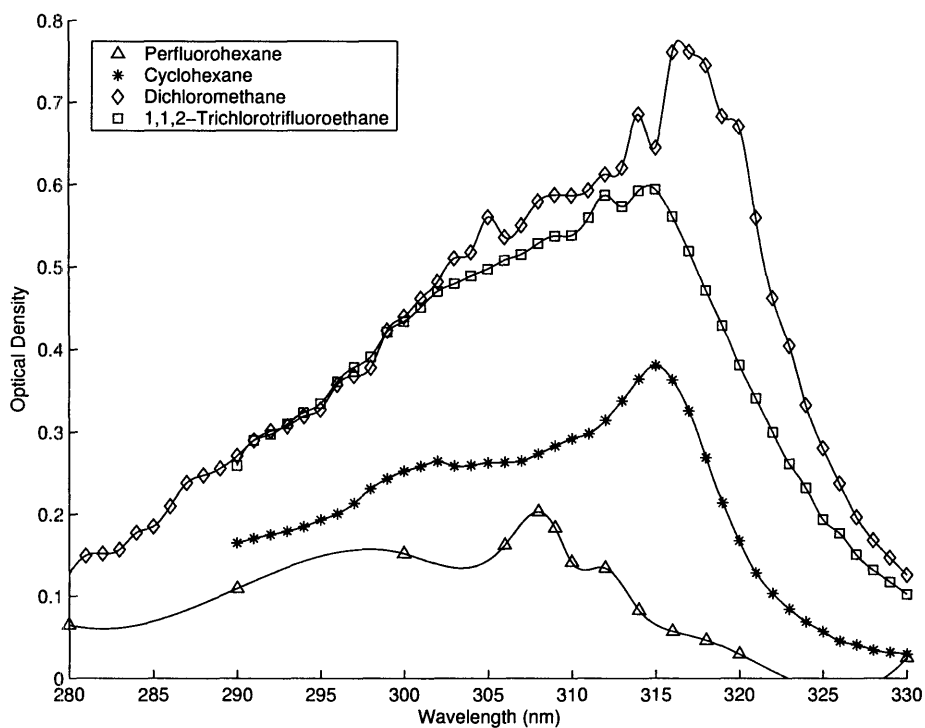
Figure 2-3 shows a visible spectrum for the cyclohexadienyl radical in cyclohexane. Absorption at the visible wavelength is much weaker than in the UV band. Error bars are shown in Figure 2-3 to indicate the signal-to-noise of this weak absorption.

The absolute absorption coefficient of c-C_6H_7 in cyclohexane at 316 nm was estimated by measuring the excimer laser fluence and the corresponding transient absorption of the probe beam, using the known di-tert-butyl peroxide absorption strength and quantum yield[6] and the known rate constant for the competing reaction of t-butoxyl with cyclohexane.[43] Our inferred absorption strength is consistent with the value of $\epsilon_{316} = 5400$ $M^{-1}cm^{-1}$ measured by Sauer et al.[59] It is also similar to the value of $\epsilon_{316} = 4400$ $M^{-1}cm^{-1}$ reported in aqueous phase by Pan and von Sonntag.[52] The gas phase peak lies at 302 nm and the absorption strength at the peak has variously been reported as 15,000 $M^{-1}cm^{-1}$ by Berho[8] and 2,700 $M^{-1}cm^{-1}$ by Bjergbakke.[11]

The absorption strength at 556 nm was estimated relative to the 316 nm absorption by rapidly scanning the monochromator between the two wavelengths. Because neither the Xe flash-lamp intensity nor the photomultiplier response is constant over this broad wavelength range, it was necessary to simultaneously adjust the voltage and thus the gain of the photomultiplier tube. The 316 nm absorptions were consistently approximately 50 times stronger than the 556 nm absorptions under identical conditions, yielding an estimated c-C_6H_7 absorption strength $\epsilon_{556} = 100$ $M^{-1}cm^{-1}$ ($\sigma = 2 \times 10^{-19}$ cm^2) in cyclohexane. To our knowledge, the green band of the cyclohexadienyl radical has not yet been detected in

Table 2.1: Observed positions of the maxima of the cyclohexadienyl radical spectrum in various organic solvents

Solvent	UV Band Position (nm)	Visible Band Position (nm)
Cyclohexane	316	556
Dichloromethane	317	558
1,1,2-Trichlorotrifluoroethane	314	555
Perfluorohexane	308	N/A

Figure 2-3: Visible absorption spectrum of cyclohexadienyl radical in cyclohexane solvent at room temperature (298 K).
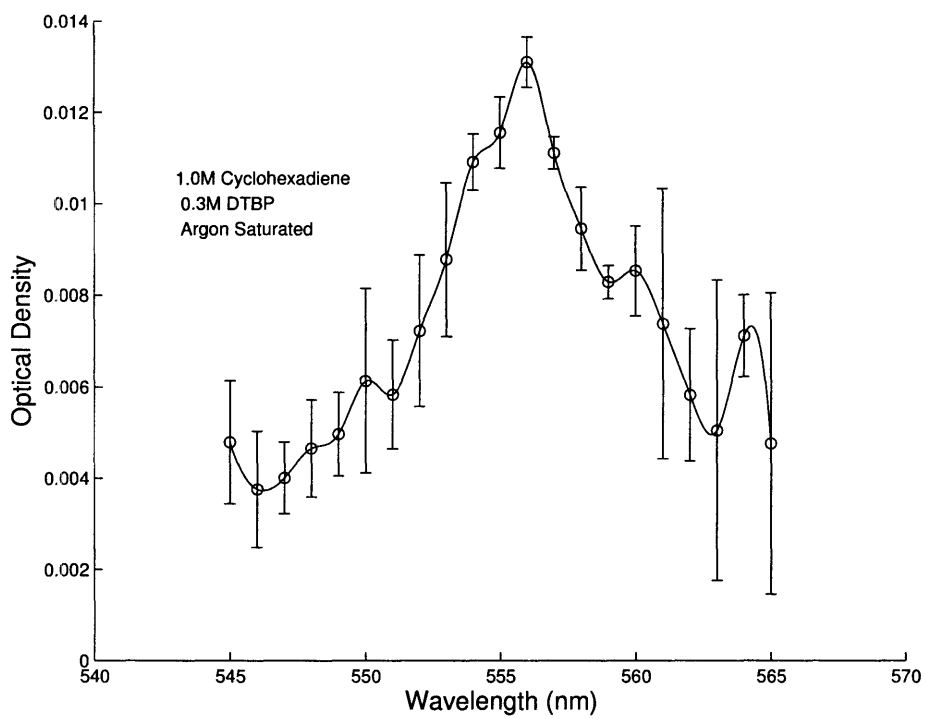
the gas phase.

2.2.1   Interferences

An interference is defined as an absorption by another radical or molecule that overlaps with the desired absorption by the radical of interest. We collected data at a wide range of detection wavelengths, to identify potential interferences. The measured transient absorptions, $A(t, \lambda)$, were analyzed using singular-value decomposition (SVD). The SVD analysis revealed that a single transient species was responsible for more than 90% of the observed signal, but weak interferences corresponding to the other singular values were detected.

The most significant interference was originally believed to be the absorption of peroxyl radicals. However, recent experiments have identified an excited state of benzene to be a significant part of the 10% interference. Experiments were performed by creating a test solution of cyclohexane with 3% benzene to approximate the amount of benzene in the stock solution of 1,4-cyclohexadiene. Benzene is always a contaminant of 1,4-cyclohexadiene since industrial production of the diene is by hydrogenating benzene.

The test solution was used in several experiments in place of the 1,4-cyclohexadiene stock solution. A 1% absorbance was recorded that appeared within 1 μs and remained constant for a period of 50-100 μs. Given the concentration of benzene in solution, an absorption coefficient of ~ 1 M^{-1}cm^{-1} (1.66×10^{-21} cm^2) is attributed to this state. It is unknown if this is an excited state of benzene or a radical formed by the degradation of benzene by photolysis. The benzene interference is, however, not as important as other interferences, since its long lifetime has a negligible effect on the measured decay rate of the cyclohexadienyl radical. In addition, the presence of cyclohexadiene would perturb this long-lived state.

The interference due to the weak absorption of peroxyl radicals (ROO) is not as strong as that of benzene, but its change over the lifetime of the experiment makes it more important to account for. The main source of peroxyl radicals is from cyclohexadienyl via Reaction 1.2, and from side reactions (e.g. abstraction of an H atom from the solvent). The absorption strength of the ROO radicals at 316 nm is not accurately known (this is the weak long-

wavelength tail of the well-known peroxyl radical UV band); we use $\epsilon = 200$ M^{-1}cm^{-1}.[61] The t-butoxyl radical also absorbs at 316 nm, $\epsilon_{316} \sim 500$ M^{-1}cm^{-1},[73] but the t-butoxyl transient has a short lifetime, so this interference is not as important.

For safety reasons, a small amount of hydroquinone is added as a stabilizer to the 1,4-cyclohexadiene by the manufacturer, so the semiquinone radical should be formed in our experiments. However, hydroquinone is only sparingly soluble in our nonpolar solutions, and, in fact, was undetectable by UV-VIS spectrophotometry at the part per million level. Due to the extremely low concentration of hydroquinone, the semiquinone interference is not expected to be detectable at our signal-to-noise level.

The peroxyl radicals are the most important interference with the cyclohexadienyl measurements at 316 nm, so it is vital to understand the time-dependence of their signals. This was done by tuning off the cyclohexadienyl peak to shorter wavelengths, where the peroxyl radicals absorb more strongly. The peroxyl radical interference can also be avoided by using the green band; however, the signal-to-noise ratio on this weak band is not sufficient to draw definite conclusions about cyclohexadienyl kinetics. In our models we account for the peroxyl radical interference by including it specifically in our predicted absorption signal.

2.3 Time-domain results

Most previous work on c-C$_6$H$_7$ had utilized either the UV band or the green band, but not both. The only exceptions were matrix studies. In the matrix studies, electron spin resonance (ESR) confirmed that c-C$_6$H$_7$ was present, but the experiments were not able to demonstrate that both absorption bands arose from the same species.[35] Here, we measure the time-dependence of the transient absorptions using both bands. In Figure 2-4, we demonstrate that the two absorptions have equivalent time-dependence under widely different conditions of oxygen concentration, implying that the absorptions arise from the same species. The two absorption bands could arise from two species in rapid equilibrium, e.g. two isomers of c-C$_6$H$_7$, but these species would have to equilibrate on a sub-microsecond time-scale at room temperature to be consistent with the observations.

Figure 2-4: Transient absorptions measured using the ultraviolet and visible bands of the cyclohexadienyl radical in cyclohexane solution (0.4M 1,4-C_6H_8 and 0.1M DTBP, T = 298K). Argon saturated solutions are shown in (A), while oxygen saturated solutions are shown in (B). The peak heights of the two absorption bands were normalized, and show identical time-dependence confirming that both absorption bands arise from the same species.
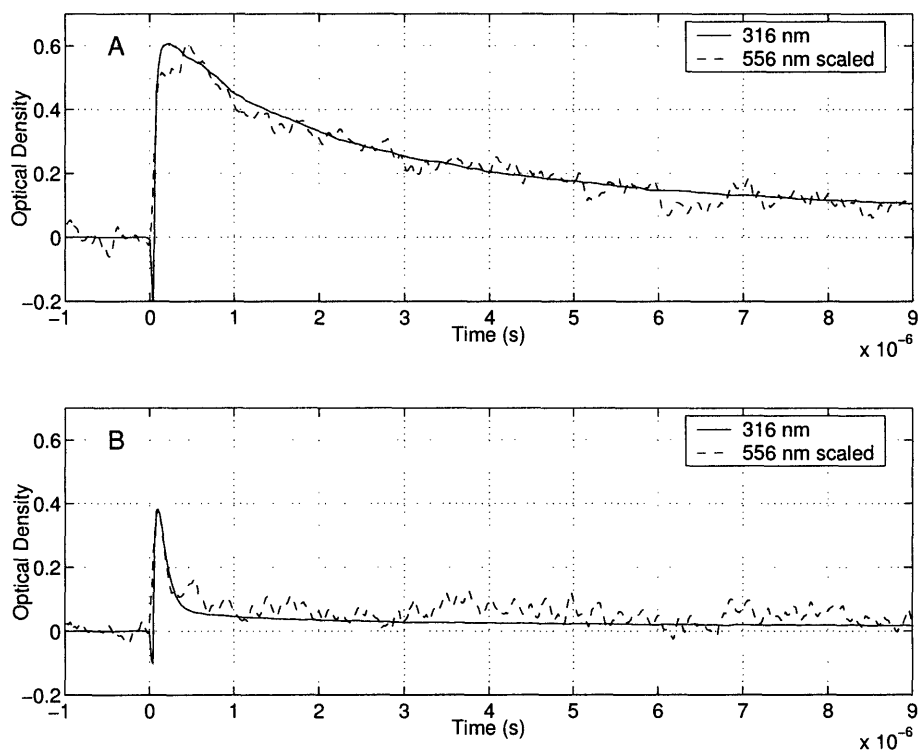
A typical time-resolved absorption measurement of the c-C_6H_7 radical is shown in Figure 2-4. Initially, 10% of the data set is recorded before the photolysis pulse to ensure an accurate measurement of the signal before absorption. After the photolysis pulse, scattered fluorescence creates a small negative signal, which then rises to peak absorbance over a period of approximately 100 ns. The peak occurs where the rate of generation of c-C_6H_7 is equal to its rate of decay. From the peak, the absorption decays at a rate an order of magnitude slower than the initial rise.

In the absence of oxygen, the c-C_6H_7 radical decays on a 10 μs timescale, presumably through radical-radical recombination. However, in the presence of oxygen, the c-C_6H_7 radical decays on a 1 μs timescale, due to the title reaction. Changes in temperature do not significantly change the fast decay rate under oxygenated conditions, as shown in Figure 2-5.

Figure 2-5: Comparison of the decay of cyclohexadienyl at different temperatures. Initial concentrations were 0.1M 1,4-C_6H_8 and 0.1M DTBP in cyclohexane solvent saturated with either Ar or O_2. At 323 K, the slow component decays at twice the rate at lower temperatures. The fast component of the decay in the presence of O_2 is relatively temperature independent.
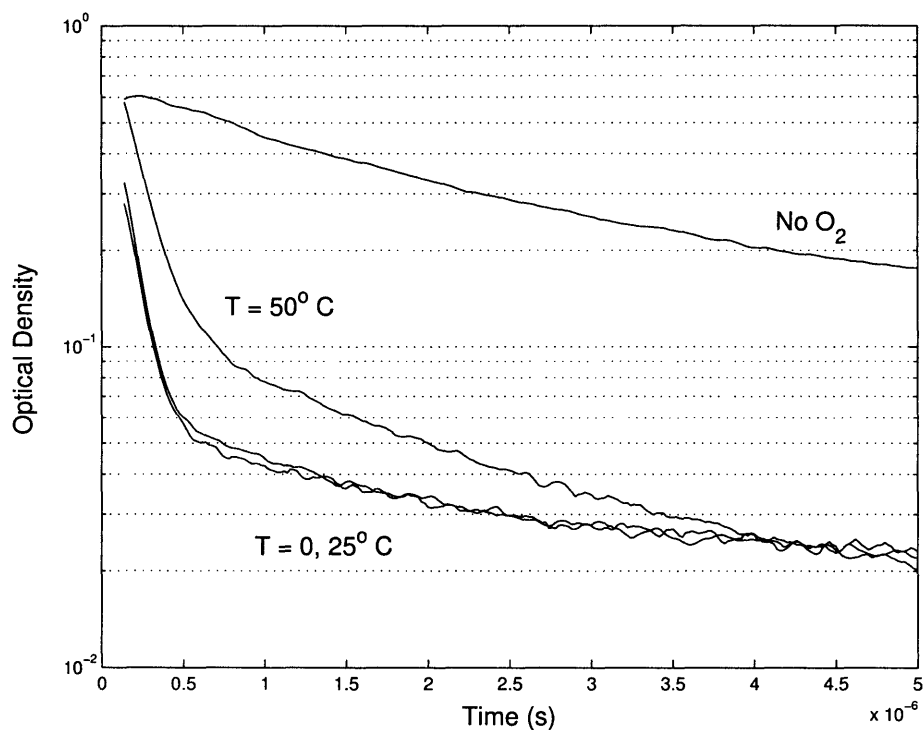
2.4 Oxygen dependence

The conventional method for determining rate constants from flash photolysis is to determine the c-C_6H_7 decay time-constants for each absorption experiment, then plot those with respect to the oxygen concentration to obtain a pseudo-first order approximation of the rate constant, $k_{1.2}$. These decay time-constants are typically calculated by fitting the absorbance signal from its peak using a single exponential model with an offset.

$$a = a_0 e^{-t/\tau} + b \tag{2.3}$$

Below a partial pressure of 0.25 atm of O_2, the single exponential fits to the data were excellent with $R^2 = 0.998$ or above for all parity plots.

Figure 2-6 shows that the reciprocal of the decay constants for the cyclohexadienyl radical (τ in Equation 2.3) are linearly dependent upon the oxygen concentration. Using linear regression, we derived the pseudo-first order rate constants for c-$C_6H_7 + O_2$ at various temperatures. These rate constants are listed in Table 2.2 at various temperatures in cyclohexane solvent along with a corrected value based on a procedure used in Chapter 3.

Although the pseudo-first order rate constants obtained are reasonably close to the diffusion limit, there are several drawbacks to this approach. First, as the oxygen concentration increases, the timescales for cyclohexadienyl generation and decay become comparable, which causes this procedure to underestimate the true rate constant, $k_{1.2}$. Second, at higher oxygen concentrations, cyclohexadienyl radical decay is not a single exponential, as shown in Figure

Table 2.2: Pseudo-first order rate constants for cyclohexadienyl in cyclohexane at several temperatures.

Temperature [K]	$k_{1.2}$ obtained from Equation 2.3 $[\mathrm{M^{-1}s^{-1}}]$	$k_{1.2}$ obtained from Equation 3.6 $[\mathrm{M^{-1}s^{-1}}]$
273	$9.1 \pm 1.1 \times 10^8$	$1.14 \pm 0.59 \times 10^9$
298	$8.1 \pm 1.8 \times 10^8$	$1.23 \pm 0.31 \times 10^9$
323	$6.3 \pm 0.6 \times 10^8$	$1.22 \pm 0.34 \times 10^9$

Figure 2-6: Time-dependent cyclohexadienyl absorption data were fit to single exponential curves to determine the effective rate of decay of the radical at various oxygen concentrations (0 - 1 mM) and temperatures ($\star$ = 323K, o = 298K, $\square$ = 273K). The slopes differ from the true value for $k_{1.2}$ due to the effects of other reactions affecting c-C_6H_7 with comparable timescales (see Section 3).

The plot shows $1/\tau$ versus $[O_2]$ (M) with the following fitted equations:

$$1/\tau_{273} = (9.1 \pm 1.1) \times 10^8 \, [O_2] + 3.12e{+}05$$

$$1/\tau_{298} = (8 \pm 1.8) \times 10^8 \, [O_2] + 1.6e{+}05$$

$$1/\tau_{323} = (6.3 \pm 0.62) \times 10^8 \, [O_2] + 2.63e{+}05$$
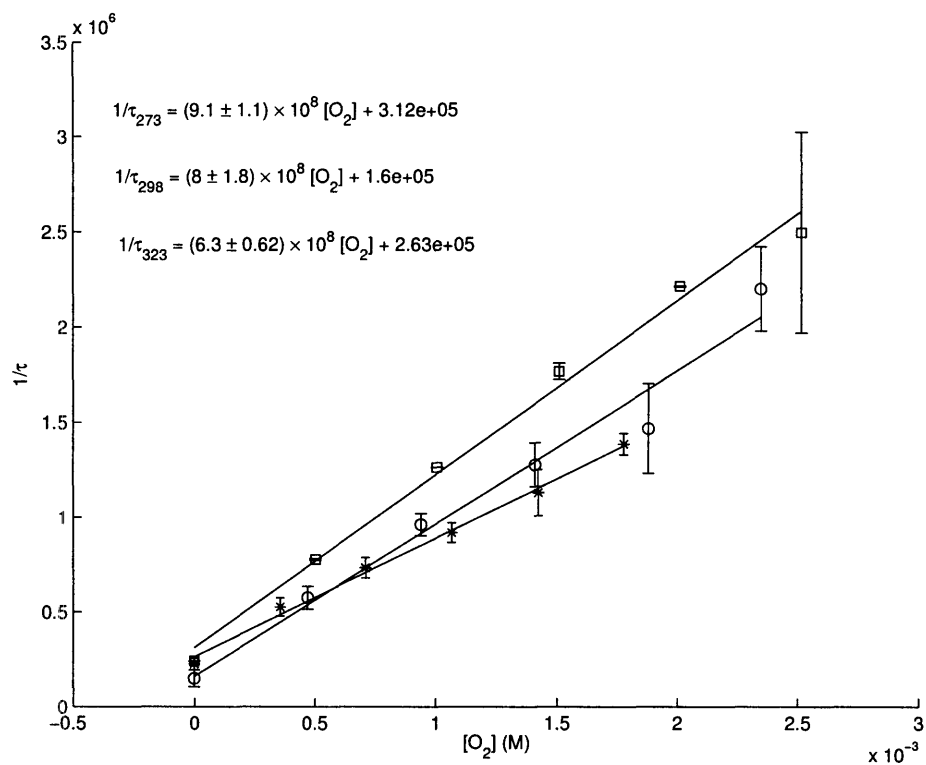
2-7. In Section 3, several more complex models are used to explain the bi-exponential decay of Figure 2-7.

Figure 2-7: Comparison of cyclohexadienyl decay at 316 nm ($[O_2]$ = 7.5 mM, T = 25 °C) to a single exponential fit with an offset. Measurements at 316 nm and 556 nm both show a multiexponential decay, implying that the signal can be attributed to cyclohexadienyl, not an interference.
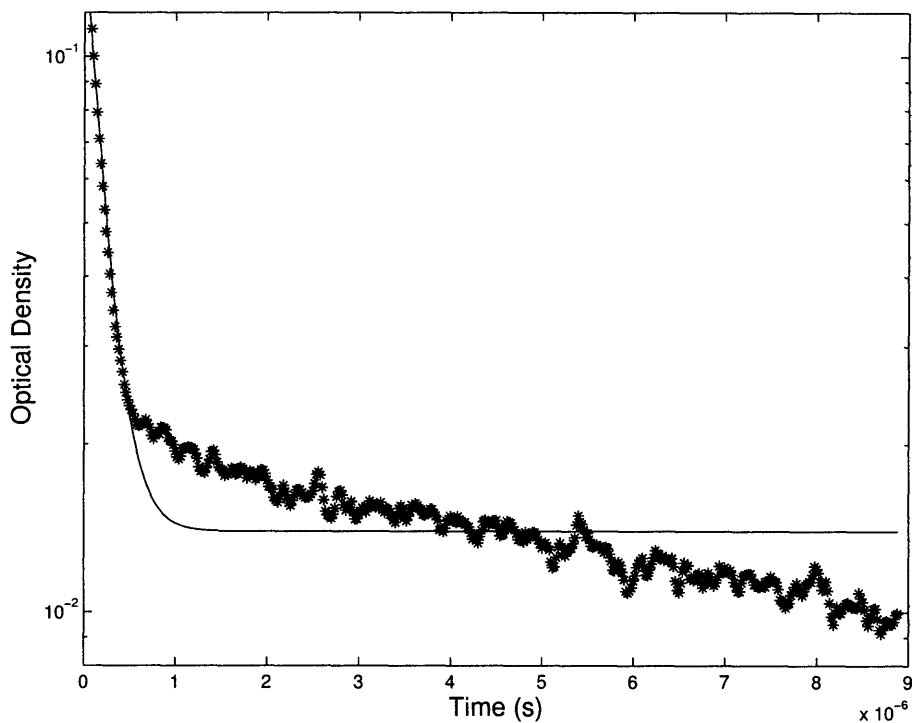
2.5   GC/MS analysis of products

Gas chromatography with mass spectrometry (GC/MS) was performed on the products of laser flash photolysis in cyclohexane solution. The solution experienced 100 laser flashes at the standard experimental conditions described above. Samples were analyzed on an HP 6890/5973 GC/MS system, equipped with a J&W DB-35 MS capillary column. The column is 30 m long with an internal diameter of 0.25 mm and a film thickness of 0.25 μm. The mass selective detector was operated in electron impact mode at 70 eV with a quadrupole

Figure 2-8: GC analysis of the photolysis products of 1,4-cyclohexadiene photolysis.

File   : C:\HPCHEM\1\DATA\KTJT420B.D
Operator   . KOL1/James
Acquired   : 20 Apr 2005 14:73   using AcqMethod KTJT0405
Instrument : GC/MS Ins
Sample Name: Uv9 240 nm)1,4 cyclohexadiene
Misc Info   : HP-17 MS, 30 M
Vial Number: 1
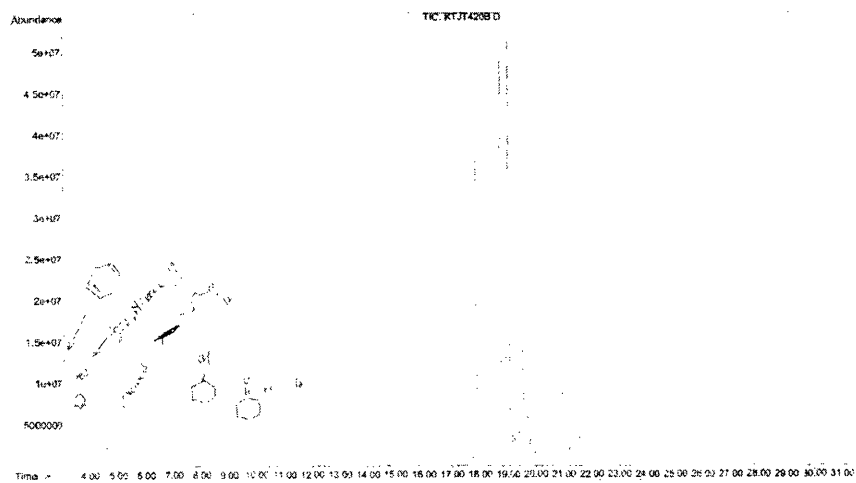
temperature of 150 °C, a source temperature of 230 °C, and a transfer line temperature at 280 °C. A 1 μl sample was injected into the GC in splitless mode operating at 250 °C with a continuous flow of He a 1 ml/min. The oven program began with an isothermal hold at 32 °C for 1.5 min., ramped to 280 °C at the rate of 6 °C/min. and then ramped to the final temperature of 310 °C at the rate of 25 °C/min. The final temperature was held for a period of three minutes. The MS was scanned from m/z 40 to 350 with the rate of 4.5 scans/second. Data were collected and analyzed with a PC using the HP ChemStation software.

The results are consistent with the presence of cyclohexadienyl radicals. Figure 2-8 shows the presence of the reactants in the cyclohexane solution along with some oxygenated products. If we zoom in on the large product peaks, we observe several species with a large molecular weight.

Figure 2-9: Increased magnification of the peaks of the heavier components in Figure 2-8. The mass-spec assignments confirm these peaks to be recombination products of the cyclohexadienyl radical.
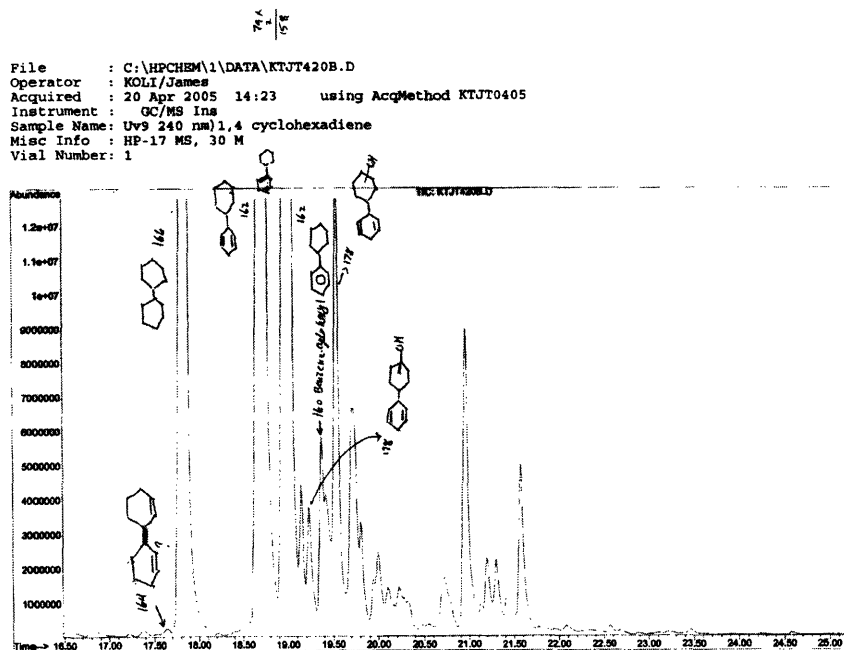
Figure 2-9 shows the presence of dimers of cyclohexadiene and benzene that occur due

to a combination of cyclohexadienyl radicals with solvent, benzene, and itself. The size of the GC peaks suggest that radical recombination is a significant pathway in liquid phase.

In Appendix C the GC traces and mass-spec assignments for all the species found are shown. Several species in solution were methylated forms of the reactants, suggesting a source of methyl radicals. It is likely that the methyl radicals come from the degradation of t-butoxyl radicals to form acetone, as shown in Reaction 2.4.

$$(CH_3)_3CO \rightarrow CH_3 + (CH_3)_2CO \tag{2.4}$$

Another source of methyl radicals could be the ring-opening of 1,4-cyclohexadiene to form a pentatriene and a methyl radical. However, in the GC/MS analysis no pentatriene were found making it likely that the only source of methyl radicals is from Equation 2.4.

2.6 Future extensions of liquid phase experiments

The liquid-phase apparatus is an extremely useful tool for measuring spectra and kinetics for a variety of radicals. However, several improvements and additions to the system would create the opportunity to do detailed experiments on a wide variety of photochemical systems. One such improvement would be combining the current apparatus with a GC/MS system.

The addition of a GC/MS to the current setup would allow detection of a number of radical intermediates and products under a variety of conditions. Adding an online GC/MS would allow quantitative determination of product species, which along with an observability analysis, would provide access to a large quantity of chemical state data.

Another simple experiment would be to observe the results of 193 nm photolysis of pure 1,4-cyclohexadiene. At this wavelength cyclohexadienyl radical is formed and an H atom is ejected. Since no peroxide is needed it is likely that a simpler product study could be done which might yield more chemical information. The results from this experiment would definitively determine if the source of the methyl radicals is t-butoxyl fragmentation or ring-opening of 1,4-cyclohexadiene.

In addition, other chemical systems are amenable to analysis in the liquid phase and may have results useful to the kinetics community at large. For example, previously Hans Carstensen found an absorption spectrum for the 2-phenylethyl radical. It is likely that if 2-phenylethyl's spectrum can be duplicated then its kinetics can be observed. Its structure is also resonantly stabilized and could provide an interesting comparison to 1,4-cyclohexadienyl kinetics.

2.7 Conclusions

1. Cyclohexadienyl radical was observed in the liquid phase using Laser-flash photolysis.

2. Absorption peaks were found in both the UV and visible regions of the spectrum. An overlay of the absorption with time at both peak wavelengths showed identical time-dependence.

3. Cyclohexadienyl decay has a direct correlation to oxygen concentration.

4. The primary interference, once thought to be peroxyl radical absorption, has been determined to be an excited state of benzene.

5. GC/MS analysis has found recombination products of cyclohexadienyl radical proving the existence of the radical in solution.

Chapter 3

Theoretical calculations and kinetic models

"The sciences do not try to explain, they hardly even try to interpret, they mainly make models. By a model is meant a mathematical construct which, with the addition of certain verbal interpretations, describes observed phenomena. The justification of such a mathematical construct is solely and precisely that it is expected to work." – John Von Neumann

3.1 Introduction

In this chapter we analyze the data obtained in the liquid phase and create models to explain the puzzling behavior in both the liquid and gas phases described in Chapter 1. First, we calculate thermodynamic values for radicals that are formed in our experiment. Using these values, we postulate different reaction schemes that explain the liquid phase results. Starting with very basic assumptions, we create analytical models that provide insight into the chemistry and gradually add complexity to describe more phenomena. After attempts to explain the liquid and gas phase phenomena by pure analytical means becomes difficult, we turn to numerical simulations to handle more complex reaction networks. By

gradually adding complexity, we determined that the simplest explanation for the phenomena in the gas phase is a shift in the equilibrium concentrations to the cyclohexadienyl and its corresponding peroxyl radicals. Several novel analysis techniques that were useful in looking at large reaction networks are also discussed.

3.2 *Ab initio* calculations of cyclohexadienyl radical properties

The B3LYP Density Functional Method, as implemented in the Gaussian 98W suite of programs[24] on a PC, is used to calculate the energies, equilibrium geometries, and vibrational frequencies of c-C_6H_7 and C_6H_7OO. Gas phase properties are calculated at B3LYP/6-311+G(2d,p) // B3LYP/6-31G(d), B3LYP/6-311+G(3df,2p) // B3LYP/6-31G(d), and B3LYP/6-311+G(3df,2df,2p) // B3LYP/6-31G(d) levels using the ultra-fine grid option in the last two geometry optimizations. In order to capture electrostatic solvation effects, we also perform calculations for cyclohexane and dichloromethane solutions using the Polarizable Continuum Model of Wiberg and coworkers[21] at the B3LYP/6-311 + G(2d,p) // B3LYP/6-31G(d) level. In the polarizable continuum models, we use a dielectric constant of 2.023 for cyclohexane and 8.93 for dichloromethane.

Most density functional methods, including B3LYP, do not give accurate absolute values for peroxyl radical thermochemistry.[76] In order to improve the accuracy of the calculations, the results are calibrated by comparison to B3LYP calculations for allyl and allylperoxyl radicals, where the experimental gas phase thermochemistry is available.[53,67] This procedure is similar to the common practice of using isodesmic reactions, reactions in which the types of bonds that are made are the same as those which are broken, to predict thermochemistry.

The results from quantum chemistry calculations are also checked against empirical estimates. The gas phase values are compared with group-additivity estimates made using the THERM program.[58] Empirical solvation corrections are based on analogies with known compounds as discussed below.

The pressure-dependent falloff of Reaction 1.2 is computed using the Master Equation method as implemented in MULTIWELL.[5,4] The densities of states are computed using the Stein - Rabinovitch variant of the Beyer-Swinehart direct-count algorithm.[68] The C-O single bond is treated as a free internal rotor. For the falloff calculation, the rate for the barrier-less adduct formation reaction

$$c\text{-}C_6H_7 + O_2 \rightarrow C_6H_7OO^{\ddagger} \tag{3.1}$$

in the gas phase was assumed to be 1.5 $\times 10^9$ $M^{-1}s^{-1}$ and both temperature and energy independent. This calculation confirms that Reaction 1.2 is in the high-pressure limit under the conditions of Berho and Lesclaux, as stated by those authors.[8]

3.2.1 Density functional calculations

Ab initio calculations were performed at the B3LYP level to get an estimate of the R-OO bond strength in cyclohexadienylperoxyl radicals, as well as of the free energies of Reactions 1.2a and 1.2b. Thermal energy contributions and entropies were directly taken from the Gaussian frequency calculations at the B3LYP/6-31G(d) level. Of the six stable minima found on the C_6H_7OO potential energy surface, three structures correspond to $p\text{-}C_6H_7OO$ and the remaining three to the corresponding *ortho* conformers (see Figure 1-2 for nomenclature). The conformations which are trans about the C-O bond are 0.9 kcal/mol ($o\text{-}C_6H_7OO$) and 1.4 kcal/mol ($p\text{-}C_6H_7OO$) more stable than the corresponding gauche conformations at the B3LYP/6-31G(2df,p) level. The gauche conformers are all comparable in energy to each other. The relative stabilities are insensitive to size of the basis set. The calculated entropy for Reaction 1.2 using density functional theory (DFT) was determined to be $\Delta S^o = -35$ cal/mol/K and is similar to other values in literature.[39]

The enthalpy of the isodesmic Reaction 3.2 was determined using DFT to be $\Delta H^o = -8.5$ kcal/mol.

$$p\text{-}C_6H_7OO + CH_2CHCH_2 \rightarrow c\text{-}C_6H_7 + CH_2CHCH_2OO \tag{3.2}$$
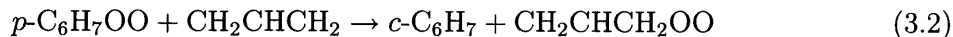
Combining this value with the known literature value[60] for the addition of O_2 to allyl ($\Delta H^o = -18.5$ kcal/mol), we obtain a bond dissociation energy for $C_6H_7OO \rightarrow c\text{-}C_6H_7 + O_2$ of 10 kcal/mol. Based on other peroxyl radical calculations in the literature, we estimate an uncertainty of 2 kcal/mol for this computed value.

In order to incorporate solvation effects, we performed polarizable continuum (PCM) calculations with cyclohexane and dichloromethane as solvents. These calculations account for the electrostatic interaction between the dipolar C_6H_7OO and the dielectric medium. This interaction increases the bond strength in cyclohexane solution by 1 kcal/mol.

3.2.2 Empirical solvation corrections

There are additional solvation effects beyond electrostatics (e.g. due to London forces) which are difficult to calculate from first principles. The free energy of solvation of O_2 in many solvents, including cyclohexane, has been measured (in the form of the Henry's Law coefficient, k_{O_2}). Of course, no measurements have been made of the vapor pressure of $c\text{-}C_6H_7$ and C_6H_7OO radicals. However, their solvation energies and entropies can be estimated from experimental data for other molecules. For example, the enthalpies and entropies of solvation of many stable $C_5\text{-}C_8$ organics in hydrocarbon solvents have been measured using gas-liquid chromatography.[47,46] The differences between the values for nonpolar C_8 and C_6 species fall in a narrow range:

$$
\begin{aligned}
\Delta\Delta H_{solv} &= \Delta H_{solv}^{C_8} - \Delta H_{solv}^{C_6} = -2 \pm 1 \text{ kcal/mol} \\
\Delta\Delta S_{solv} &= \Delta S_{solv}^{C_8} - \Delta S_{solv}^{C_6} = -2 \pm 1 \text{ cal/mol-K}
\end{aligned}
$$

Excluding electrostatics, the solvation enthalpy of C_6H_7OO and $c\text{-}C_6H_7$ can be approximated as similar to a C_8 molecule and a C_6 molecule, respectively. Electrostatic effects can then be incorporated using the polarizable continuum model to obtain a solvation enthalpy

50

contribution to Reaction 1.2 of $\Delta\Delta H_{solv} = -3 \pm 1$ kcal/mol. The solvation entropy remains unchanged by PCM and is $\Delta\Delta S_{solv} = -2 \pm 1$ cal/mol/K. Combining these corrections with the gas phase quantum chemical values, we predict the change in enthalpy for Reaction 1.2 in cyclohexane solution to be -13 ± 3 kcal/mol, consistent with the measurements of -12 ± 1 kcal/mol made by Kranenburg et al.[39] in other organic solvents.

3.2.3 Summary of computed thermochemistry and equilibria for Reaction 1.2

To summarize, our best thermodynamic estimates for Reaction 1.2b in gas phase at 298 K are as follows:

$$\Delta H^o{}_{(1.2b)} = -10 \pm 2 \text{ kcal/mol}$$
$$\Delta S^o{}_{(1.2b)} = -35 \pm 1 \text{ cal/mol-K} \qquad (3.3)$$

which corresponds to

$$K_p{}^o(1 \text{ atm}, 298 \text{ K}) = e^{5000\,K/T - 18} = 0.5$$

The equilibrium constants for the optical isomers of o-C_6H_7OO are computed to be nearly identical. Because of the error bars in the computed ΔH^o and ΔS^o, we can only be certain that $25 \geq K_p{}^o(1\,\text{atm}, 298\,\text{K}) \geq 0.01$.

In dilute cyclohexane solution, following the notation of Meyer,[47]

$$K_c{}^o(1\text{M}) = \frac{[C_6H_7OO]}{[c\text{-}C_6H_7][O_2]} = \left(\frac{\rho_{C_6H_{12}}K_p}{M_{C_6H_{12}}k_{O_2}}\right) e^{-\left(\frac{\Delta\Delta H_{solv} - T\Delta\Delta S_{solv}}{RT}\right)} \qquad (3.4)$$

Evaluating the expression using Suresh's value[69] for k_{O_2} yields the following:

$$K_c{}^o(1\,\text{M}, 298\,\text{K}) = 46\,e^{\left(\frac{6500\,K}{T} - 18\right)} = 2100 \qquad (3.5)$$

The uncertainty in this computed $K_c{}^o$ is quite large, more than two orders of magnitude.

However, Kranenburg's experimental data indicate $K_c^o > 100$ in iso-octane (otherwise Reaction 1.2a would not proceed forward to any significant extent at the oxygen concentration employed). Our present kinetic data further constrain K_c^o, as discussed below. With the computed K_c^o, if the O_2 concentration were equal to 476 μM, the equilibrium concentrations of c-C_6H_7 and C_6H_7OO are predicted to be equal; in cyclohexane this oxygen concentration will be in equilibrium with an O_2 partial pressure of 0.4 torr. Most solution phase experiments have been run under much higher O_2 partial pressures of 76 - 760 torr, where the equilibrium is predicted to strongly favor C_6H_7OO over c-C_6H_7 consistent with the observed rapid disappearance of c-C_6H_7.

3.3 Analytical models for cyclohexadienyl chemistry with oxygen

In Chapter 2, a single exponential model, Equation 2.3, was used to create a first-order rate constant measurement of the reaction of c-C_6H_7 with O_2. Although this model shows excellent agreement with data, it ignores certain aspects of the chemistry. Notably, pseudo-first order models make the assumption that there is no generation of the decaying species. Although the generation of c-C_6H_7 by Reaction 2.2 is on the 100 ns timescale, the decay of c-C_6H_7 at high $[O_2]$ is almost as fast as its generation. A simple analytical model based on reactions 1.2 and 2.2 was constructed to decouple radical decay rates from cyclohexadienyl generation. According to this model,

$$[c\text{-}C_6H_7] = \left(\frac{\alpha}{\beta - 1/\tau}\right) e^{-t/\tau} - \left(\frac{\alpha}{\beta - 1/\tau}\right) e^{-\beta t} \tag{3.6}$$

where

$$\tau = \frac{1}{k_{2.2}[1,4\text{-}C_6H_8] + k_0}$$

$$\alpha = k_{2.2}[(CH_3)_3CO]_0 \, [1,4\text{-}C_6H_8]_0$$

$$\beta = k_{1.2}[O_2]_0$$

$$(3.7)$$

The constant, k_0, is a fitted parameter to account for all first-order rate processes that are not dependent upon 1,4-cyclohexadiene concentration.

Figure 3-1: Data taken at 298 K and $p_{O_2} = 0.25$ bar overlaid with a fit to the model shown in Equation 3.6.
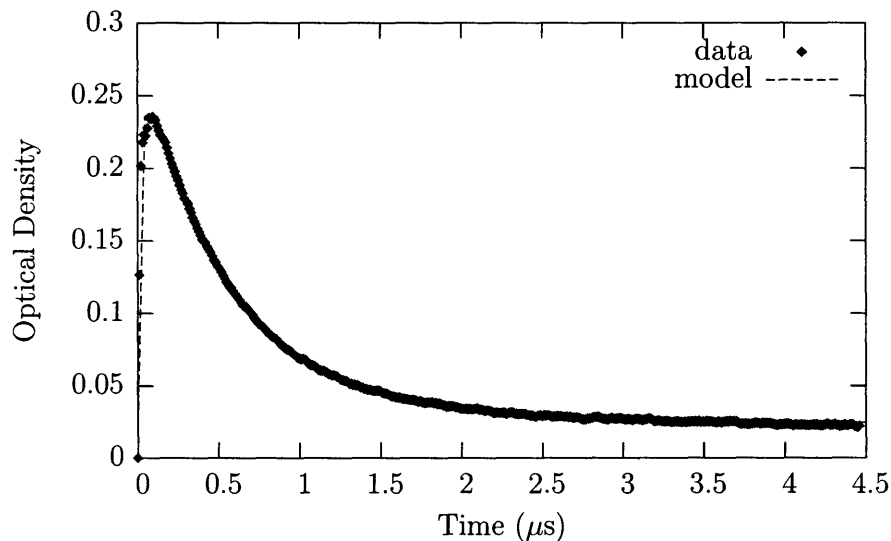
Nonlinear least-squares regression was performed to fit the data at 298 K to Equation 3.6. Figure 3-1 shows that an excellent fit was obtained with the analytical model with a baseline correction. In order to fit the data well, a good initial guess was required or else the fit would be poor due to the noise in the data creating spurious minima. In Chapter 4 we discuss a better way for performing these fits that avoids the problem of spurious minima.

Fitting all of the data measured at 298 K in cyclohexane yielded a $k_{1.2} = 1.23 \pm 0.31 \times 10^9$ M^{-1} s^{-1}, about 50% greater than the value obtained using the conventional approach

described in Section 2.4. This value is close to the predicted diffusion limit in cyclohexane, and is expected for a reaction with a low energy barrier.

Despite the excellent fits obtained with this simple model, it does not account for the significant reduction in the gas phase rate compared to the liquid phase. The analytical model above would predict the rate constants to be nearly the same in both cases, excluding a small solvent effect. For this reason, more reactions need to be included in the model to determine what pathways may be responsible for the difference in the rates between the gas and liquid phases.

Table 3.1: Important reactions used in simulations of the liquid experiments

#	Reaction	k_{298} [$M^{-1}s^{-1}$ or s^{-1}]	References
2.2	$(CH_3)_3CO + 1,4\text{-}C_6H_8 \rightarrow c\text{-}C_6H_7 + (CH_3)_3COH$	5.3×10^7	16
1.2b	$c\text{-}C_6H_7 + O_2 \rightarrow p\text{-}C_6H_7OO$	4.0×10^8	43, Sec. 3.3
-1.2b	$p\text{-}C_6H_7OO \rightarrow O_2 + c\text{-}C_6H_7$	1.9×10^5	Sec. 3.2.3
1.2a	$c\text{-}C_6H_7 + O_2 \rightarrow o\text{-}C_6H_7OO$	8.0×10^8	43, Sec. 3.3
-1.2a	$o\text{-}C_6H_7OO \rightarrow O_2 + c\text{-}C_6H_7$	1.9×10^5	Sec. 3.2.3
1.5a	$o\text{-}C_6H_7OO \rightarrow C_6H_6 + HO_2$	8×10^5	51
R	$2c\text{-}C_6H_7 \rightarrow Products$	1.2×10^9	3

Table 3.1 lists a reaction scheme that includes several likely reactions that might be occurring in tandem with cyclohexadienyl oxidation. Rate constants for these reactions were determined by making several assumptions: first, that the forward rate, $k_{1.2}$, is the diffusion-limited rate constant in cyclohexane, 1.2×10^9 $M^{-1}s^{-1}$ and second, that Reactions 1.2a and 1.2b are reversible and that their equilibrium constants can be calculated. Section 3.2 describes the calculation of these equilibrium constants in more detail. Third, $k_{1.2a} = 2k_{1.2b}$ due to the two enantiomers of $o\text{-}C_6H_7OO$. Lastly, a small absorption (200 $M^{-1}cm^{-1}$) was attributed to cyclohexadienylperoxyl in order to account for the residual baselines observed. All radical recombination rates were assumed to be diffusion-limited, and other rate constants were taken from literature, as cited in Table 3.1.

Assuming that reactant concentrations are constant over the time-scale of the experiment

and that $k_{1.5}$ is much faster than $k_{-1.2a}$, the reaction network can be solved analytically for the concentrations of c-$C_6H_7$and p-C_6H_7OO. Although the concentration of $(CH_3)_3CO$ varies significantly over the lifetime of the cyclohexadienyl radical, it can be modeled with a first order decay,

$$[(CH_3)_3CO] = [(CH_3)_3CO]_0 \, e^{-t/\tau} \tag{3.8}$$

$$\tau = \frac{1}{k_{2.2}[1,4\text{-}C_6H_8] + k_0}$$

where k_0 represents the sum of the other losses of $(CH_3)_3CO$ due to side-reactions and decomposition. This term presents a non-homogeneous component to the linear differential equations governing the system.

The resulting system of differential equations is shown in matrix form in equation 3.9.

$$x' = \mathbf{A}x + g(t) \tag{3.9}$$

where,

$$\mathbf{A} = \begin{bmatrix} -(k_{1.2a} + k_{1.2b})[O_2] & k_{-1.2b} \\ k_{1.2b}[O_2] & -k_{-1.2b} \end{bmatrix}$$

$$g(t) = \begin{bmatrix} k_{2.2}[(CH_3)_3CO]_0[1,4\text{-}C_6H_8] \\ 0 \end{bmatrix} e^{-t/\tau}$$

The solution procedure follows that of a standard textbook example in Boyce and DiPrima.[13] The matrix, $\mathbf{A}$, is solved to obtain its eigenvalues, $\lambda_\pm$, and eigenvectors, $\xi_\pm$.

$$\lambda_\pm = \frac{(k_{1.2a} + k_{1.2b})[O_2] - k_{-1.2b} \pm \sqrt{(k_{1.2a} + k_{1.2b})^2[O_2]^2 + 2k_{-1.2b}(k_{1.2a} + k_{1.2b})[O_2] + k_{-1.2b}^2}}{2}$$

$$\tag{3.10}$$

Using $\lambda_\pm$ and $\boldsymbol{\xi}_\pm$, we can transform the differential equations and decouple them by writing them in the form,

$$\boldsymbol{y}' = \mathbf{D}\boldsymbol{y} + \mathbf{T}^{-1}g(t) \tag{3.11}$$

where

$$\mathbf{D} = \begin{bmatrix} \lambda_+ & 0 \\ 0 & \lambda_- \end{bmatrix}$$

$$\mathbf{T} = \begin{bmatrix} \boldsymbol{\xi}_+ & \boldsymbol{\xi}_- \end{bmatrix}$$

Once the equations are decoupled, they can be solved using an integrating factor approach to get the solution in the transformed variable, $\boldsymbol{y}$. To transform back into $\boldsymbol{x}$, the relation used to create $\boldsymbol{y}$, $\boldsymbol{x} = \mathbf{T}\boldsymbol{y}$, is inverted to yield the following multi-exponential decay model.

$$[c\text{-}C_6H_7] = C_1 e^{-\lambda_+ t} + C_2 e^{-\lambda_- t} + C_3 e^{-t/\tau} \tag{3.12}$$

where the constants, C_1 to C_3 are determined by the method outlined above. Alternatively, one could also use the method of undetermined coefficients to obtain the constants.

The complex analytical model is an elegant representation of the cyclohexadienyl reaction network: however, there are a number of assumptions made to allow for an analytical solution. It is not guaranteed that $k_{1.5}$ is much faster than $k_{-1.2a}$, which makes relying on the analytical model dangerous. These relationships need to be corroborated with a technique that does not need to make these assumptions.

3.4   Numerical models

The assumptions underpinning the complex analytical model are not certain and depend on certain experimental conditions. A more general model based on Table 3.1 requires a numer-

ical simulation of cyclohexadienyl kinetics. Simulations were performed using Matlab with the ODE23S stiff solver. Regular Runge-Kutta ODE solvers were not capable of handling the large differences in lengthscales within the model.

Figure 3-2: A reaction scheme that is consistent with the observed multi-exponential decay of cyclohexadienyl in cyclohexane. The measured data are sufficient to determine $k_{1.2} = k_{1.2a} + k_{1.2b}$, but cannot uniquely determine all 6 rate constants.
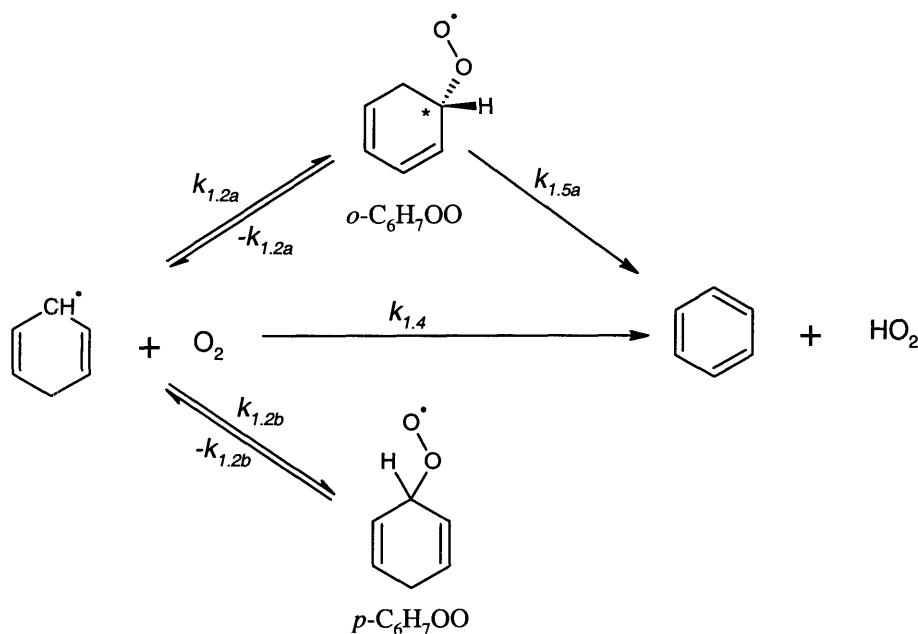
Using the values in Table 3.1, simulations adequately predicted the overall kinetics of the reactions, as shown in Figure 3-3 and Figure 3-4. These parameters were not adjusted to try to improve the fit, as there are not enough data to uniquely determine so many parameters.

Figure 3-3: Predictions of a numerical simulation of cyclohexadienyl chemistry at 298 K for p_{O_2} ranging from 0.05 to 0.25 atm. Lines represent simulation predictions, while points represent experimental data and their error bars for cyclohexadienyl decay at each oxygen concentration. At low oxygen partial pressures, the equilibrium concentrations of C_6H_7OO and c-C_6H_7 are comparable, resulting in a large, slowly-decaying baseline. Reactions used in the simulation and their rate constants are listed in Table 3.1.
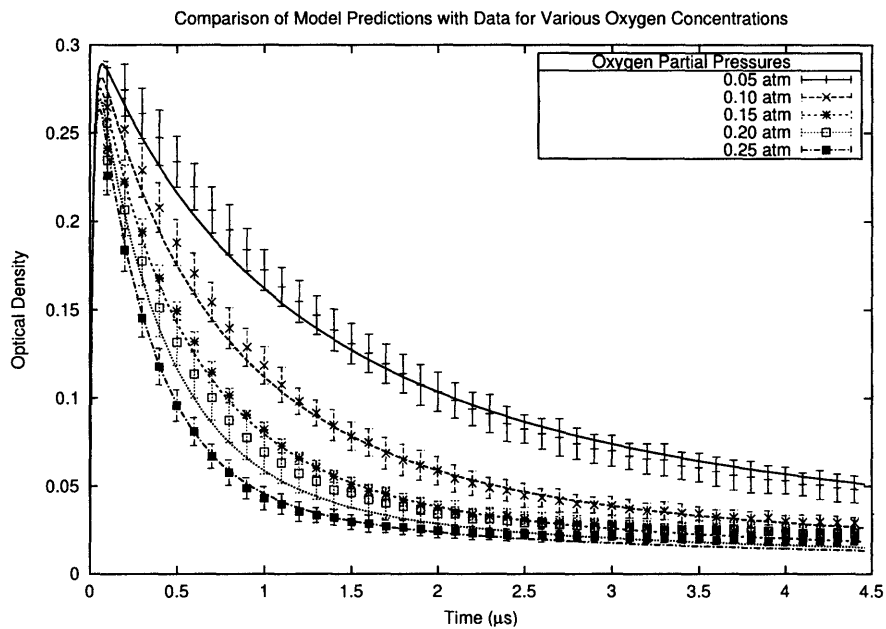
Figure 3-4: Predictions of a numerical simulation of cyclohexadienyl chemistry at 298 K for p_{O_2} ranging from 0.20 to 1.00 atm. Lines represent simulation predictions, while points represent experimental data and their error bars for cyclohexadienyl decay at each oxygen concentration. At high oxygen concentrations, the equilibrium shifts toward the products of Reaction 1.2, which have a smaller absorption on the order of 200 $M^{-1}cm^{-1}$. This interference is primarily responsible for the baseline absorbance at higher oxygen concentrations. Reactions used in the simulation and their rate constants are listed in Table 3.1.

Comparison of Model Predictions with Data for Various Oxygen Concentrations
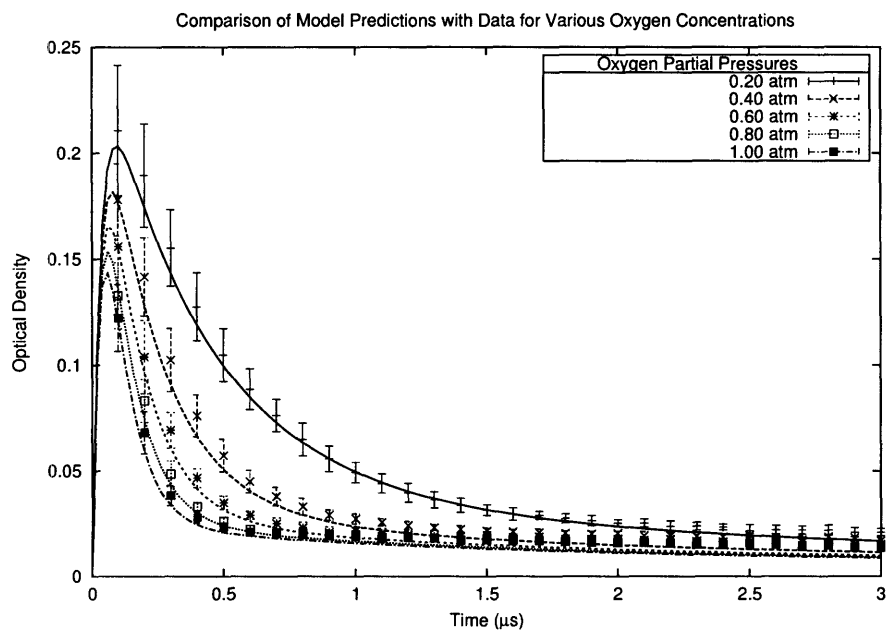
3.5 Discussion of model results and an explanation of the liquid and gas phase cyclohexadienyl oxidation rates

3.5.1 Comparison with previous liquid-phase experiments

Experimental data obtained in these experiments are comparable to other liquid-phase studies, which all conclude that Reaction 1.2 is diffusion-limited in their respective solvents. The current experiments determine the rate constant for Reaction 1.2 in cyclohexane (see Table 2.2).

In comparison to the values in Table 2.2, Maillard's rate constant[43] in benzene at 298 K was determined to be 1.67×10^9 $M^{-1}s^{-1}$. Multiplying Maillard's rate constant by the ratio of benzene / cyclohexane viscosities gives an expected rate constant of 1.1×10^9 $M^{-1}s^{-1}$, within the expected error bars of the corrected values in Table 2.2. Using the Stokes-Einstein relation between diffusivity and viscosity, the diffusion-limited rate constant in cyclohexane was calculated to be 1.5×10^9 $M^{-1}s^{-1}$ at 298 K, within 50% of the measured rate constants.

Hendry[28] proposed that the major products of the fast reaction of c-C_6H_7 and O_2 in the liquid-phase are benzene and HO_2. However, Pan[51] and Maillard[43] proposed that C_6H_7OO is the primary product of the reaction. Pan also observed that in aqueous solution, HO_2 generation was significantly slower than the cyclohexadienyl decay, implying an intermediate step. However, the most convincing evidence that C_6H_7OO is the main product in the liquid phase comes from thermodynamic data determined by Kranenburg et al. using photoacoustic calorimetry. Kranenburg determined in organic solvents, at microsecond timescales, that the decay of cyclohexadienyl radicals generated 12 kcal/mol of energy. This is consistent with the calculated enthalpy of Reaction 1.2, but much less than the 23 kcal/mol expected if the dominant products were HO_2 and C_6H_6. At this time-scale, Reaction 1.2 must dominate other pathways with greater heats of reaction.

3.5.2 Deviation from single exponential behavior and equilibrium

Single exponential decay models do not adequately fit the data as shown in Figure 2-7. Both the 316 nm and 556 nm bands exhibit the same multi-exponential decay with time, indicating that the signal must be attributable to the cyclohexadienyl radical itself or to another molecule in equilibrium with cyclohexadienyl on the sub-microsecond timescale, as opposed to interference by other molecules.

Based on these results and our thermochemistry calculations, we propose that Reactions 1.2 are in equilibrium under our reaction conditions.

$$c\text{-}C_6H_7 + O_2 \rightleftharpoons o\text{-}C_6H_7OO \tag{3.13a}$$

$$c\text{-}C_6H_7 + O_2 \rightleftharpoons p\text{-}C_6H_7OO \tag{3.13b}$$

A similar equilibrium has been proposed for hydroxycyclohexadienyl by von Sonntag.[75] A possible explanation for the oxygen-dependent multi-exponential decay could be the c-C_6H_7 radical coming into equilibrium with the corresponding peroxyl radicals, followed by a slower decay of the equilibrated radicals. The experimental data in cyclohexane suggests that Reaction 3.13 becomes equilibrated within 2-3 μs for $[O_2] > 2.5$ mM.

3.5.3 Experimental bounds on equilibrium 1.2

Our best information on the equilibrium constant for Reaction 1.2 in the gas phase comes from the calculations discussed in Section 3.2.3. However, experiments also allow bounds on K_c^o to be determined in solution. The experiments of Kranenburg et al.[39] prove that, at high oxygen concentrations, most of the c-C_6H_7 is converted into C_6H_7OO on a sub-microsecond timescale, bounding $K_c^o > 100$ in iso-octane and ethyl acetate. The present experiments provide tighter bounds on K_c^o in solution. The observation that c-C_6H_7 is quantitatively converted by reaction with O_2 even at sub-atmospheric concentrations of O_2 indicates that $K_c^o > 1 \times 10^3$.

As discussed above, we attribute the fast component of the bi-exponential decay to

Table 3.2: Comparison of inferred Reaction 1.2 and Reaction 1.3 equilibrium constants

Equilibrium Constants at 25°C	Reaction 1.2	Reaction 1.3
$K_p^{\,o}(1\,\text{atm})$	0.5	0.14 [a]
$K_c^{\,o}(1\text{M})$	2.1×10^3 [b]	2.5×10^3 [c]

[a] Bohn in 1999 , ref 12
[b] Cyclohexane Solvent, present work
[c] Pan, 1988 in Water, ref 51

equilibration of Reaction 1.2. With this interpretation of the data, the ratio of the amplitudes of the slow to the fast components of the multi-exponential in principle provides a direct measure of $K_c^o/[O_2]$. However, accurate measurement of this ratio is only feasible over a limited range, and there are several interferences and secondary reactions which need to be modeled in order to extract a value for K_c^o. From these bounds and the simulations at 298 K, we derive

$$2 \times 10^4 > K_c^o(1\,\text{M}, 298\,\text{K}) > 1 \times 10^3$$

The temperature dependence of $K_c^{\,o}$ derived by the fitting procedure over the range 0 to 50°C is consistent with the measured[39] and calculated values of $\Delta H = 12 - 13$ kcal/mole, but the kinetic data are not sufficient to determine ΔH more precisely. In other words, the data indicate that $k_{-1.2b} \approx 2 \times 10^5$ s^{-1} at 298 K, with an $E_a \approx 12$ kcal/mole. The corresponding $A \sim 10^{14}$ s^{-1} is in the range expected for a barrierless dissociation. The large A factor for the reverse reaction and the observation that Reaction 1.2 is diffusion-controlled even in low viscosity, weakly-interacting solvents at 273 K strongly suggest that Reaction 1.2 has no significant barrier in non-polar solvents. In the gas phase, however, several published quantum chemical calculations[2,25] and a recent study on hydroxycyclohexadienyl[27] report barriers to this reaction.

The calculations in Section 3.2.3 predict that 2 atm of O_2 are required to convert half of the gas phase $c\text{-}C_6H_7$ to C_6H_7OO at equilibrium, while a partial pressure of only 0.05 atm would suffice to achieve that condition in cyclohexane solution. This predicted two order

of magnitude variation between the behavior in solution and in the gas phase is consistent with all experimental data on Reaction 1.2 and similar to that observed experimentally for Reaction 1.3.[19,12] It is interesting to directly compare the literature equilibrium constants for Reaction 1.3 with our calculated values for Reaction 1.2, as shown in Table 3.2.

3.5.4 Subsequent reactions responsible for the overall decay of cyclohexadienyl at equilibrium conditions

At least two possible mechanisms exist that can explain the decay of c-C_6H_7 after Reactions 1.2 equilibrate. Pan et al. have proposed that the product of Reaction 1.2a, o-C_6H_7OO, decomposes irreversibly through Reaction 1.5a. Reaction 1.5b is expected to be much slower, and can be neglected in this model. Berho and Lesclaux,[8] and more recently Estupiñán[17] proposed Reaction 1.4, the direct abstraction of a hydrogen from cyclohexadienyl, as the dominant loss channel in the gas phase. Both these potential pathways are shown in Figure 3-2.

Analysis of the overall decay in the gas phase

Using the calculated equilibria determined in Section 3.2.3 for Reactions 1.2a and 1.2b, reported gas phase experiments[17,8] operate in a regime where the equilibria strongly favor c-C_6H_7 over C_6H_7OO. Thus, only a negligible amount of c-C_6H_7 is consumed before equilibrium is reached. The observed experimental decay of c-C_6H_7 to C_6H_6 and HO_2 ($k_{exp} = 8.4 \times 10^7 e^{(-0.6\,\text{kcal}/RT)}$ $M^{-1}s^{-1}$) must primarily be due to either Reaction 1.4 and/or Reaction 1.5a.

Using the quasi-steady-state approximation on the peroxyl radical intermediates allows the determination of a rate-law for the gas phase, as shown in Equation 3.14:

$$\frac{d[c\text{-}C_6H_7]}{dt} = \left(\frac{k_{-1.2a}k_{1.2a}}{k_{-1.2a} + k_{1.5a}} - (k_{1.2a} + k_{1.4}) \right) [c\text{-}C_6H_7][O_2] \qquad (3.14)$$

Several direct conclusions can be made using Equation 3.14. First, the decay in the gas phase cannot be due to $k_{1.2a}$ alone. In order for this to be true, $k_{1.5a} \gg k_{-1.2a}$, such that

63

$k_{exp} \sim k_{1.2a}$. However, for $k_{1.2a}$ to be the primary loss channel, the reaction rate would have to decrease by two orders of magnitude from the liquid phase to the gas phase. The observed small activation energy of 0.6 kcal/mol is inconsistent with such a large change in reaction rate.

Second, if, on the other hand, $k_{-1.2a} \gg k_{1.5a}$, then the direct abstraction of hydrogen (Reaction 1.4) is the primary pathway in the gas phase, as stated by Estupiñán et al.[17] The low value of the rate constant coupled with the small activation barrier is unusual for H-abstraction, but this reaction is atypical in many respects.

However, a final possibility exists: Pan argues that peroxyl rearrangement to form benzene and HO_2 (1.5a) dominates the direct abstraction pathway (1.4), but not the equilibrium back Reaction (-1.2a). The observed decay could then be explained by equilibrium 1.2 in combination with the decomposition of o-C_6H_7OO.

$$\frac{d[c\text{-}C_6H_7]}{dt} = -\left(\frac{k_{1.2a}k_{1.5a}}{k_{-1.2a} + k_{1.5a}}\right)[c\text{-}C_6H_7][O_2] \qquad (3.15)$$

The weak temperature dependence would in this case be due to the overall decay being a combination of the exothermic equilibrium 1.2a and the endothermic Reaction 1.5a. Of course, it is also possible that both Reactions 1.5a and 1.4 contribute comparably to the overall decay, and that this combination would also exhibit little temperature dependence. The available experimental data are currently not sufficient to determine whether Reaction 1.4 or Reaction 1.5a is dominant in the gas phase. Since the dominant reaction pathway is in doubt, we recommend the use of Equation 3.14, which allows for both channels in interpreting experimental data.

Analysis of the overall decay in the liquid phase

Unfortunately, on the short timescale of the liquid-phase experiments, the steady-state approximation cannot be applied to the peroxyl intermediates, significantly complicating the interpretation of the data. However, a perturbation analysis of the cyclohexadienyl kinetic model in Figure 3-2 does provide analytical approximations for the eigenvalues of the system.

The following parameters correspond to the calculated zeroth and first-order terms of the eigenvalues, where the small parameters were defined as $k_{1.4}/k_{-1.2b}$ and $k_{1.5a}/k_{-1.2b}$. Details of the derivation are included in a Maple input file in Appendix B.

$$\lambda_1 = -k_{-1.2a} - (k_{1.2a} + k_{1.2b})[O_2] - \frac{k_{1.4}(K_{1.2a} + K_{1.2b})[O_2]^2}{(1 + (K_{1.2a} + K_{1.2b})[O_2])} - \frac{2k_{1.5a}}{3(1 + (K_{1.2a} + K_{1.2b})[O_2])}$$

$$\sim -(k_{1.2a} + k_{1.2b} + k_{1.4})[O_2] \tag{3.16}$$

$$\lambda_2 = -\left(k_{-1.2a} + \frac{k_{1.5a}K_{1.2b}}{K_{1.2a} + K_{1.2b}}\right)$$

$$\sim -\left(k_{-1.2a} + \frac{k_{1.5a}}{3}\right) \tag{3.17}$$

$$\lambda_3 = -\left(\frac{(k_{1.4} + k_{1.5a}K_{1.2a})[O_2]}{1 + (K_{1.2a} + K_{1.2b})[O_2]}\right)$$

$$\sim -\frac{2k_{1.5a}}{3} \tag{3.18}$$

The approximations are valid when $k_{1.2b}[O_2] \gg 1$, and assume $k_{1.2a} \approx 2k_{1.2b}$. Also, the approximation for λ_3 requires that $k_{1.5a}K_{1.2a} \gg k_{1.4}$. The fast component of c-C_6H_7 decay observed in solution is dominated by the title reaction. However, several other effects compete in addition to the effects of convolution with the time constant of the decay of t-butoxyl in the formation of c-C_6H_7 discussed in Section 2.4.

Once Reactions 1.2a and 1.2b reach equilibrium, the observed cyclohexadienyl decay occurs with time constants corresponding to $1/\lambda_2$ and $1/\lambda_3$, which both are functions of $k_{1.5a}$. Note that λ_3 is similar, but not identical to Equation 3.14; both agree that Reaction 1.4 is favored if $k_{1.2b}[O_2]$ is small, while Pathway 1.5a is favored if $k_{1.2b}[O_2]$ is large. The temperature dependence in the slow component of cyclohexadienyl decay, shown in Figure 2-5, thus depends mainly on the interplay between the back reaction, Reaction -1.2a, and the reactions which lead to HO_2 and C_6H_6, Reactions 1.4 and 1.5a. The large increase in the slow component decay observed between 298 K and 323 K would be consistent with an emergence of $\lambda_2 \sim -k_{-1.2a}$, since Reaction -1.2a is expected to have a high activation barrier. The difficulties with determining the relationship between the measured time constants of

the c-C_6H_7 decay in the presence of oxygen, and the underlying elementary steps, suggest that theoretical estimates of the rate constants, not just the thermochemistry, are necessary to understand this system in detail.

Estimates for rate constants

Reactions 1.2 and 1.4

All solution-phase experiments agree that the reaction of the cyclohexadienyl radical with oxygen is diffusion-limited. The experiments performed in this work determine this rate constant to be $\approx 1.2 \times 10^9$ $M^{-1}s^{-1}$. Due to the statistical factor associated with the *ortho* and *para* forms, we expect $k_{1.2a} \approx 2k_{1.2b}$, making $k_{1.2a} \approx 8 \times 10^8$ $M^{-1}s^{-1}$ and $k_{1.2b} \approx 4 \times 10^8$ $M^{-1}s^{-1}$. Using the computed K_c, we infer $k_{-1.2a}$ (for each enantiomer) and $k_{-1.2b}$ to range from 0.4 to 8×10^5 s^{-1} at 298 K. The rate constant $k_{1.4}$ must be less than 3×10^8 $M^{-1}s^{-1}$ in solution to be consistent with Kranenburg's calorimetry data and our calculated thermochemistry, taking error bars into account. The fact that Reactions 1.2a and 1.2b appear to be diffusion-controlled indicates that the intrinsic chemistry rates are faster than the diffusion rate. In the gas phase, A factors for R + O_2 reactions are normally in the range of 10^9 to 10^{10} $M^{-1}s^{-1}$; if $k_{1.2}$ has a similar A factor, yet $k_{intrinsic} > k_{diffusion} \approx 1 \times 10^9$ $M^{-1}s^{-1}$ at $T = 0^\circ C$ we can infer that $E_a < 1.3$ kcal/mol (in solution). There is likely some solvent effect on the E_a for Reaction 1.2 similar to that on the product C_6H_7OO, which could increase the barrier in the gas phase. However, the fact that the analogous allyl radical reaction with O_2 in the gas phase at room temperature is known to be quite fast $(3.6 \times 10^8$ $M^{-1}s^{-1})$[33] suggests the true gas-phase E_a for Reaction 1.2 is 2 kcal/mol or less. Some quantum calculations reported in the literature show high barriers to Reactions 1.2 and 1.3. However, long-distance floppy transition states that involve considerable changes in electronic structure are extremely difficult to compute accurately. The more plausible hypothesis can be based on experimental analogy with allyl radical and the fact that this reaction runs at the diffusion-limited rate even in weakly-interacting non-polar solvents.

Little is known theoretically regarding Reaction 1.4, which is much more exothermic

than typical H-abstractions by O_2. The floppy bi-radical transition state is expected to be extremely difficult to calculate accurately with available quantum chemistry techniques. Normal A factors for H-abstractions and radical-radical disproportionations are typically $\sim 10^9$ $M^{-1}s^{-1}$. If Reaction 1.4 has an A factor in this range, $k_{1.4} < 3 \times 10^7$ $M^{-1}s^{-1}$ in the gas phase would imply $E_a > 2.3$ kcal/mol in the gas phase, comparable with barriers seen in comparably exothermic H-abstractions by OH. Less is known about the barrier to Reaction 1.4 in solution phase; if we again assume $A_{1.4} \sim 10^9$ $M^{-1}s^{-1}$, we infer that $E_a > 0.6$ kcal/mol in order to be consistent with the experimental upper bound on $k_{1.4}$.

Reactions 1.5a and 1.5b

Almost nothing is known for certain about Reactions 1.5. The A factor for Reaction 1.5a is probably similar to the 5×10^{11} s^{-1} A factor for the analogous reaction

$$C_2H_5OO \rightleftharpoons C_2H_4 + HO_2 \tag{3.19}$$

which has been thoroughly studied experimentally[36] and theoretically.[57,48] However, the barrier height is certainly very different, since the thermochemistry of Reaction 3.19 is dramatically different than that for Reaction 1.5a. An upper bound on $k_{1.5a}$ can be determined, however, using Equation 3.15 and the calculated value for the equilibrium constant, $K_{1.2a}$. This bounds $k_{1.5a}$ and $k_{1.5b} < 1 \times 10^6$ s^{-1} in the gas phase at $T = 298$ K, and they must be even less if there is competition with $k_{1.4}$.

3.6 An experiment to resolve the discrepancy

The models proposed provide a framework for resolving the discrepancy between the gas and liquid phase cyclohexadienyl oxidation rates. However, knowing the rate of cyclohexadienyl decay with time is not enough to determine the rates of Reactions 1.5a and 1.4 or to prove that an equilibrium exists. Is there an experiment that could prove the equilibrium exists and resolve theses rates?

Two possible experiments exist that could determine these rates. The first involves trying to observe the fast reactions, Reactions 1.2. Observing these reactions requires increasing the partial pressure of oxygen in the gas phase such that appreciable amounts of o-C_6H_7OO and p-C_6H_7OO are formed. Based on our calculations, a $p_{O_2} = 2$ atm is required to achieve equal amounts of c-C_6H_7 and C_6H_7OO in the gas phase. Unfortunately, this means that the time constant for the fast reaction is on the order of

$$\frac{1}{k_{1.2}[O_2]} = \frac{1}{(1.2 \times 10^9)(0.082)} = 1 \times 10^{-8} s$$

or 10 ns. Since the excimer pulse itself is on the order of the time-constant it would be difficult to accurately measure the rate. However, using this method one could disprove Berho and Lesclaux's rate, since

$$\frac{1}{k_{1.2}[O_2]} = \frac{1}{(4 \times 10^7)(0.082)} = 3 \times 10^{-7} s$$

any verifiable rate greater than 300 ns would show their measurement to be in error.

The other experiment would be able to resolve all the rates, by simultaneously measuring the concentrations of c-C_6H_7 and HO_2 or c-C_6H_7 and benzene. This experiment would require either a product study to quantify the number of benzene molecules formed or would require monitoring two distinct wavelengths simultaneously to capture the formation of HO_2. Benzene is a natural contaminant of 1,4-C_6H_8 so in order to perform a product study the 1,4-C_6H_8 would have to be purified to levels where the benzene product could be reliably detected. HO_2 measurement would require another source of light in the infrared or at 280 nm in the UV. Either experiment would be difficult and would require a large amount of control over the laser power, chemical concentrations, and pressure. An interesting possibility would be the detection of c-C_6H_7 by UV absorption coupled with the detection of HO_2 by microwave absorption.

Several experiments were performed in the gas phase on c-C_6H_7 and the preliminary results are shown in Chapter 5.

3.7 Conclusions

1. In contrast to previous reports, cyclohexadienyl radical decay is not a single exponential decay. The multi-exponential decay is due to equilibration of Reaction 1.2, followed by slow decay of the equilibrated system.

2. The equilibrium constant of Reaction 1.2 has been computed. Under low oxygen concentrations, the computed value favors the reactants in most gas-phase experiments. In contrast, at the higher oxygen concentrations of liquid-phase experiments, equilibrium favors the products, in part due to solvation effects.

3. Gas phase experiments measure the rate of a process other than Reaction 1.2. We propose these experiments actually measure the combination of rate constants shown in Equation 3.14. If Reactions 1.2 or 1.5a are negligible in gas phase then Reaction 1.4, as proposed by Estupiñán,[17] is the dominant pathway. Available data are insufficient to determine the primary peroxyl decay channel.

Chapter 4

Global optimization of rate parameters

"Premature optimization is the root of all evil." – Donald E. Knuth

4.1 Summary

In Chapter 3 analytical and numerical models were presented which had several unknown constants. These constants could be determined using the available data through regression. However, most of these models were nonlinear with respect to the constants, requiring techniques which do not guarantee optimum fits. In fact, due to noise or other artifacts in the data, many of these nonlinear fits failed to determine physically meaningful parameters. These numerical difficulties led to a search for a method to guarantee an optimum solution to a nonlinear fit. The method found, global dynamic optimization or GDOC, was developed by Adam Singer and Paul Barton in 2004.[62]

In this chapter, we present the first application of this method to a least-squares (χ^2) fit of experimental data by a nonlinear kinetic model. Several important advantages of knowing with certainty the best possible fit rather than a locally optimum fit are discussed and demonstrated using data from the experiments in Chapter 2. This is particularly important

for c-C_6H_7 since many chemical mechanisms are possible and it is important to determine which models are inconsistent with the experimental results. With GDOC, one can rigorously demonstrate that a nonlinear kinetic model with several adjustable rate parameters is inconsistent with measured experimental data. The numerical method presented is a valuable tool in evaluating the validity of a complex kinetics model.

4.2 Introduction

Kineticists frequently desire to validate or disprove a proposed chemical reaction network by comparing it with experimental data. Models for chemical kinetics experiments are usually systems of nonlinear ordinary differential equations (ODEs) with several unknown adjustable parameters, p, posed as an initial value problem as shown in Equation 4.1.

$$\frac{\mathrm{d}x}{\mathrm{d}t} = f(t, x, q, p), \quad x(t_0) = x^0(p) \tag{4.1}$$

where the vector of state variables, x, usually includes time-dependent species concentrations or mass-fractions and might also include other quantities like temperature or density if they are time-varying during the experiment. The vector q represents values that are constant throughout the process, such as rate constants for an isothermal system at atmospheric pressure. There are often dozens of numerical parameters q and x^0; here we assume that most of these parameters are well-established and can be safely held fixed, but that some of them are significantly uncertain and should be adjusted to improve the agreement between the model and the experiment.

Generally, the adjustable parameter vector, p, includes several unknown rate constants but could also include unknown molecular properties or initial conditions or both. Examples of uncertain initial conditions that could be adjusted to obtain a better fit are the temperature in a shock tube or the initial concentration of radicals formed in a flash photolysis experiment.

Once a kinetics model is formulated, the first question a kineticist asks is whether or not

the model is consistent with experimental data. In other words, are there any physically reasonable values of p that would allow the kinetic model to match the data within its limits of uncertainty? The usual approach to try to answer this question is to vary p within a physically reasonable range to try to minimize the $\chi^2(p)$ defined in Equation 4.2,

$$\chi^2(p) = \sum_{i=1}^{N_{data}} \left(\frac{d_i - m_i(p)}{\sigma_i} \right)^2 \tag{4.2}$$

where d is the vector of data, m is the vector of model predictions, and σ is the vector of standard deviations. The value for d_i is the average over j replicate measurements, d_{ij}, such that $d_i = (1/N_{replicates}) \sum_j d_{ij}$. The standard deviation used here is the unbiased indicator associated with the χ^2 distribution.

$$\sigma_i = \left(\sqrt{\frac{1}{N_{replicates} - 1} \sum_{j=1}^{N_{replicates}} (d_{ij} - d_i)^2} \right) \tag{4.3}$$

The model prediction , $m_i(p)$, is usually a simple linear function of the state variables at the time, t_i, where the corresponding data point, d_i, was measured, i.e. $m_i(x(t_i))$, where $x(t_i)$ is the solution of Equation 4.1 for the specified choice of p.

An important value in the χ^2 distribution is the number of degrees of freedom in the system, ν, defined as the number of data points minus the number of adjustable parameters.

$$\nu = N_{data} - N_{parameters} \tag{4.4}$$

For the large values of ν typical in kinetics, the χ^2 distribution is sharply peaked near its expectation value, $\langle \chi^2 \rangle = \nu$. If the model and the data are consistent, we expect that Equation 4.2 will give a $\chi^2 \sim \nu$; if it gives a value significantly larger than ν, it is unlikely that the data and the model are consistent. If the model is correct, the probability that a data set would have a weighted sum of squares value greater than χ^2 is given by Equation

$$Pr(\chi^2) = \int_{\chi^2}^{\infty} \frac{t^{\nu/2-1}e^{-t/2}}{2^{\nu/2}\Gamma(\frac{\nu}{2})}dt = \frac{\Gamma\left(\frac{\nu}{2},\frac{\chi^2}{2}\right)}{\Gamma\left(\frac{\nu}{2}\right)} \tag{4.5}$$

The Pr-value is the measure of likelihood that the data is consistent with the specified model, given the specified error, σ_i. The implicit assumptions associated with using this measure are that the model structure and all the numbers in the model are exactly correct and all the deviations between d_i and $m_i(\boldsymbol{p})$ are due to normally distributed random errors. If we measure data, $\boldsymbol{d}$, that yield $Pr(\chi^2) > 0.75$ we have a lot of confidence that the data is consistent with the model, but if $Pr(\chi^2) < 0.25$ the data and the model are likely inconsistent. Intermediate values of Pr suggest that there would be value in repeating the experiment in order to reach an unambiguous conclusion.

If we could show that the Pr-value is small, or correspondingly that $\chi^2(\boldsymbol{p})$ is large for *all* physically reasonable values of the adjustable parameters $\boldsymbol{p}$, then we could say the model is inconsistent with the data, or equivalently that the data disproves the model. The most obvious way to do this would be to find the lowest possible $\chi^2(\boldsymbol{p})$ over the entire physically reasonable range of parameters. This can be accomplished by using an optimization algorithm to find the minimum of the $\chi^2(\boldsymbol{p})$.

Many algorithms exist for finding the minimum of objective functions like χ^2. One of the best of these algorithms is the Levenberg-Marquardt (LM)[42,44] method. However, all of these methods have difficulty relating kinetic data to nonlinear chemical kinetic models for several reasons:

1. Usually several of the unknown parameters are correlated, i.e. the $\chi^2(\boldsymbol{p})$ surface is typically very flat in some regions of $\boldsymbol{p}$ space, and in these regions its Hessian is near-singular making it difficult for many methods to identify a minimum.

2. Experimental data often contain noise, which roughens the objective function surface. These rough patches can trap an optimization algorithm into a local minimum. That minimum, however, may not be the global minimum of $\chi^2(\boldsymbol{p})$ over the whole parameter

space.

Until recently, it was impossible to determine if the minimum obtained from optimizing this class of problems was a local minimum or the global minimum. In many situations, despite the numerical problems, kineticists would nonetheless be able to find a set of parameters that made the model consistent with experimental data, i.e. Pr > 0.75, and immediately turn to determining the range of parameters that give good fits, i.e. the uncertainties in the parameter values, as discussed extensively in the literature.[29,55,23,22]

However, a kineticist that could not find a parameter set which made the model consistent with experimental data would be left in a quandary. Is the model an incorrect description of the chemistry or did I just not find the correct set of fitting parameters?

Here we present the first numerical method which allows one to find the global minimum of $\chi^2(p)$ for nonlinear ODE IVP models that do not have analytical solutions, and so conclusively determine whether a proposed kinetic model is inconsistent with a set of experimental data. The method is demonstrated using data and a kinetic model drawn from a recent study[72] of the reaction of cyclohexadienyl radical with oxygen.

Being able to reliably identify global optima would be useful in many problems that arise in physical chemistry. Because good numerical methods for global optimization of nonconvex problems were not available, the most common approach has been to restrict oneself to models which yield convex (often linear) optimization problems, or to approximate the objective function with a convex response surface, so that there was only one minimum to be found.[23,22,10] This is probably one of the main reasons that "textbook" models which lead to linear least-squares optimizations are so popular. Unfortunately, many chemical systems are in reality nonlinear and nonconvex, so that approximations are required to make the resulting optimization problems convex, and it can be difficult to bound the errors introduced by these approximations. A popular approach which does not approximate the model or the objective function is multistart, a stochastic method where a large number of local optimizations are performed from various initial guesses, in the hope that at least one of them will hit the global optimum.[74] In practice, multistart and the convex approximation

methods are effective ways to find good fits for cases where the model and the data are consistent. However, none of these methods are guaranteed to find the best fit and, therefore, cannot disprove a model with confidence.

Several global optimization methods exist for solving chemical engineering and kinetics problems.[20,1] However these methods require an explicit nonconvex algebraic model,[20,1] and cannot solve problems that can only be expressed as a system of differential equations. Here we present the first method suitable for the common situation where the objective function is only known implicitly, through the numerical solution of a system of differential equations.

4.3   Theory and implementation

A simple example of local and global minima is shown in Figure 4-1. For an objective function that is convex only one minimum exists, and that minimum is the global minimum. Most kinetic models, however, lead to nonconvex least-squares problems, or, as Figure 4-1 shows, problems containing a concave and a convex portion. When an objective function contains both concave and convex regions, multiple local minima can exist.

The first algorithm guaranteed to find the global minimum was created in the late 1960's by Falk and Soland,[18] and is called branch and bound. What branch and bound does is to subdivide the region containing the minima into two separate regions. The algorithm then determines an upper and lower bound on the minima for each region. For example, in Figure 4-2, if the upper bound on the minimum of the objective function (bold curve) in region B is lower than the lower bound on the objective function in region A, then region A is rejected because it cannot contain the global minimum. Region B is then divided and the process repeated, narrowing in on the region in p space where the global minimum lies. Subdivision and evaluation of the upper and lower bounds continue until the bounds converge to within a specified tolerance on the global minimum.

For this algorithm to work, one must be able to determine upper and lower bounds on the minimum in any subregion, and the bounds must tighten as the region is subdivided. Determining an upper bound on the global minimum is easy: choose any point p_{guess} in

Figure 4-1: A simple example of a convex and nonconvex function. Convex functions have only one minimum, while nonconvex functions can have more than one minimum.[62]
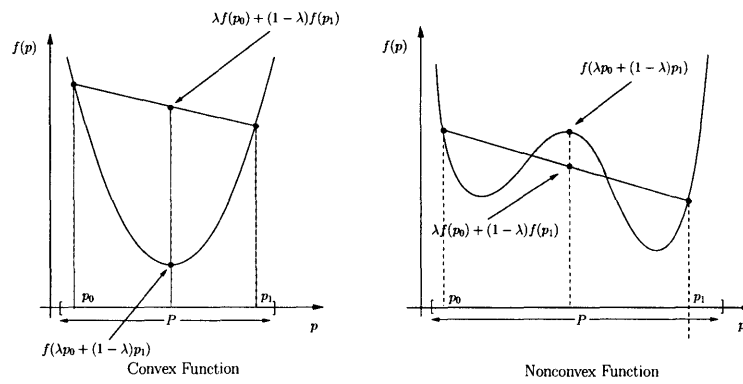
Figure 4-2: An example of a convex relaxation of a nonconvex function. The large parabola represents the first convex lower bound of the function. The region is then bisected at the convex minimum to form regions A and B. The relaxation is repeated to find new lower bounds for each region. By finding a point p in region B where $f(p)$ is less than the convex lower bound for region A, one can show that the global minimum cannot exist in region A. Region A can now be discarded from the search.
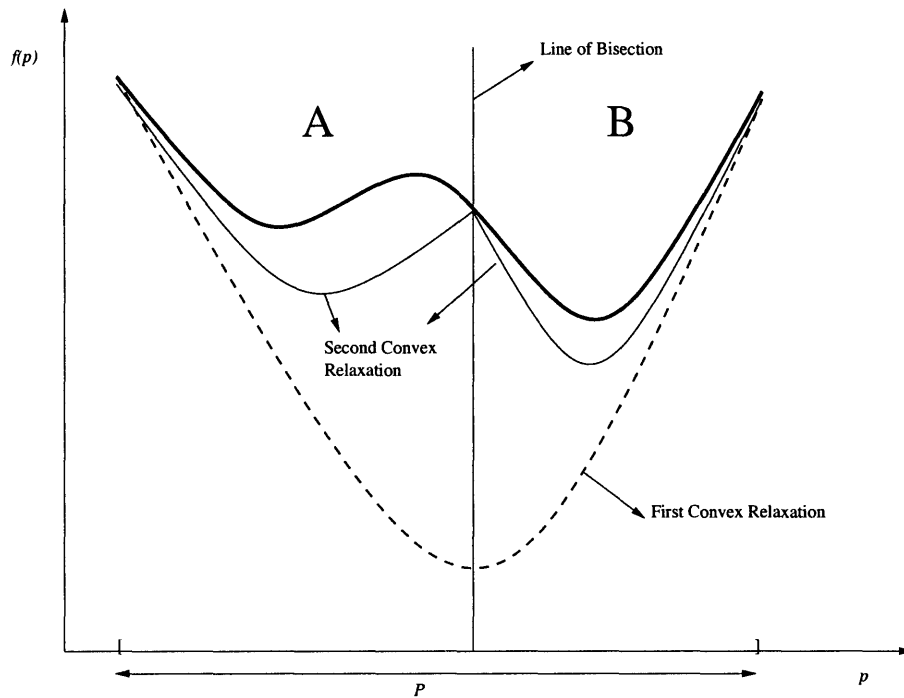
the range, then $\chi^2(p_{guess})$ is an upper bound on the minimum of $\chi^2(p)$. A tighter upper bound can found by performing a standard optimization starting from p_{guess} to find a local minimum. Unfortunately, it is much more difficult to determine provable lower bounds that tighten appropriately as the region is subdivided. Performing a local optimization does not guarantee a lower bound since the region may contain more than one local minimum.

The success of the new algorithm used here comes from its ability to construct convex relaxations to $\chi^2(p)$ in any specified subregion, Figure 4-2. A convex relaxation, $c(p)$, is a curve that is convex and underestimates the objective function at all points:

$$c(p) \leq \chi^2(p), \forall p \in [p_0, p_1] \tag{4.6}$$

Because $c(p)$ is convex, if you find a minimum at p_{min} it is guaranteed to be the global minimum of c:

$$c(p_{min}) \leq c(p), \forall p \in [p_0, p_1] \tag{4.7}$$

Combining the two,

$$c(p_{min}) \leq \chi^2(p), \forall p \in [p_0, p_1] \tag{4.8}$$

Thus, the minimum of the relaxation is a rigorous lower bound, which can be used in the branch and bound algorithm.

The hard part is to construct $c(p)$ so that it is guaranteed to be a convex relaxation of $\chi^2(p)$, even though $\chi^2(p)$ is only known implicitly as the solution of a system of nonlinear ODEs. Here we give a brief synopsis of how this is done. All the details, with proofs, are given in References 62 and 65, 66, 64. Information on global optimization in general can be found in the excellent book by Horst and Tuy.[31]

The procedure for constructing rigorous convex relaxations for problems with nonlinear ODEs embedded involves a sequence of bounding operations. First, bounds are placed on adjustable parameters p. If physical bounds for the state variable values, x are known, they

are also included to ensure the relaxation remains finite. A subtle, but theoretically crucial difference exists between the bounds placed on p and those placed on x. The bounds on p can be arbitrarily chosen to restrict the search domain of the adjustable parameters. However, the bounds on x cannot be arbitrary. The additional bounds placed on the state variables must represent a superset of any possible values that x may take; such bounds are often derived from physical insight and are often simple constants. From the bounds on p (and x if available), two sets of differential equations are derived. The first set of equations relax a special optimization problem on the right hand side (RHS) of Equation 4.1 (often via interval arithmetic); these equations yield rigorous bounds on x that converge to x as the search space is refined. The second set of differential equations derives from generating convex and concave relaxations of the RHS of Equation 4.1 on the space defined by the bounds on p and the solution of the first set of differential equations bounding x. Because this space is a subset of $\mathbb{R}^n$ for fixed points in time, any consistent convex bounding operation, such as the method of McCormick,[45] may be employed. Given the initial conditions x^0, integration of these two coupled sets of differential equations yields convex relaxations for the original differential equation. Singer and Barton[66] have shown that as the bounding set on p converges to a single point p^*, the convex relaxations derived utilizing this method converge to $f(x, p^*)$.

In order to numerically solve the global optimization problem for $\chi^2(p)$, an in-house software package, GDOC (Global Dynamic Optimization Collection), was written. The global optimizer for $\chi^2(p)$ consists of many distinct parts: a branch and bound algorithm, a local optimizer, a numerical integrator, software for constructing the convex relaxations, and a residual evaluator, which is used to evaluate the right-hand sides (RHS) of the ODEs. The branch and bound performed on the Euclidean space of the parameters is done using an in-house branch and bound library, libBandB version 3.2.[63] Local optimization is performed using NPSOL version 5.0.[26] NPSOL is a proprietary package and does not come with the GDOC distribution; instead SLSQP, a free optimization code is included. Numerical integration is performed using an extended discontinuity-locked version of CVODES,[30] which

is discussed in Reference 62. Residual evaluation is performed via code generated by the compiler component of the GDOC package.[62] Together, these components form the global dynamic optimization code (GDOC) used in this work. In order to solve parameter estimation problems, the end user needs only to define a problem in the GDOC input language, which the GDOC package then parses.

The GDOC global optimization package and the example cases are available for download over the Internet at http://yoric.mit.edu/gdoc/. All of the details, including information on obtaining key numerical packages such as NPSOL and CVODES, which are neither developed nor distributed by the authors, are explained at http://yoric.mit.edu/gdoc/#HowCanIGetIt. The algorithm appears to scale as a low power of the number of state variables but scales exponentially with the number of adjustable parameters. Hence even models involving large reaction mechanisms with many reacting species can be handled, but only a relatively small number of parameters can be optimized simultaneously.

4.4 Case study: transient absorption experiments and model

GDOC was applied to the numerical model studied extensively in Chapter 3. Two data traces measured at 298 K and 323 K were used to provide data for the fits. For details on how the data was produced see Chapter 2.

The first data trace, Figure 4-3, was measured after photolyzing a solution at 298 K containing 0.4 M 1,4-cyclohexadiene and 0.1 M di-tert-butyl peroxide in equilibrium with 0.2 bar O_2 and 0.8 bar Ar. The second data trace, Figure 4-4, was measured under identical conditions but at 323 K. The measured absorbance, d, is modeled using Equation 4.9

$$m_i = (\epsilon_{c\text{-}C_6H_7}[c\text{-}C_6H_7](t_i) + \epsilon_{ortho}[o\text{-}C_6H_7OO](t_i) + \epsilon_{para}[p\text{-}C_6H_7OO](t_i))\ell \qquad (4.9)$$

The spectrometer averages 30 individual laser shots then sends the data set to the computer. Equation 4.2 treats each of these data points as if they are single shots and not the

Figure 4-3: Globally and locally optimal fits to c-C_6H_7 absorption at 298 K with three adjustable parameters. Error bars shown are $\pm\sigma_i$ and, for clarity, only every fifth data point is shown. The local optimum ($\chi^2 = 500$) is not significant at the 25% confidence level, while the global optimum ($\chi^2 = 128$) is consistent with the data (>99% confidence). The GDOC program found a global solution for the three parameter fit which shows the numerical model to be statistically significant.
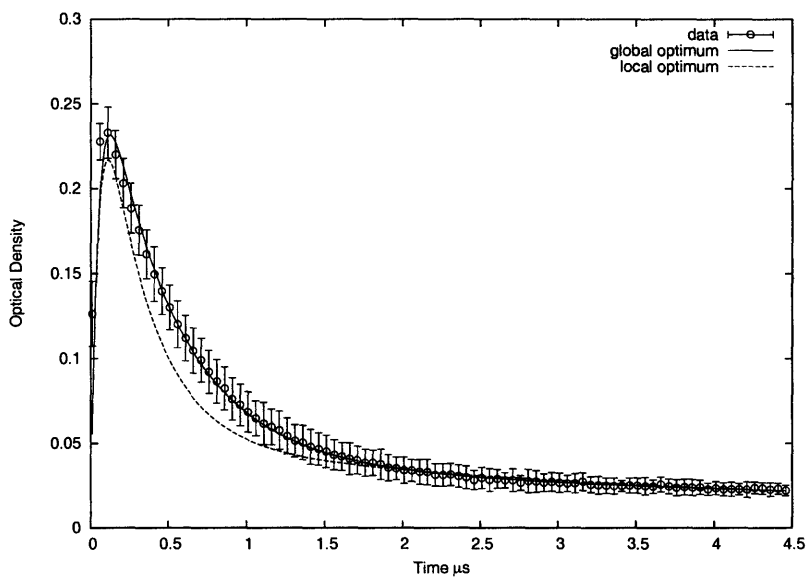
Figure 4-4: Globally and locally optimal solutions to a fit of c-C$_6$H$_7$ absorption at 323 K with three adjustable parameters. Error bars shown are $\pm\sigma_i$ and, for clarity, only every fifth data point is shown. The local optimum ($\chi^2 = 500$) corresponds to a 5% level of confidence in the model fit, while the global optimum ($\chi^2 = 476$) corresponds to only a 16% level of confidence. Since the GDOC program was unable to find a global optimum with a level of confidence greater than the cutoff of 25%, we can reject the model as fitting the data. There are no sets of parameters which will improve the fit.
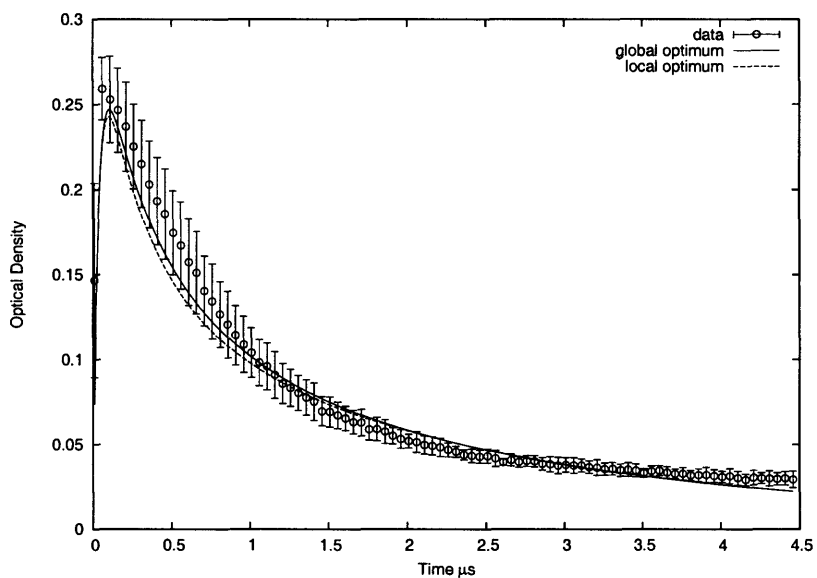
result of 30 replicates. The means of the data are, thus, well-determined and the standard deviations are slightly overestimated by this procedure.

The mechanism we are trying to disprove with the data is shown in Table 4.1. In this proposed mechanism, Reactions 2.2, 1.5a, and R were assumed to be irreversible, while Reactions 1.2b and 1.2a were treated as reversible. In the fits, the rate constants were constrained to lie within a physically reasonable range.

There are too many parameters in the model to determine them all from one or even several transient absorption data traces. Most parameters were fixed based on prior literature information or on the calculations in Chapter 3, as shown in Tables 4.1 and 4.2. For example, the rate constants for Reactions 2.2 and R were taken from the literature,[16,3] and the reverse rate constants for Reactions 1.2b and 1.2a were set using equilibrium constants computed in Section 3.2.3. The values for ϵ, ℓ, and the initial concentration of $1,4\text{-}C_6H_8$ were measured, and the published[69] Henry's law coefficient for O_2 along with controlled flowrates were used to determine O_2 concentration.[72,71] In this model it is assumed that the only radical formed by the laser flash is $(CH_3)_3CO$, i.e. $[c\text{-}C_6H_7]_0 = [C_6H_7OO]_0 = [HO_2]_0 = 0$. The concentration of $(CH_3)_3CO$ was determined using the known absorption cross-section of $DTBP$[6] and a measurement of the UV light power density exiting the reaction cell. This left three adjustable parameters to be determined in the least-squares fitting procedure: $k_{1.2b}$, $k_{1.2a}$, and $k_{1.5a}$. The dynamic model has 6 important state variables: $[c\text{-}C_6H_7]$, $[o\text{-}C_6H_7OO]$, $[p\text{-}C_6H_7OO]$, $[(CH_3)_3CO]$, $[O_2]$, and $[c\text{-}C_6H_7]$; these are the components of $x(t)$.

The estimates for the variation in the data were taken by comparing three different

Table 4.1: Proposed kinetic model. $k_{2.2}$ and k_R were fixed; $k_{1.2b}$, $k_{1.2a}$, and $k_{1.5a}$ were adjusted to fit the data within the stated bounds.

#	Reaction	k_{298} $[M^{-1}\mu s^{-1}$ or $\mu s^{-1}]$
2.2	$(CH_3)_3CO + 1,4\text{-}C_6H_8 \rightarrow c\text{-}C_6H_7 + (CH_3)_3COH$	53
1.2b	$c\text{-}C_6H_7 + O_2 \rightleftharpoons p\text{-}C_6H_7OO$	[1, 1200]
1.2a	$c\text{-}C_6H_7 + O_2 \rightleftharpoons o\text{-}C_6H_7OO$	[1, 1200]
1.5a	$o\text{-}C_6H_7OO \rightarrow C_6H_6 + HO_2$	[0.001, 100]
R	$2\,c\text{-}C_6H_7 \rightarrow$ Products	1200

experimental runs taken under identical conditions for each temperature. The average and standard deviations (Equation 4.3) were used to create the data points with error bars in Figures 4-3 and 4-4. The error bars drawn consist of one standard deviation on either side of the data point on the y-axis.

The tolerance for NPSOL was set to 10^{-5}, and the ATOL for CVODES was set to 10^{-10}. A multistart analysis[37] showed that these two cases have hundreds of local minima. However, many of these local minima have similar p and objective (χ^2) values. Presumably, they arise because the noise in the data, d, roughens the $\chi^2(p)$ surface. From an analysis of the roughness,[62] we set the objective function tolerance for the branch-and-bound procedure $= 10$ (the smallest χ^2 values are O(100)).

4.5 Results

For the data set shown in Figure 4-3, the best local fit obtained previously[72,71] using the kinetic model detailed in Table 4.1 had a significant discrepancy from the experimental data. However, the globally optimized fit obtained fits the data set very well with a χ^2 value of 128, as shown in Figure 4-3. The model actually is consistent with the data and there is no discrepancy that needs to be explained! The local optimization routine used previously was trapped in a local minimum and produced an erroneous result due to a poor initial guess.

The previous study did not identify the global optimum of the objective function, since a good initial guess is needed to find the best overall fitted parameters. Using the multistart algorithm over 1000 different nonlinear local optimizations were run from random initial guesses spanning the physical boundaries of the parameters. Only 4 of the initial guesses found the global optimum and one-third of the guesses led to poor fits (Pr≤0.25). A histogram of the 1000 multistart optima found is shown in Figure 4-5.

A second data set measured at 323 K is displayed in Figure 4-4. Again, the fit obtained using the conventional local least-squares minimization approach does not fall within the experimental error bars. Using global optimization, the fit improves and has a χ^2 value of 476, which corresponds to a probability of 0.16. Even with this best possible choice for the 3

Figure 4-5: Histogram of the local minima found from nonlinear χ^2 fits to the data in Figure 4-3. Each of the 1000 different local optimizations performed began from a random initial guess spanning the physically reasonable range of the adjustable parameters. The local optima were binned based on the probability the model is consistent with the data, i.e. by the level of confidence. At 298 K many different parameter sets exist which provide significant fits (Pr > 0.75), however, there is a reasonable likelihood of finding fits that are not consistent with the data. Only 4 of the 1000 initial guesses converged to the globally optimal best fit.
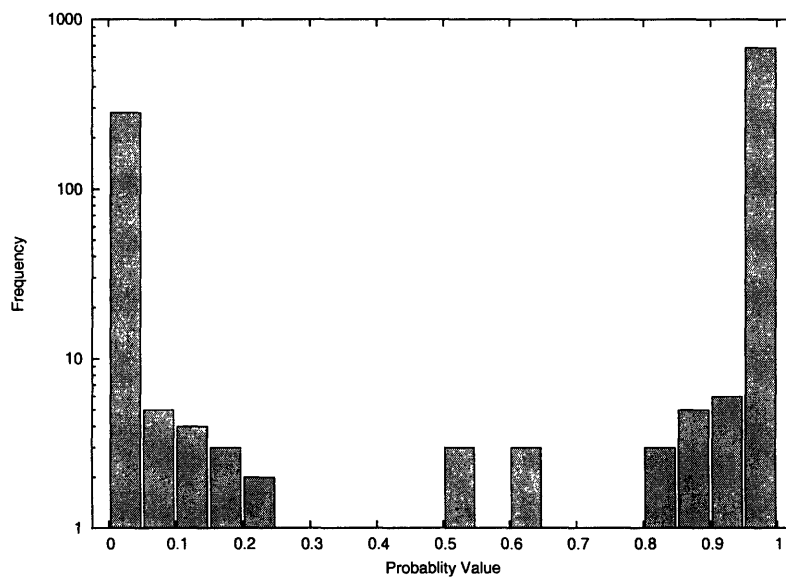
Figure 4-6: Histogram of the local minima found from nonlinear χ^2 fits to the data in Figure 4-4. Each of the 1000 different local optimizations performed began from a random initial guess spanning the physically reasonable range of the adjustable parameters. The local optima were binned based on the probability the model is consistent with the data, i.e. by the level of confidence. Only 1 of the 1000 initial guesses converged to the globally optimal best fit. The best fit in this example has a $Pr(\chi^2) = 0.163$, which indicates that the model and the data are inconsistent.
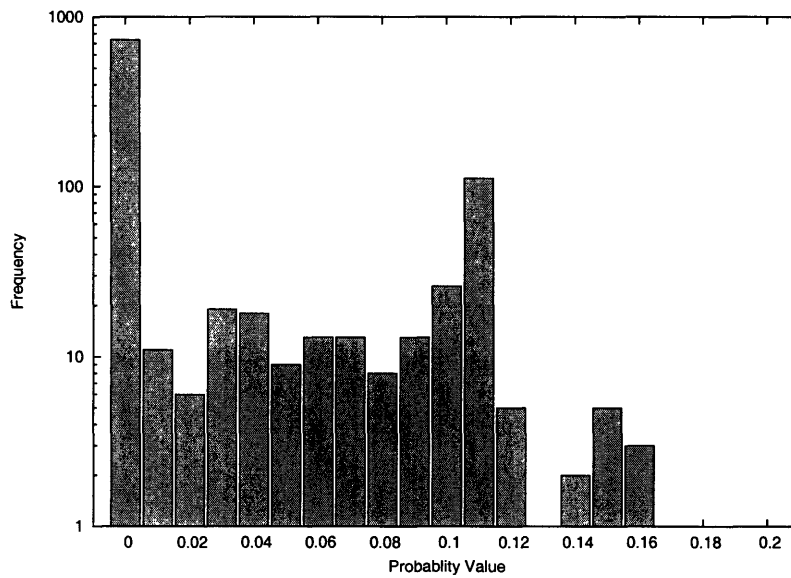
parameters the deviations between the model and data are significantly larger than expected from the error bars on the data. We can conclude with a high degree of confidence that the model is not consistent with the data for any choice of the parameters.

Again, using the multistart algorithm, 1000 local optimizations of the model parameters were performed against the data shown in Figure 4-4. Figure 4-6 shows that finding the significant optima is much more difficult compared to the 298 K data. The chances of randomly finding the best possible fit to the data are, literally, 1 in a 1000.

There are of course many possible reasons why a model could be inconsistent with data, and this particular model is based on quite a large number of assumptions. In this particular case, it seems most likely that the heats of reaction for steps 1.2b and 1.2a computed in Section 3.2.3 are slightly off, causing the computed equilibrium constants $K_{1.2b}$ and $K_{1.2a}$ to have the wrong temperature dependence. These values have error bars of more than a few kcal/mole, more than enough to resolve the discrepancy in Figure 4-4.

The application of GDOC to the parameter fits for the cyclohexadienyl numerical model results in two unique solutions. In the 298 K case, GDOC found a set of parameters that indicated the model cannot be proven false at a 75% confidence level. However, in the 323 K case, GDOC found that no parameter set is possible that can make the data consistent with the proposed model. Unlike other forms of optimization, GDOC can show with a high level of confidence when models and data don't mix.

4.6 Conclusions

A computer program has been developed suitable for finding the global solution of the most common type of least-squares problem that arises in chemical kinetics, based on the recent breakthroughs in global dynamic optimization by Singer and Barton.[65,66,64] Using this new mathematical method one can for the first time rigorously determine whether a model with several adjustable parameters can be made to fit kinetic data, or whether it is fundamentally inconsistent with the data. The model has been applied to transient absorption traces of $c\text{-}C_6H_7$ oxidation in cyclohexane. In the 298 K example, the new method showed that the

model was consistent with the data. However, it was proven that the globally optimum set of parameters was not consistent with the data at 323 K. Probably, this is due to the specifying the equilibrium constant rather than allowing it to be a free parameter within its wide range of error (see Section 3.2.3). This new addition to the kineticists' numerical toolkit is expected to prove useful for properly comparing models and data in future experiments. The software described here and the associated documentation has been made available via the Internet at http://yoric.mit.edu/gdoc.

Table 4.2: Model parameters which were not adjusted in the fit.

Model Parameter	298 K	323 K
$\epsilon_{c\text{-}C_6H_7}$	2100 $M^{-1}cm^{-1}$	2100 $M^{-1}cm^{-1}$
$\epsilon_{o\text{-}C_6H_7OO}$, $\epsilon_{p\text{-}C_6H_7OO}$	200 M^{-1} cm^{-1}	200 M^{-1} cm^{-1}
ℓ	0.7 cm	0.7 cm
$[1,4\text{-}C_6H_8]_0$	0.400 M	0.400 M
$[(CH_3)_3CO]_0$	1.53 $\times 10^{-4}$ M	1.53 $\times 10^{-4}$ M
$[O_2]_0$	0.0019 M	0.0014 M
$[c\text{-}C_6H_7]_0$, $[o\text{-}C_6H_7OO]_0$, $[p\text{-}C_6H_7OO]_0$	0 M	0 M
$K_{1.2b} = k_{1.2b}/k_{-1.2b}$	2081 M^{-1}	385 M^{-1}
$K_{1.2a} = k_{1.2a}/k_{-1.2a}$	4162 M^{-1}	770 M^{-1}
$k_{2.2}$	53 $M^{-1}\mu$ s^{-1}	73 $M^{-1}\mu$ s^{-1}
k_R	1200 $M^{-1}\mu$ s^{-1}	1750 $M^{-1}\mu$ s^{-1}

Chapter 5

Gas phase experiments

"Ride like fury! If you run out of gas, get ethyl. If Ethel runs out, get Mabel!"

–Rufus T. Firefly (Groucho Marx), Duck Soup, 1933

5.1   Summary and motivation

In this section, gas phase experiments were performed to verify the behavior of c-C_6H_7 in the presence of O_2 and to learn the rate of H-abstraction from 1,4-C_6H_8 by t-butoxyl radical.

There are at least four distinct advantages to performing gas phase experiments with radical reactions versus liquid phase experiments. First, solvents create a dielectric medium that perturb the thermodynamic energies of the reactants and products. Second, reactions in gas phase are not limited by diffusion, which allows for a better measurement of the upper bound of the radical reaction rate. Third, spectroscopic measurements have a higher resolution in the gas phase. Lastly, gas phase reactions are more relevant to fields such as combustion and atmospheric chemistry.

Gas phase reactions of cyclohexadienyl radical were studied using laser-flash photolysis. The probe beam was a solid-state pico-second laser system instead of a flash lamp or dye laser. The advantages of this system are manifold:

- The 80 MHz pulse train from the probe laser is fast enough to probe the radical's

absorption thousands of times during its lifetime in the gas phase. Radical generation and decay can be recorded with a single photolysis pulse, which makes the results much less sensitive to fluctuations in the photolysis energy. Other techniques, such as pLIF and flow-tube experiments are often limited by these fluctuations.

- The pico-second pulses are frequency doubled and tripled efficiently, making the probe beam tunable in the UV, visible, and infrared regions.

- The solid-state technology produces at least 10 milliwatts of power at most wavelengths with a high signal-to-noise ratio.

Transient absorption signals were observed and recorded. The transient signals were observed to decay in the presence of oxygen in accord with the experiments of Berho and Lesclaux[8] and Estupiñán.[17] Attempts to measure the rate at which t-butoxyl radical abstracts hydrogen from 1,4-C_6H_8 are discussed. Specific issues related to using the pico-second laser and the chemical system used to generate the radical are discussed. The chapter ends with a discussion of future work and experiments based on recent findings.

5.2 Introduction

Gas-phase studies of cyclohexadienyl oxidation kinetics have been performed before by Berho et al. Berho reported an unusually slow rate constant for the reaction of cyclohexadienyl radical with oxygen of 2.41×10^7 $M^{-1}s^{-1}$. In chapters 2 and 3, we dispute this rate because it is likely that Berho measured a combination of several rates, which together appeared to be a single slow decay.

Berho et al. were able to create cyclohexadienyl radical in gas phase[8] using a complicated mechanism involving chlorine dissociation in the presence of H_2. Estupiñán et al. improved on the methods of Berho and Lesclaux and used the reaction scheme shown in Equation 5.1 to create c-C_6H_7 radical.

$$Cl_2 + h\nu_{(>290)} \quad \rightarrow \quad 2\,Cl \qquad (5.1)$$
$$Cl + 1,4\text{-}C_6H_8 \quad \rightarrow \quad HCl + c\text{-}C_6H_7$$
$$Cl + 1,4\text{-}C_6H_8 \quad \rightarrow \quad C_6H_8Cl$$
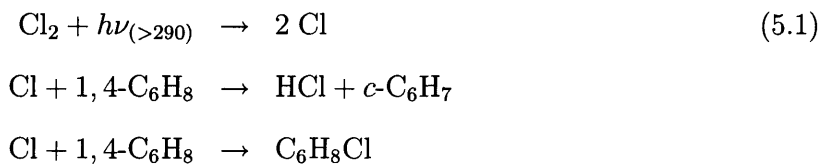
Estupiñán et al. had the primary goal of determining the rate of c-C_6H_7 oxidation, which is discussed in detail in Chapters 2 and 3 Estupiñán found the rate to be slightly higher at 4×10^7 $M^{-1}s^{-1}$. However, Estupiñán's results do not indicate the rate at which chlorine atom abstracts the hydrogen from $1,4$-C_6H_8. This rate is unknown in literature, and would be a valuable addition of the rate rules in several combustion mechanisms.

Since Estupiñán new methods have been discovered to measure c-C_6H_7 radical in gas phase. Kumar et al.[40] found that c-C_6H_7 radical can be generated directly using 193 nm light with Reaction 5.2.

$$1,4\text{-}C_6H_8 + h\nu_{193} \rightarrow c\text{-}C_6H_7 + H \qquad (5.2)$$
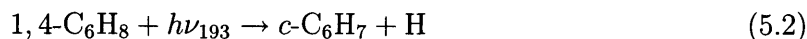
With 193 nm photolysis, Kumar observed excited benzene absorption peaks that were much larger than the cyclohexadienyl peaks at 300 nm. Despite this interference, Kumar

93

was able to distinguish benzene from cyclohexadienyl radicals due to the different time dependence. Kumar and Berho claim c-C_6H_7 reacts with NO at a rate of approximately 9.0×10^8 $M^{-1}s^{-1}$ and 1.0×10^9 $M^{-1}s^{-1}$ respectively. Imamura recently measured the laser-induced fluorescence spectrum of c-C_6H_7, but did not perform kinetic measurements.

In this study we attempt to measure the rate of H-abstraction from $1,4$-C_6H_8 by $(CH_3)_3CO$ radical by probing the rise in absorbance due to generation of the c-C_6H_7 radical. The determination of this key rate would allow comparison with a similar rate in the liquid phase measured by Effio et al.[16]

5.3   Experimental approach

Figure 5-1: Diagram of the experimental setup used to measure cyclohexadienyl radical kinetics in the gas phase. The sequence of the experiment works as follows: (1) The Ti-Sapph laser emits a probe beam of pico-second pulses at a repetition rate of 80MHz. The beam is then tripled in frequency to the UV. (2) The excimer laser fires initiating the chemistry. (3) The change in the intensity of the probe beam over the timescale of the experiment is measured by photodiode or photo-multiplier tube (PMT) and recorded by the digital oscilloscope. (4) The final trace is transferred from the oscilloscope to computer and stored.
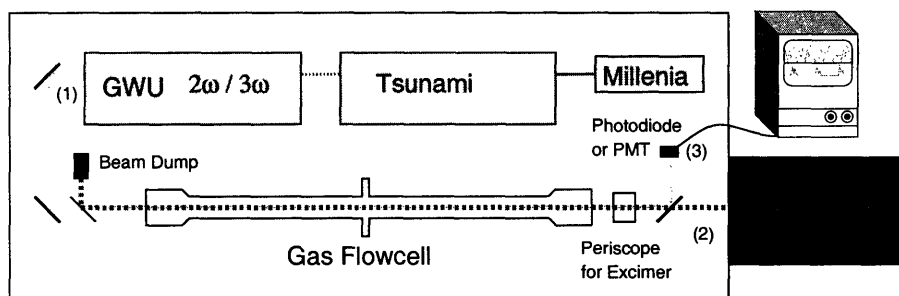
Gas phase cyclohexadienyl radicals were experimented on using techniques and methods similar to those used in the liquid phase. c-C_6H_7 was produced by laser flash photolysis with the same chemical mechanism used in Chapter 2 (Reactions 2.1 and 2.2). The transient absorption of light from the third harmonic of a pico-second pulse Titanium-Sapphire laser (Spectra-Physics Tsunami) was measured using a UV sensitive photodiode (ThorLabs Det 210 or ThorLabs PDA155). A diagram depicting the layout of the experiment is shown in

Figure 5-1.

Figure 5-2: Diagram of the gas distribution system for the stainless-steel flowcell. A–C are Sierra flow controllers and control the window purge streams as well as the addition of oxygen. D–E are MKS flow controllers and govern the Ar flow through bubbler F and G. Check valves are placed between the bubblers and the MKS flow controllers to prevent liquid from flowing backwards.
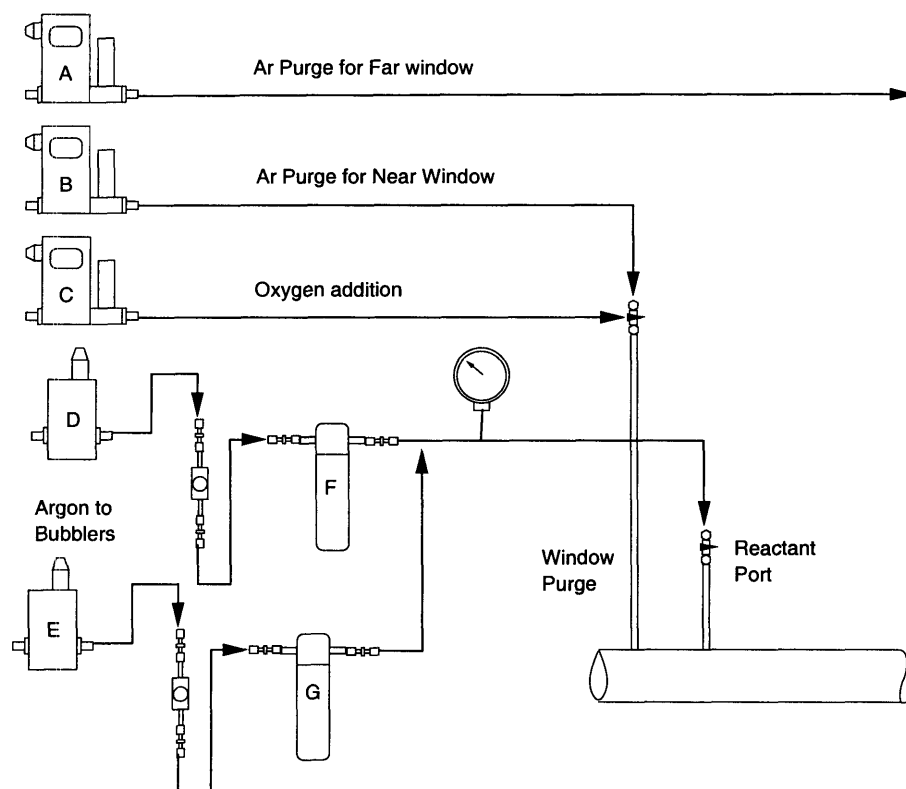
The vapor mixture was created by sparging Argon (AirGas, Grade 6.0) through two Ace glass bubblers, one containing 1,4-cyclohexadiene (Aldrich, 97%) and the other di-tert-butyl peroxide (Aldrich, 98%), as shown in Figure 5-2. Each bubbler was jacketed and temperature controlled using re-circulating water baths. The Argon flow into the bubblers was controlled using MKS mass flow controllers and constrained to rates which allowed time for vapor-liquid equilibrium to occur. These rates were verified by observing the changes in pressure with time due to flow from the bubblers.

Additional Ar was added as a purge gas to prevent chemical deposition on the windows

to the flowcell. O_2 could also be added as an additional reactant. Both the flow of additional Ar and O_2 were controlled using Sierra mass flow controllers. In order to determine correct reactant concentrations these additional flowrates were added to the amounts coming from the bubblers to get a total molar flowrate, n_{total}. Total flowrates through the cell were anywhere from 200–1000 cm^3/min.The pressure in the cell, P, was controlled by hand using several bypass valves to be $\approx$ 360 torr within $\pm$ 5% over the course of the experiments. The combination of control over the Ar flowrate, bubbler temperature, cell pressure, and cell temperature allows for accurate determination of the flowrates of 1,4-C_6H_8 and DTBP using Equations 5.3–5.6.

$$y_i = \frac{p_i^*(T_{bubbler})}{P} \tag{5.3}$$

$$\log_{10} p_i^* = A_i + \frac{B_i}{T_{bubbler}} + C_i \log_{10}(T_{bubbler}) + D_i T_{bubbler} + E_i T_{bubbler}^2 \tag{5.4}$$

$$n_i = \frac{y_i n_i^{Ar}}{1 - y_i} \tag{5.5}$$

$$c_i = \frac{P}{RT_{cell}} \left(\frac{n_i}{n_{total}} \right) \tag{5.6}$$

In Equations 5.3–5.6, y_i is the mole fraction of reactant i, p_i^* is the partial pressure, and P is the total pressure in both the bubblers and the flowcell. The pressure drop between the two values is negligible. The variable n_i is the reactant molar flowrate out of the bubbler, while n_i^{Ar} is the flowrate of Argon into the bubbler. Equation 5.4 is a modified Antoine equation that given temperature in K calculates the vapor pressure in torrs. Constants A–E are the coefficients for this modified Antoine equation[78] and are shown in Table 5.1. The gas mixture flows continuously through a stainless steel flow cell with quartz windows at each end and exits to an exhaust line pumped by a Roots Vacuum System.

A Lambda Physik Compex 102 Excimer Laser containing a KrF gas mixture generated 25 ns photolysis pulses at a wavelength of 248 nm. About 30 mJ of this light was directed into the gas cell through an iris. The amount of photolysis light entering and leaving the sample cuvette was measured using a calibrated power meter from Ophir Optronics. Depending

Table 5.1: Modified Antoine coefficients for 1,3-cyclohexadiene and di-tert-butyl peroxide (DTBP). Vapor pressures for 1,3-cyclohexadiene and 1,4-cyclohexadiene are essentially identical. Values were taken from Reference 78.

Chemical Name	Coefficient	Value		
1,3-cyclohexadiene	A	32.7055		
	B	-2.7281	$\times$	10^3
	C	-8.8297		
	D	4.2152	$\times$	10^{11}
	E	3.1600	$\times$	10^{-6}
	T_{min}	161 K		
	T_{max}	556 K		
di-tert-butyl peroxide (DTBP)	A	-17.3901		
	B	-2.1221	$\times$	10^3
	C	-1.3506	$\times$	10^1
	D	-3.0330	$\times$	10^{-2}
	E	1.7215	$\times$	10^{-5}
	T_{min}	233 K		
	T_{max}	547 K		

on the concentration of the gas mixture, between 10% and 99% of the 248 nm light was absorbed by the reactants. Once the beam exits the cell, the remaining light is directed into a beam dump by a 248 nm 45° incidence mirror.

The probe beam was generated by a tunable laser system consisting of a diode-pumped cw visible laser (Millennia Xs), Titanium-Sapphire oscillator (Tsunami), and a second and third harmonic generator (GWU23) provided by Spectra Physics Corp. The Millennia Xs outputs up to 10 W of 532 nm light which pumps the Tsunami's Ti-Sapph crystal. The crystal emits a train of pulses lasting only 2 ps each at a rate of 80 MHz in the infrared region. The Tsunami output wavelength is tunable over the range of 700–1000 nm. The infrared pulses are then directed into the GWU23 where the photons are combined in BBO and LBO crystals to create more energetic photons in the UV and visible regions. Second harmonic output is half the wavelength of the Tsunami input, while the third harmonic output is one-third of the entering wavelength. For most experiments the Tsunami output was set to 924 nm, such that the third harmonic output was 308 nm, near the absorption peak for cyclohexadienyl radical in the gas phase.[8] The output power is stable to within 1% over the lifetime of the experiments. However, systematic noise is present which complicates

interpretation of the data. The probe beam is directed through the quartz windows of the flowcell in a direction counter to that of the excimer.

After exiting the flowcell the probe beam is directed by a mirror through a Schott WG 305 filter to suppress scattered light from the photolysis beam. The beam is incident upon a a UV sensitive photodiode (ThorLabs Det 210 or ThorLabs PDA155) which registers a voltage in proportion to the intensity of light. In configurations that used an integrating sphere (Melles Griot) a Hamamatsu 1P28 side window photomultiplier (200-650 nm wavelength range) was used in place of the photodiodes. The voltage was amplified using a Femto amplifier until the signal was ~ 1 V. Low-pass signal filters were used in conjunction with the Femto's internal low-pass filter to reduce noise above the 50 MHz frequency range. The resulting signal was sent to an HP54642A digital oscilloscope. The data were typically averaged between 10-100 times and contained 500 temporal data points for each transient absorption. The data are collected so that 10% of the acquisition period provides pre-trigger information.

The transient absorption data from the spectrometer was then analyzed using standard numerical techniques with Microsoft Excel, Matlab and Gnuplot programs.

5.4 Results

5.4.1 Time-dependent absorptions

Data traces for four different cyclohexadiene bubbler temperatures are shown in Figure 5-3 with their experimental conditions listed in Table 5.2. For each of the signals, a sharp rise in absorbance from the excimer pulse to a peak at around 10–100 μs was observed.

To confirm that the signal was due to cyclohexadienyl radical, we performed a variety of tests. First, we added the chemicals in a stepwise fashion to determine if the signal was due to another mechanism than the one proposed in Reactions 2.1 and 2.2. No signal was observed with Ar alone, but when DTBP was added a small signal was evident, however, the timescale was not consistent with cyclohexadienyl absorption. Instead the signal can be attributed to the formation of methyl radical and acetone($\epsilon_{308} = 500$ M^{-1}cm^{-1}), as shown

98

in Equation 2.4. With the addition of 1,4-C_6H_8 another small signal was evident and was attributed to excited benzene, which is a contaminant in 1,4-C_6H_8. With the addition of all the gas components, the full absorption signal in Figure 5-3 was observed. Likewise, both the probe and the excimer laser beams were blocked to determine if the signal was based on the excimer and probe interaction. From these studies, it was determined that the signals found only occurred when both laser beams were present and interacted with both reactants in the flowcell.

The timescale of the subsequent decay is on the order of ms, in agreement with our expectations for the gas-phase decay of cyclohexadienyl radical in the absence of oxygen. However, the 1,4-C_6H_8 concentration dependence of the rise-time signal is not monotonically increasing. The rise-time constant is observed despite the substantial difference in 1,4-cyclohexadiene concentrations when the bubbler temperatures were varied from 25 °C and 45 °C.

Table 5.2: Experimental conditions for data traces at different 1,4-C_6H_8 bubbler temperatures taken on February 17, 2005.

1,4-C_6H_8 Bubbler		DTBP Bubbler		Purge	Flowcell	
$T(°C)$	$n^{Ar}_{1,4\text{-}C_6H_8}(\text{sccm})$	$T(°C)$	$n^{Ar}_{DTBP}(\text{sccm})$	$n^{Ar}_{Purge}(\text{sccm})$	$T(°C)$	$P(\text{torr})$
15	31	25	31	104	50	379
25	31	25	31	104	50	379
35	32	25	32	102	52	367
45	31	25	31	104	50	379

5.4.2 Cyclohexadienyl radical concentration dependence

At each bubbler temperature, the rise in absorbance was fit to a simple exponential model, shown in Equation 5.7.

$$a = -a_o e^{-bt} + c \tag{5.7}$$

Using data taken at different 1,4-C_6H_8 bubbler temperatures a plot of b against 1,4-C_6H_8 concentration can be constructed. The slope of the plot provides a value for the rate constant

Figure 5-3: Recorded signal from the photolysis of 1,4-C_6H_8 and DTBP at various 1,4-C_6H_8 bubbler temperatures.
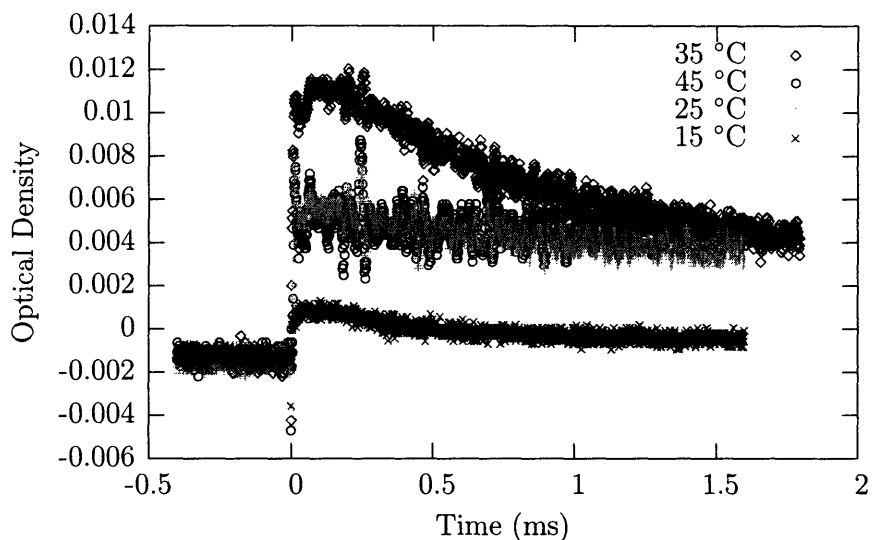
for H-abstraction from 1,4-C_6H_8 to form c-C_6H_7 radical. Figure 5-4 shows a plot of these values with a negative slope of -3×10^6 and an intercept of 1.67×10^5. Rate constants can never be negative, which indicates that effects other than reaction are important in these decay traces.

5.4.3 Decay rate in the presence of oxygen

Oxygen was added to determine its effect on the rate of c-C_6H_7 decay. The decay of c-C_6H_7 was measured by fitting the region from the peak of absorption to a data point approximately two-thirds the height of the peak. This region was fit to a simple exponential decay, shown in Equation 2.3 Figure 5-5 shows the change in the rate of decay with increasing oxygen concentration. The results show significant changes in the rate constant with increasing oxygen concentration. The oxidation rate constant found is $6.6 \pm 1.7 \times 10^6$, about a factor of five smaller than that found by Berho and Lesclaux[8] and Estupiñán.[17] The change in the decay rate with oxygen indicates the presence of a radical intermediate that reacts with oxygen, or an excited state that is quenched by oxygen.

100

Figure 5-4: Rise-time constants of experimental absorption with respect to the 1,4-C_6H_8 concentration.
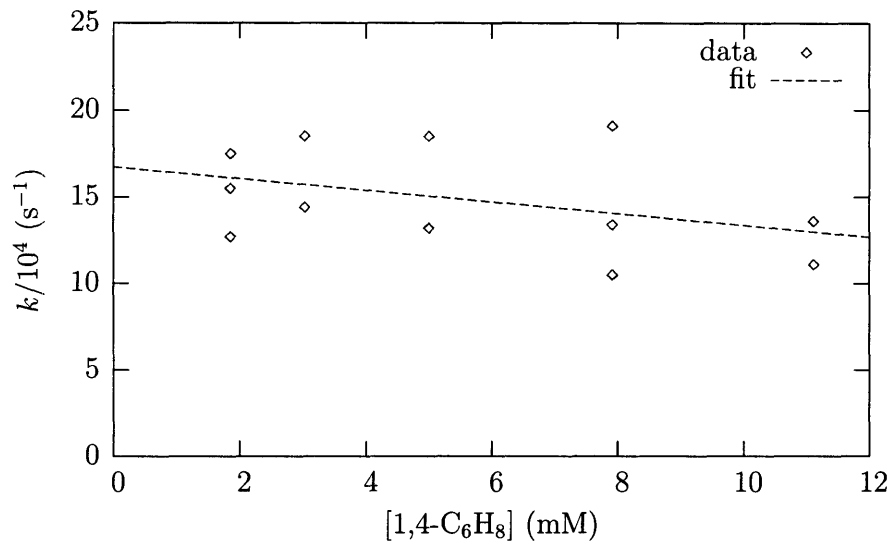
Figure 5-5: Decay rate constants of experimental absorption with respect to the O_2 concentration.
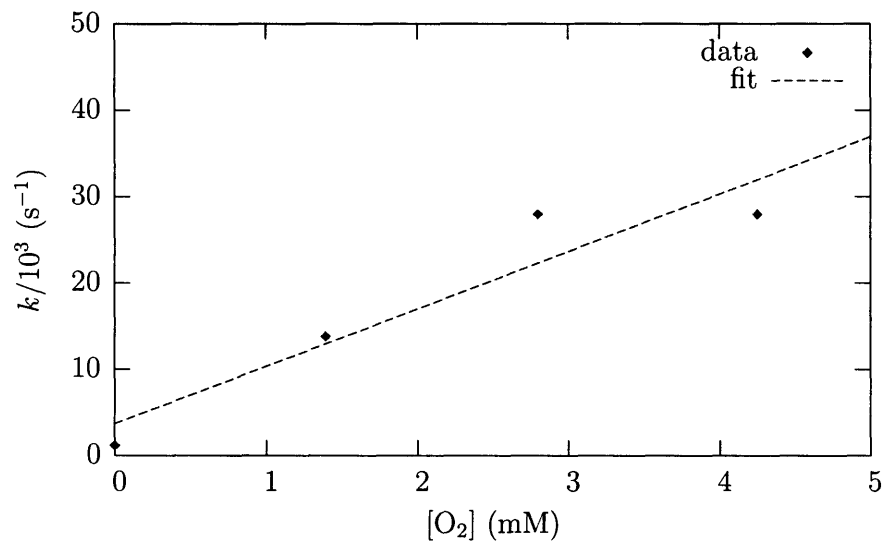
5.5 Discussion

One of the primary goals of this experiment is to measure the rate at which $(CH_3)_3CO$ abstracts hydrogen from 1,4-C_6H_8, as shown in Equation 2.2. The product of this reaction is c-C_6H_7 and t-butyl alcohol. Based on experiments done by Berho and Estupiñán,[8,17] we know the UV absorption bands for the c-C_6H_7 radical and should be able to detect its presence in the gas phase. The expected absorption signal would increase sharply due to Reaction 2.2 then decay due to radical recombination processes.

Initially, the increasing absorption signal would be due entirely to c-C_6H_7 formation, which is equal to the rate of H-abstraction. Effio et al.[16] measured the H-abstraction rate in liquid phase and reported a value of 5.3×10^7 $M^{-1}s^{-1}$. Using this rate as a basis, we would expect a time-constant of 9.5 μs in the gas phase. Figure 5-6 shows a transient absorption that has been magnified in the 10 μs region. Indeed, the transient appears to reach its peak on the order of 10 μs.

Figure 5-6: A transient absorption signal taken at 35 °C at the μs timescale. The rise time is consistent with the expectation of 10 μs.
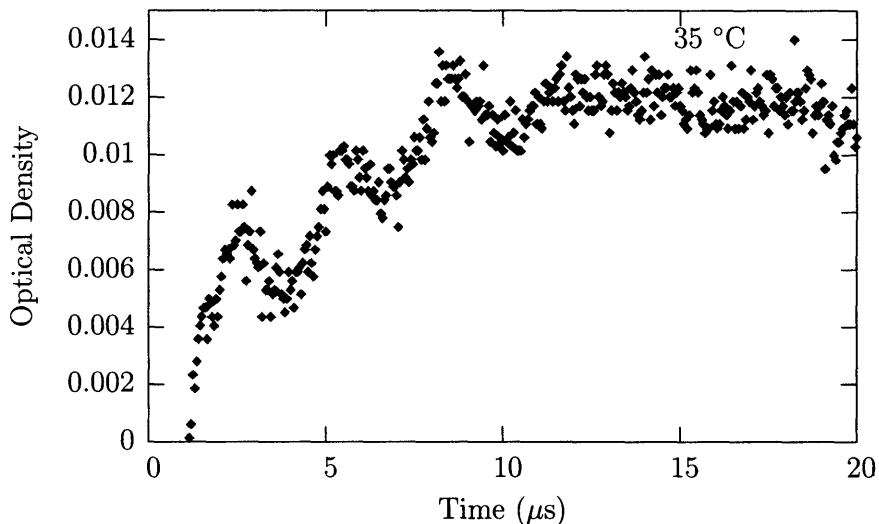
Assuming that the H-abstraction reaction is first-order, this rate can be determined from the slope of a plot of rise-time constants with 1,4-C_6H_8 concentration. Due to the inconsistency of the results, this plot, shown in Figure 5-4, has a negative slope, which is

not possible with first-order kinetics. There are several likely reasons for this inconsistency, however the most likely reason is that the reaction measured is not following first-order kinetics. A possible scenario is that 1,4-C_6H_8 itself absorbs 248 nm photons and decomposes into H and c-C_6H_7. This would be similar to Kumar's mechanism, but at with a lower yield due to the lower energy photons. The H atom could then add to the benzene contaminant creating c-C_6H_7 using a chain mechanism further confusing the results. However, several other phenomenon could be responsible and must be ruled out.

5.5.1 Laser noise

One source of interference is a non-random series of spikes that appear on the ms timescale which we can attribute to the Millennia Xs laser. Figure 5-7 shows noise due to the Millennia Xs laser system.

Figure 5-7: A transient absorption signal taken at 35 °C at the 10 ms timescale displaying the laser noise of the Millennia Xs. Note there is a sinusoidal component as well as a sharply spiked component synchronized to the line.
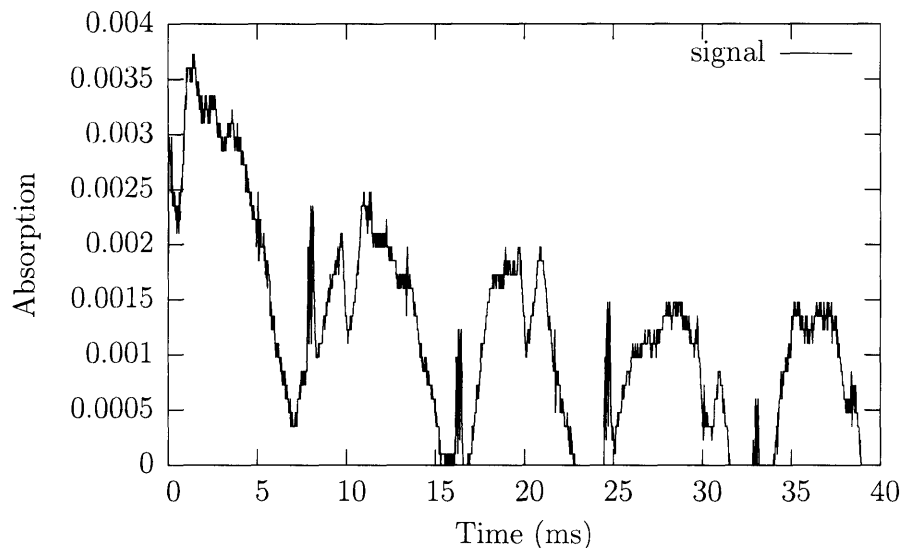
The noise is synchronized with the 60 Hz of the line such that the noise occurs in phase with the line-triggered excimer pulses. The magnitude of this noise is such that it is responsible for 0.4% of the absorption measured. Random noise can be easily removed by averaging

signals, however, periodic noise can only be eliminated by subtracting a reference beam or through eliminating the Fourier component. Unfortunately, the timescale of the noise overlaps the expected timescale of the c-C_6H_7 radical decay and removing the Fourier component responsible through filtering would distort the kinetic data. Subtracting a reference would require exact timing to ensure a proper overlap of the signals.

However, if one triggers the Compex randomly, one can still average away the line-synchronous noise, because to the experiment the noise is random. With 100 averages most of the noise due to this component can be removed. This procedure, however, did not change the rise time, since at 10 μs the rise time only samples the noise spikes once every 1000 times making it already out of the range of the noise. This procedure does however, make measuring decays with oxygen possible with very little noise, as shown in Figure 5-3.

5.5.2 Thermal lensing and photoacoustic phenomena

Whatever is responsible for the rise-time interference must have the following characteristics:

- It must be insensitive to changes in partial pressure of $1,4$-C_6H_8.

- It creates a small scale signal that acts on the μs timescale and repeats at intervals of 250 μs, as shown in Figure 5-8.

- It depends on a conjunction of all the reactants, excluding O_2 and both laser beams. Remove any component and the signal disappears.

All of these clues led to the conclusion that a thermal lensing event was occurring. The definition of thermal lensing, according to the IUPAC Compendium of Chemical Technology is as follows:

A technique that determines the alteration in the refractive index of a medium as a result of the temperature rise in the path of a laser beam absorbed by the medium. The lens produced (usually divergent) causes a change (usually a decrease) in the irradiance measured along the laser beam axis.

104

Figure 5-8: Fluctuation in signal with a periodicity of 250 μs.
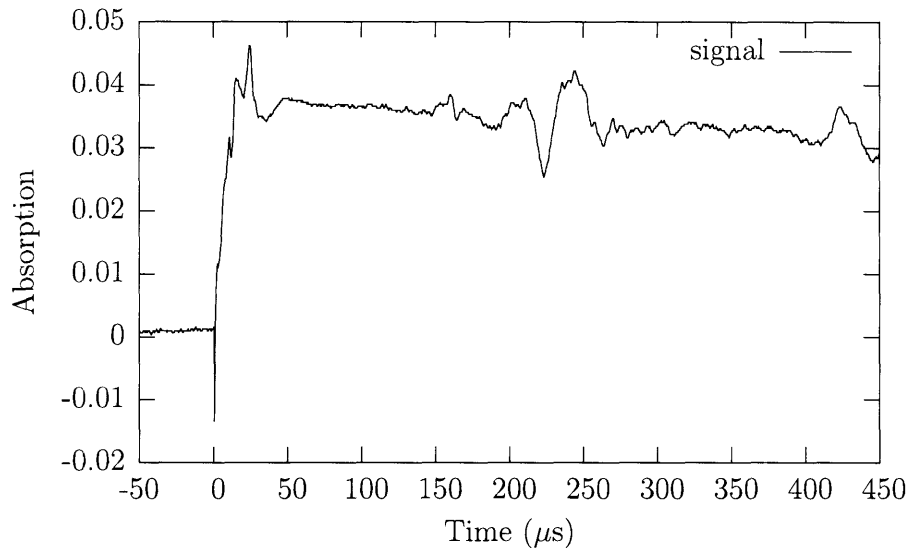
Basically, the heat absorbed by the gas changes the refractive index of the medium steering the laser beam off the detector. Such a phenomena is hard to account for since it looks and acts like a real signal. In fact, many experiments use this phenomena to find heat capacities and to test thermodynamic properties of radicals by fitting the lensing signals.

We attempted to remove the lensing signal through the use of an integrating sphere. By carefully aligning the laser and placing the beam in the center of the 1.5 in. opening to the sphere, small deviations could be integrated out spatially by having the beam reflect several times off the reflective interior surface of the sphere. The sphere diminished the 250 μs signal by 90%, but the time-constant associated with the rise in absorbance did not change. Further work is planned to unravel this mystery.

5.6 Future extensions of gas phase experiments

5.6.1 Alternative means of generating cyclohexadienyl radical

If, for the moment, we abandon H-abstraction as a means for creating cyclohexadienyl radical, several experiments could be performed which would could test the spectrometer's capability to detect cyclohexadienyl radical.

Generation of c-C_6H_7 by 193 nm photolysis of 1,4-C_6H_8 is a simple method that would provide a direct source of radicals for study.[40] Using an ethanol / dry ice bath one could operate at low reactant concentrations where very little of the excimer energy would be absorbed, minimizing the thermal lensing effect yet producing a detectable amount of c-C_6H_7 radicals. The rate of cyclohexadienyl oxidation would be determined easily by running different partial pressures of O_2 and comparing the decay rates using the same methods as in the liquid phase. It would be interesting to run this experiment at high partial pressures of oxygen, where C_6H_7OO might be trapped allowing a direct test of our re-interpretation of Estupiñán's data.

Using this mechanism, experimental conditions could be optimized and a spectrum obtained to confirm the presence of c-C_6H_7. The Arrhenius behavior of the radical recombination and oxidation could be evaluated and compared to our expectations based on the models in Chapter 3. This information could then be used in planning future H-abstraction experiments.

In experiments involving reagents other than oxygen, generating c-C_6H_7 using 193 nm light may not be feasible if the other reagent can also be excited by high-energy photons. In such cases, H-abstraction from 1,4-C_6H_8 may be the only viable way of generating c-C_6H_7. In future gas phase experiments, I would recommend using OH as the means of abstracting H from 1,4-C_6H_8 instead of $(CH_3)_3CO$ generated by photolysis of DTBP. $(CH_3)_3CO$ radicals can undergo a beta-scission reaction to form acetone and methyl radical (Reaction 2.4). Methyl radical is a much weaker hydrogen abstractor than $(CH_3)_3CO$. The net result of the beta-scission is a reduction in the number cyclohexadienyl radicals that can be created. On

the other hand, OH radical can be generated easily by the photolysis of HNO_3 at 248 nm. Using OH, no such beta-scission pathway exists and the full quantity of OH radicals can be used to abstract hydrogen atom from 1,4-cyclohexadiene.

5.6.2 Improvements to experimental setup

Apart from the chemistry, another problem which needs addressing is the amount of scattered excimer light that is detected. Even in a cross-beam arrangement, light from the excimer laser can contaminate the probe beam and is added to the signal measured. Scattered light can limit the detection-limit of the absorber by swamping the signal such that absorption is undetectable.

The two most important improvements to reduce scatter would be to collimate the excimer beam and to use a glass flowcell. Collimation would allow much greater control of the excimer fluence and would allow the ability to detect smaller absorption signals. At this point, the detection is limited by the 248 nm scattered light which saturates the detection methods. A glass cell or a blacked out stainless steel cell would absorb stray excimer and prevent scatter from entering the detector, which is off-axis to the excimer beam.

To a lesser extent than the scatter, another limitation to the detection limit of cyclohexadienyl is the probe laser noise. The laser noise due to the Millennium has been greatly reduced due to a new power supply, but to reduce the noise further would require random triggering or the subtraction of a reference beam. Without these techniques the single-shot detection limit of the spectrometer will always be limited by the overlap of the ($\sim$ 0.4%) noise at the ms timescale.

5.6.3 Simultaneous determination of two radicals

From an observability analysis[50] of the reaction mechanism, the rates of the unknown reactions in the systems can be fully-determined by observing two radical concentrations simultaneously. If one could observe the rate of c-C_6H_7 decay, while observing the generation of HO_2, the rate of direct abstraction (Reaction 1.4) and the rate of *ortho* rearrangement

107

(Reaction 1.5a) could be determined. Alternatively, benzene formation could also be observed, but benzene is already a contaminant of 1,4-C_6H_8. Determining the concentration due to formation would be difficult against this background concentration. Observing HO_2 is possible using microwave absorption, thus a possibility would be to combine a microwave cavity with an absorption experiment and trigger off the excimer pulse. Such an experiment would be novel in that it would obtain the simultaneous kinetic measurement of two species. Another possible addition would be a GC/MS system to sample the exit gas and determine the concentrations of products to determine the ultimate fate of some of the radical species. The combination of a product study in tandem with absorption studies could elucidate many pathways which require some form of corroboration.

5.6.4   Alternative means of detecting cyclohexadienyl radical

If absorption measurements are not feasible, laser-induced fluorescence could be another method of detecting c-C_6H_7 radical. Imamura[32] reports that c-C_6H_7 fluorescence can be observed at 560 nm. This wavelength can be reached using the available OPO with the GWU doubling crystal or with a Millennia pumped dye laser and would be away from many of the interferences experienced.

To conclude, many interesting experiments remain to be tried with cyclohexadienyl radical and many vistas remain to be explored.

5.7   Conclusions

1. Gas phase experiments were performed using a pico-second laser beam to probe radical concentrations. This approach is novel in its application to observing radical chemistry.

2. Experiments showed a transient absorption with a decay rate at the ms timescale affected by the concentration of oxygen.

3. The rate of rise in the absorption signal was unresponsive to 1,4-C_6H_8 concentration.

4. Several phenomena were identified that could obscure the transient absorption. Using random triggering and spatial integration these phenomena were reduced to acceptable levels. However, the rise in the absorption signal was unaffected by these measures.

5. A zeroth-order process with respect to cyclohexadiene concentration is responsible for the rise in the observed transient absorption. Whether this is due to a mode of thermal lensing or a different chemical mechanism is uncertain. More experiments should be conducted to determine the exact pathway through which cyclohexadienyl radical is formed.

6. Gas phase GC/MS on the photolysis products could help solve the mystery of the rise in the transient absorption.

7. Several additional mechanisms can generate gas phase c-C_6H_7 and could be used in other experiments of interest.

Appendix A

GDOC input and data files

A.1   chi298.oai

```
# This is the full problem formulation for James's problem. I will write
# separate input files for different reduced variants.

# fp <=> from paper
DECLARATION
# x(1) = C_A, x(2) = C_Z, x(3) = C_Y, x(4) = C_D, x(5) = C_B
  state: x(1:5)
# p(1) = k2, p(2) = k3, p(3) = k4
  parameter: p(1:3)
  time: [0, 4.46]
# k(1) = k1, k(2) = k5, k(3) = C_{0_2}, k(4) = K1, k(5) = K2
  constant: k(1:5)
  data: xdata(1:2)
END
# this is scaled
PARAMETER VALUES
  p(1)= 470.596 : [10.0, 1200.0]
  p(2)= 1107.833 : [10.0, 1200.0]
  p(3)= 0.3690 : [0.001, 40.0]
END

# this is not scaled
EQUATION
```

```
    $x(1) = k(1)*x(2)*x(3) - k(3)*(p(1)+p(2))*x(1) + p(1)/k(4)*x(4)
          + p(2)/k(5)*x(5) - k(2)*x(1)^2;
    $x(2) = -k(1)*x(2)*x(3);
    $x(3) = -k(1)*x(2)*x(3);
    $x(4) = p(1)*x(1)*k(3) - p(1)/k(4)*x(4);
    $x(5) = p(2)*k(3)*x(1) - (p(3)+p(2)/k(5))*x(5);
END

REFERENCE
   xRef(1) = xL(1);
   xRef(2) = xL(2);
   xRef(3) = xL(3);
   xRef(4) = xL(4);
   xRef(5) = xL(5);
   pRef(1) = pL(1);
   pRef(2) = pL(2);
   pRef(3) = pL(3);
END

INITIAL
   x(1)=0;
   x(2)=1.4E-4;
   x(3)=4.0E-1;
   x(4)=0 ;
   x(5)=0 ;
END

OBJECTIVE
   ((2100.0*x(1)+200.0*(x(4)+x(5))-xdata(1))/xdata(2))^2;
END

NATURAL BOUNDS
   x(1):[0,1.4E-4]
   x(2):[0,1.4E-4]
   x(3):[0,4.0E-1]
   x(4):[0,1.4E-4]
   x(5):[0,1.4E-4]
END

CONSTANT VALUES
   k(1) = 53;
   k(2) = 1200;
```

```
  k(3) = 0.0019;
  # 46*exp(6500/T-18)
  k(4) = 2081;
  # 2*k(4)
  k(5) = 4162;
END

PLOT
  2100.0*x(1)+200.0*(x(4)+x(5));
END
```

A.2 chi323.oai

```
# This is the full problem formulation for James's problem. I will write
# separate input files for different reduced variants.

# fp <=> from paper
DECLARATION
# x(1) = C_A, x(2) = C_Z, x(3) = C_Y, x(4) = C_D, x(5) = C_B
  state: x(1:5)
# p(1) = k2, p(2) = k3, p(3) = k4
  parameter: p(1:3)
  time: [0, 4.46]
# k(1) = k1, k(2) = k5, k(3) = C_{0_2}, k(4) = K1, k(5) = K2
  constant: k(1:5)
  data: xdata(1:2)
END
# this is scaled
PARAMETER VALUES
  p(1)= 340.548 : [10.0, 1200.0]
  p(2)= 1118.710 : [10.0, 1200.0]
  p(3)= 1.403 : [0.001, 40.0]
END

# this is not scaled
EQUATION
  $x(1) = k(1)*x(2)*x(3) - k(3)*(p(1)+p(2))*x(1) + p(1)/k(4)*x(4)
          + p(2)/k(5)*x(5) - k(2)*x(1)^2;
  $x(2) = -k(1)*x(2)*x(3);
  $x(3) = -k(1)*x(2)*x(3);
  $x(4) = p(1)*x(1)*k(3) - p(1)/k(4)*x(4);
  $x(5) = p(2)*k(3)*x(1) - (p(3)+p(2)/k(5))*x(5);
END

REFERENCE
  xRef(1) = xL(1);
  xRef(2) = xL(2);
  xRef(3) = xL(3);
  xRef(4) = xL(4);
  xRef(5) = xL(5);
  pRef(1) = pL(1);
```

```
  pRef(2) = pL(2);
  pRef(3) = pL(3);
END

INITIAL
  x(1)=0;
  x(2)=1.4E-4;
  x(3)=4.0E-1;
  x(4)=0 ;
  x(5)=0 ;
END

OBJECTIVE
  ((2100.0*x(1)+200.0*(x(4)+x(5))-xdata(1))/xdata(2))^2;
END

NATURAL BOUNDS
  x(1):[0,1.4E-4]
  x(2):[0,1.4E-4]
  x(3):[0,4.0E-1]
  x(4):[0,1.4E-4]
  x(5):[0,1.4E-4]
END

CONSTANT VALUES
  k(1) = 73;
  k(2) = 1750;
  k(3) = 0.0014;
  # 46*exp(6500/T-18)
  k(4) = 385;
  # 2*k(4)
  k(5) = 770;
END

PLOT
  2100.0*x(1)+200.0*(x(4)+x(5));
END
```

A.3 chi298.inp

0	0	0.76403
0.01	0.1264	1.905238
0.02	0.201625	1.879847
0.03	0.2178	1.376977
0.04	0.22305	2.386762
0.05	0.222225	1.070401
0.06	0.227625	1.076209
0.07	0.234875	1.052849
0.08	0.23385	1.949385
0.09	0.235325	1.854587
0.1	0.234675	1.710095
0.11	0.232875	1.511828
0.12	0.22905	1.346217
0.13	0.226025	1.337943
0.14	0.223025	1.356868
0.15	0.22155	1.436442
0.16	0.21985	1.421208
0.17	0.217875	1.418882
0.18	0.21405	1.322787
0.19	0.21025	1.47342
0.2	0.206675	1.45809
0.21	0.20305	1.445095
0.22	0.20045	1.453605
0.23	0.197625	1.504468
0.24	0.19445	1.577181
0.25	0.19165	1.562338
0.26	0.1883	1.467015
0.27	0.184975	1.37764
0.28	0.182725	1.332476
0.29	0.1792	1.401499
0.3	0.17765	1.410402
0.31	0.1755	1.462213
0.32	0.172225	1.469521
0.33	0.169575	1.398818
0.34	0.16595	1.378465

0.35	0.163525	1.399676
0.36	0.1614	1.434132
0.37	0.158625	1.377616
0.38	0.1563	1.397593
0.39	0.153775	1.534566
0.4	0.1512	1.653138
0.41	0.149675	1.599633
0.42	0.148725	1.669359
0.43	0.146275	1.612831
0.44	0.14435	1.513726
0.45	0.142125	1.526922
0.46	0.139675	1.372476
0.47	0.13675	1.436999
0.48	0.1354	1.395134
0.49	0.133	1.395015
0.5	0.131625	1.297957
0.51	0.130125	1.314823
0.52	0.128225	1.375751
0.53	0.12605	1.368174
0.54	0.12395	1.385797
0.55	0.1216	1.343701
0.56	0.12015	1.386759
0.57	0.118	1.389844
0.58	0.1177	1.431736
0.59	0.115275	1.410777
0.6	0.11355	1.350099
0.61	0.11193	1.340575
0.62	0.110312	1.322727
0.63	0.109095	1.304482
0.64	0.107023	1.269436
0.65	0.105385	1.240821
0.66	0.10463	1.334878
0.67	0.10442	1.362047
0.68	0.103282	1.301396
0.69	0.101913	1.255533
0.7	0.10018	1.287233
0.71	0.099062	1.302835

0.72	0.09704	1.313451
0.73	0.095622	1.234534
0.74	0.093967	1.278809
0.75	0.092747	1.246626
0.76	0.092088	1.266542
0.77	0.09105	1.36547
0.78	0.090463	1.382982
0.79	0.08896	1.365841
0.8	0.087352	1.2446
0.81	0.086535	1.283935
0.82	0.08529	1.201481
0.83	0.08433	1.168722
0.84	0.083507	1.199769
0.85	0.082808	1.25855
0.86	0.082358	1.266017
0.87	0.08049	1.191246
0.88	0.079675	1.141727
0.89	0.077948	1.218428
0.9	0.07758	1.240335
0.91	0.076097	1.243502
0.92	0.075343	1.212762
0.93	0.075012	1.196119
0.94	0.074508	1.163676
0.95	0.07348	1.243321
0.96	0.07257	1.229458
0.97	0.0714	1.167755
0.98	0.070483	1.169839
0.99	0.069528	1.187068
1	0.069255	1.237532
1.01	0.06848	1.192854
1.02	0.068705	1.243019
1.03	0.068182	1.129882
1.04	0.067767	1.176993
1.05	0.06607	1.159281
1.06	0.06485	1.037528
1.07	0.064325	1.002653
1.08	0.064185	1.005197

1.09	0.063817	1.072395
1.1	0.063255	1.147396
1.11	0.06166	1.246455
1.12	0.060937	1.259367
1.13	0.060685	1.176962
1.14	0.060373	1.223205
1.15	0.060542	1.143596
1.16	0.059673	1.056173
1.17	0.059375	1.043142
1.18	0.057982	0.997339
1.19	0.057885	1.066451
1.2	0.057278	1.110592
1.21	0.057688	1.130122
1.22	0.057127	1.125724
1.23	0.056618	1.193042
1.24	0.055833	1.142607
1.25	0.054777	1.093271
1.26	0.054275	1.063288
1.27	0.05395	1.056727
1.28	0.053343	1.012882
1.29	0.053367	1.029791
1.3	0.052705	1.030744
1.31	0.051445	0.952707
1.32	0.051475	1.046537
1.33	0.050577	1.036729
1.34	0.050795	1.029166
1.35	0.050182	0.962814
1.36	0.050415	1.018472
1.37	0.049695	0.948782
1.38	0.048892	0.967873
1.39	0.048795	1.013935
1.4	0.04782	1.07953
1.41	0.047965	1.037097
1.42	0.047198	1.062752
1.43	0.047425	1.006277
1.44	0.047285	1.017186
1.45	0.046582	0.943923

1.46	0.046677	0.960311
1.47	0.046645	0.856865
1.48	0.046698	0.915679
1.49	0.04672	0.945154
1.5	0.046375	0.882938
1.51	0.045198	0.959823
1.52	0.044885	0.899031
1.53	0.044665	0.895385
1.54	0.044605	0.916488
1.55	0.044033	0.901798
1.56	0.043145	0.891876
1.57	0.042757	0.846828
1.58	0.042798	0.805478
1.59	0.042392	0.865432
1.6	0.042255	0.864329
1.61	0.042175	0.818418
1.62	0.041745	0.885278
1.63	0.041217	0.887969
1.64	0.040888	0.932798
1.65	0.040918	0.946757
1.66	0.040822	0.936836
1.67	0.040435	0.892504
1.68	0.040392	0.89793
1.69	0.04007	0.880978
1.7	0.040208	0.846603
1.71	0.040015	0.82114
1.72	0.039598	0.874605
1.73	0.038942	0.854116
1.74	0.039285	0.842605
1.75	0.039282	0.772305
1.76	0.038582	0.7996
1.77	0.038198	0.744573
1.78	0.038277	0.770216
1.79	0.038665	0.796472
1.8	0.038488	0.734773
1.81	0.038545	0.745427
1.82	0.038613	0.777475

1.83	0.037913	0.835276
1.84	0.03831	0.86735
1.85	0.037498	0.869816
1.86	0.03766	0.892699
1.87	0.037435	0.844175
1.88	0.037018	0.755016
1.89	0.036522	0.795446
1.9	0.036257	0.732927
1.91	0.035568	0.767447
1.92	0.035717	0.694475
1.93	0.03582	0.756242
1.94	0.035765	0.727398
1.95	0.035855	0.737898
1.96	0.035165	0.66881
1.97	0.035252	0.746418
1.98	0.034702	0.710376
1.99	0.034355	0.733805
2	0.0341	0.725429
2.01	0.034033	0.777895
2.02	0.034065	0.735723
2.03	0.034155	0.685219
2.04	0.033987	0.663487
2.05	0.03413	0.594782
2.06	0.033905	0.638937
2.07	0.033673	0.632948
2.08	0.034333	0.715031
2.09	0.034305	0.721584
2.1	0.034515	0.73909
2.11	0.033245	0.73049
2.12	0.033703	0.732427
2.13	0.033335	0.650487
2.14	0.03277	0.632444
2.15	0.032837	0.684302
2.16	0.033008	0.747071
2.17	0.032828	0.767088
2.18	0.032532	0.763857
2.19	0.031745	0.666788

2.2	0.03137	0.595172
2.21	0.031337	0.648345
2.22	0.031573	0.616882
2.23	0.031065	0.672569
2.24	0.031062	0.659443
2.25	0.031348	0.655789
2.26	0.031235	0.657955
2.27	0.031205	0.677758
2.28	0.030335	0.693052
2.29	0.03126	0.651517
2.3	0.03153	0.635746
2.31	0.031508	0.652736
2.32	0.031255	0.64805
2.33	0.030713	0.67162
2.34	0.030665	0.647041
2.35	0.030375	0.596241
2.36	0.030575	0.661197
2.37	0.030478	0.709689
2.38	0.03067	0.724917
2.39	0.030683	0.724962
2.4	0.030225	0.685177
2.41	0.029865	0.672757
2.42	0.029638	0.627764
2.43	0.029315	0.622705
2.44	0.029433	0.632588
2.45	0.028868	0.588754
2.46	0.02844	0.562306
2.47	0.02939	0.603736
2.48	0.0295	0.603653
2.49	0.02976	0.603169
2.5	0.029205	0.6054
2.51	0.029562	0.617226
2.52	0.02924	0.68638
2.53	0.029622	0.711246
2.54	0.02933	0.681893
2.55	0.028917	0.737729
2.56	0.028338	0.66441

2.57	0.028887	0.647089
2.58	0.028685	0.554115
2.59	0.02887	0.622467
2.6	0.02899	0.586516
2.61	0.028977	0.552045
2.62	0.028878	0.602332
2.63	0.02856	0.608846
2.64	0.028403	0.522442
2.65	0.028785	0.428025
2.66	0.028157	0.451083
2.67	0.02861	0.525427
2.68	0.02816	0.603309
2.69	0.028037	0.67792
2.7	0.02795	0.724335
2.71	0.028135	0.663154
2.72	0.02816	0.545993
2.73	0.027983	0.492516
2.74	0.027047	0.430991
2.75	0.026738	0.415247
2.76	0.02659	0.431982
2.77	0.02681	0.344296
2.78	0.027492	0.471155
2.79	0.027312	0.486739
2.8	0.027553	0.580844
2.81	0.027858	0.681764
2.82	0.028233	0.699815
2.83	0.028288	0.661688
2.84	0.02849	0.679763
2.85	0.028362	0.630511
2.86	0.027575	0.629457
2.87	0.027435	0.616131
2.88	0.026748	0.576243
2.89	0.027195	0.505183
2.9	0.026455	0.516204
2.91	0.026815	0.513023
2.92	0.027127	0.627909
2.93	0.027742	0.631993

2.94	0.027485	0.609946
2.95	0.027197	0.521477
2.96	0.027293	0.549957
2.97	0.02734	0.48732
2.98	0.02762	0.528483
2.99	0.02747	0.570395
3	0.02702	0.606058
3.01	0.026707	0.561164
3.02	0.02664	0.549991
3.03	0.026928	0.529086
3.04	0.02688	0.469473
3.05	0.026562	0.519337
3.06	0.026302	0.478641
3.07	0.0269	0.539019
3.08	0.027193	0.564302
3.09	0.027255	0.531389
3.1	0.026718	0.538618
3.11	0.02638	0.56306
3.12	0.025995	0.541497
3.13	0.026408	0.447996
3.14	0.026623	0.390987
3.15	0.026972	0.425766
3.16	0.02741	0.514966
3.17	0.02713	0.500129
3.18	0.026527	0.457684
3.19	0.025718	0.44108
3.2	0.025475	0.473451
3.21	0.025632	0.463978
3.22	0.026068	0.476441
3.23	0.025523	0.553676
3.24	0.025397	0.533218
3.25	0.025468	0.559525
3.26	0.025243	0.520696
3.27	0.025545	0.539341
3.28	0.025448	0.46946
3.29	0.02521	0.459653
3.3	0.024735	0.383873

3.31	0.025018	0.452359
3.32	0.025218	0.456111
3.33	0.025483	0.446465
3.34	0.02535	0.515178
3.35	0.025105	0.517015
3.36	0.02482	0.477119
3.37	0.024795	0.45188
3.38	0.02521	0.407646
3.39	0.02492	0.42237
3.4	0.025077	0.386335
3.41	0.024865	0.322954
3.42	0.025185	0.396476
3.43	0.02532	0.397661
3.44	0.025153	0.446158
3.45	0.025493	0.443117
3.46	0.025048	0.439769
3.47	0.025745	0.540048
3.48	0.02482	0.509604
3.49	0.02505	0.496136
3.5	0.025177	0.494565
3.51	0.025097	0.440846
3.52	0.025515	0.475483
3.53	0.025188	0.407525
3.54	0.025485	0.414675
3.55	0.025227	0.405395
3.56	0.024807	0.513421
3.57	0.024768	0.502027
3.58	0.02456	0.48296
3.59	0.02508	0.439314
3.6	0.024862	0.427742
3.61	0.02452	0.394615
3.62	0.025185	0.371475
3.63	0.025173	0.326135
3.64	0.025487	0.418033
3.65	0.025108	0.40993
3.66	0.025757	0.431782
3.67	0.02559	0.361498

3.68	0.02556	0.419335
3.69	0.025605	0.412997
3.7	0.025247	0.412765
3.71	0.02463	0.434171
3.72	0.023795	0.465181
3.73	0.02332	0.491864
3.74	0.023813	0.537828
3.75	0.023575	0.453274
3.76	0.023838	0.473551
3.77	0.023492	0.4314
3.78	0.023502	0.483747
3.79	0.02361	0.483251
3.8	0.0239	0.45127
3.81	0.024178	0.463795
3.82	0.02466	0.413338
3.83	0.024135	0.427923
3.84	0.024175	0.428609
3.85	0.023822	0.482425
3.86	0.024055	0.468991
3.87	0.02413	0.41687
3.88	0.024252	0.380072
3.89	0.024233	0.383034
3.9	0.024255	0.384997
3.91	0.024195	0.414689
3.92	0.02381	0.435603
3.93	0.023795	0.455152
3.94	0.023183	0.449444
3.95	0.023107	0.372996
3.96	0.02301	0.363269
3.97	0.023617	0.368179
3.98	0.023267	0.342787
3.99	0.023545	0.403489
4	0.023283	0.367711
4.01	0.023615	0.379105
4.02	0.023585	0.368947
4.03	0.02324	0.352606
4.04	0.023137	0.345217

4.05	0.02255	0.378903
4.06	0.022905	0.3787
4.07	0.02315	0.346694
4.08	0.023002	0.303806
4.09	0.02288	0.320604
4.1	0.023103	0.367634
4.11	0.022978	0.409356
4.12	0.023148	0.363779
4.13	0.02248	0.391146
4.14	0.022883	0.368275
4.15	0.022703	0.350699
4.16	0.022985	0.327561
4.17	0.022935	0.420024
4.18	0.023265	0.409784
4.19	0.023035	0.40712
4.2	0.023207	0.361938
4.21	0.02279	0.453288
4.22	0.022818	0.392674
4.23	0.0227	0.394447
4.24	0.023145	0.322704
4.25	0.023295	0.345513
4.26	0.023825	0.337716
4.27	0.02352	0.38462
4.28	0.022775	0.400048
4.29	0.022795	0.359504
4.3	0.022815	0.315098
4.31	0.023488	0.334119
4.32	0.02262	0.29789
4.33	0.022855	0.360078
4.34	0.02208	0.362953
4.35	0.0224	0.391163
4.36	0.022722	0.399178
4.37	0.023165	0.393269
4.38	0.02269	0.378202
4.39	0.02266	0.38188
4.4	0.02333	0.380949
4.41	0.023332	0.315057

4.42	0.023152	0.371274
4.43	0.022097	0.371339
4.44	0.021795	0.416209
4.45	0.02151	0.355557
4.46	0.022215	0.308681

A.4 chi323.inp

0	0.0009	10.33776
0.01	0.146687	5.715141
0.02	0.231325	1.717641
0.03	0.250375	1.518846
0.04	0.257025	1.644899
0.05	0.257	1.655798
0.06	0.2591	1.83601
0.07	0.258875	1.886962
0.08	0.258	2.084818
0.09	0.256025	2.146771
0.1	0.255075	2.409168
0.11	0.252925	2.537458
0.12	0.25125	2.638516
0.13	0.2492	2.617034
0.14	0.249125	2.574262
0.15	0.24795	2.665064
0.16	0.24665	2.472374
0.17	0.24435	2.469636
0.18	0.241475	2.607929
0.19	0.238525	2.866768
0.2	0.23695	3.008759
0.21	0.237025	2.617612
0.22	0.23615	2.39663
0.23	0.232975	2.416297
0.24	0.22995	2.434646
0.25	0.2268	2.548738
0.26	0.225325	2.481819
0.27	0.2238	2.523846

0.28	0.221625	2.464202
0.29	0.219775	2.4577
0.3	0.217525	2.475377
0.31	0.215075	2.55809
0.32	0.21215	2.583002
0.33	0.208925	2.51183
0.34	0.205925	2.515331
0.35	0.204725	2.546427
0.36	0.203125	2.549371
0.37	0.202075	2.612488
0.38	0.1998	2.608128
0.39	0.19745	2.544753
0.4	0.194775	2.639588
0.41	0.193275	2.559992
0.42	0.19105	2.586896
0.43	0.189925	2.532895
0.44	0.189275	2.643197
0.45	0.18645	2.687161
0.46	0.185625	2.655226
0.47	0.1829	2.522604
0.48	0.180125	2.388352
0.49	0.177875	2.32457
0.5	0.177125	2.464337
0.51	0.174675	2.470025
0.52	0.173075	2.444332
0.53	0.172475	2.486408
0.54	0.170925	2.55124
0.55	0.169025	2.624911
0.56	0.16715	2.567496
0.57	0.165075	2.58607
0.58	0.162075	2.494987
0.59	0.1615	2.650736
0.6	0.15905	2.511235
0.61	0.1574	2.555347
0.62	0.156675	2.512653
0.63	0.1549	2.408111
0.64	0.154725	2.398407

0.65	0.1524	2.334438
0.66	0.151225	2.424189
0.67	0.149125	2.396558
0.68	0.146325	2.282343
0.69	0.144175	2.179562
0.7	0.142325	2.112997
0.71	0.1404	2.063314
0.72	0.13835	2.03374
0.73	0.1363	1.937335
0.74	0.136475	2.137621
0.75	0.135375	2.209214
0.76	0.134325	2.210677
0.77	0.132425	2.141594
0.78	0.130675	2.042945
0.79	0.129625	2.064774
0.8	0.128075	1.976282
0.81	0.12665	1.935192
0.82	0.125725	2.033165
0.83	0.12345	1.968832
0.84	0.12225	1.934606
0.85	0.12095	1.866771
0.86	0.12055	1.962286
0.87	0.119275	1.891109
0.88	0.11825	1.830528
0.89	0.116125	1.703044
0.9	0.116072	1.793759
0.91	0.1142	1.740838
0.92	0.114108	1.823185
0.93	0.112285	1.747518
0.94	0.110963	1.693625
0.95	0.109652	1.654828
0.96	0.108842	1.65776
0.97	0.107595	1.611469
0.98	0.106478	1.572198
0.99	0.106292	1.55069
1	0.105155	1.429854
1.01	0.104038	1.461608

1.02	0.102462	1.436254
1.03	0.10081	1.47463
1.04	0.101072	1.450206
1.05	0.099513	1.286536
1.06	0.098225	1.35891
1.07	0.097695	1.356864
1.08	0.097613	1.419137
1.09	0.096475	1.441189
1.1	0.09676	1.447156
1.11	0.09595	1.383914
1.12	0.094692	1.318392
1.13	0.092878	1.297987
1.14	0.092705	1.418604
1.15	0.090493	1.29157
1.16	0.090915	1.368924
1.17	0.089975	1.337095
1.18	0.08853	1.204256
1.19	0.087555	1.305338
1.2	0.086578	1.2469
1.21	0.085818	1.172544
1.22	0.08459	1.165445
1.23	0.085028	1.174548
1.24	0.084835	1.205961
1.25	0.08503	1.227843
1.26	0.08333	1.092137
1.27	0.083235	1.003652
1.28	0.082028	1.00694
1.29	0.081735	1.101438
1.3	0.081147	1.10146
1.31	0.080367	1.027749
1.32	0.080727	1.031823
1.33	0.079685	1.008999
1.34	0.07905	1.084197
1.35	0.078168	1.066436
1.36	0.077665	1.03782
1.37	0.076035	0.985382
1.38	0.074982	0.909216

1.39	0.07498	0.938367
1.4	0.074692	1.011539
1.41	0.07526	1.103093
1.42	0.074095	1.042477
1.43	0.073468	0.990263
1.44	0.07237	0.979854
1.45	0.07096	0.914444
1.46	0.06962	0.85962
1.47	0.069795	0.875314
1.48	0.070523	0.892323
1.49	0.070135	0.794097
1.5	0.069215	0.820764
1.51	0.069295	0.889532
1.52	0.068348	0.807116
1.53	0.068087	0.852446
1.54	0.067748	0.773398
1.55	0.06823	0.808498
1.56	0.067272	0.787681
1.57	0.0681	0.935917
1.58	0.066922	0.852333
1.59	0.06671	0.775438
1.6	0.065865	0.691984
1.61	0.065485	0.718721
1.62	0.064992	0.744213
1.63	0.064327	0.724612
1.64	0.06432	0.750443
1.65	0.06389	0.80013
1.66	0.06329	0.698067
1.67	0.06202	0.672602
1.68	0.062988	0.742938
1.69	0.062137	0.775145
1.7	0.062908	0.892379
1.71	0.062935	0.780975
1.72	0.062695	0.818529
1.73	0.061703	0.739872
1.74	0.060105	0.745406
1.75	0.059785	0.621622

1.76	0.058928	0.637911
1.77	0.05824	0.496247
1.78	0.05899	0.593997
1.79	0.05895	0.600349
1.8	0.05922	0.638476
1.81	0.059075	0.687468
1.82	0.059005	0.628721
1.83	0.058283	0.653827
1.84	0.05777	0.62535
1.85	0.057728	0.682449
1.86	0.05763	0.700228
1.87	0.056653	0.645781
1.88	0.056173	0.496691
1.89	0.05573	0.472141
1.9	0.05526	0.483238
1.91	0.055137	0.489467
1.92	0.05555	0.572673
1.93	0.055078	0.549268
1.94	0.05462	0.642444
1.95	0.054363	0.552216
1.96	0.053268	0.551643
1.97	0.052843	0.388063
1.98	0.052818	0.416665
1.99	0.053477	0.369249
2	0.05239	0.419825
2.01	0.05199	0.403553
2.02	0.051382	0.480729
2.03	0.05008	0.466018
2.04	0.051562	0.50668
2.05	0.051158	0.547717
2.06	0.051408	0.606289
2.07	0.050583	0.498267
2.08	0.050603	0.517709
2.09	0.05028	0.475967
2.1	0.050232	0.426266
2.11	0.04972	0.526449
2.12	0.0488	0.501881

2.13	0.04941	0.536097
2.14	0.04887	0.456954
2.15	0.048622	0.511851
2.16	0.049208	0.534665
2.17	0.04877	0.524657
2.18	0.049063	0.482414
2.19	0.04886	0.488376
2.2	0.048798	0.392817
2.21	0.048415	0.53822
2.22	0.048317	0.482965
2.23	0.048078	0.547927
2.24	0.046918	0.455102
2.25	0.046755	0.460384
2.26	0.046915	0.403942
2.27	0.047122	0.323345
2.28	0.046378	0.361563
2.29	0.046492	0.350952
2.3	0.045905	0.410568
2.31	0.045817	0.3226
2.32	0.04621	0.388343
2.33	0.046305	0.38926
2.34	0.04589	0.379362
2.35	0.044987	0.398608
2.36	0.044033	0.291184
2.37	0.044687	0.347386
2.38	0.044305	0.281478
2.39	0.044167	0.268418
2.4	0.043623	0.248614
2.41	0.04346	0.393627
2.42	0.043217	0.442812
2.43	0.043095	0.565732
2.44	0.04331	0.522615
2.45	0.043373	0.593077
2.46	0.042917	0.379666
2.47	0.042645	0.393325
2.48	0.043498	0.384306
2.49	0.043292	0.427248

2.5	0.04372	0.407047
2.51	0.04325	0.401164
2.52	0.04312	0.386932
2.53	0.04376	0.521046
2.54	0.042717	0.458504
2.55	0.04266	0.544171
2.56	0.041822	0.467501
2.57	0.042015	0.435408
2.58	0.04116	0.347763
2.59	0.041545	0.368885
2.6	0.04098	0.385459
2.61	0.039753	0.194882
2.62	0.041217	0.26309
2.63	0.041675	0.292167
2.64	0.042095	0.360038
2.65	0.041775	0.483535
2.66	0.040895	0.351041
2.67	0.041072	0.386495
2.68	0.040502	0.26793
2.69	0.041217	0.384844
2.7	0.04025	0.320975
2.71	0.039828	0.318877
2.72	0.039323	0.538217
2.73	0.039328	0.502502
2.74	0.039703	0.500578
2.75	0.039885	0.392728
2.76	0.04034	0.312811
2.77	0.039995	0.170236
2.78	0.040705	0.265277
2.79	0.040275	0.25307
2.8	0.040328	0.303998
2.81	0.040177	0.331558
2.82	0.040058	0.367172
2.83	0.039155	0.414752
2.84	0.03966	0.499193
2.85	0.038538	0.35023
2.86	0.038685	0.369438

2.87	0.038422	0.330376
2.88	0.038062	0.248894
2.89	0.039027	0.368695
2.9	0.038422	0.370703
2.91	0.038497	0.441299
2.92	0.03804	0.445757
2.93	0.037585	0.511707
2.94	0.037858	0.584356
2.95	0.037102	0.448969
2.96	0.037765	0.483295
2.97	0.038062	0.459437
2.98	0.03773	0.368341
2.99	0.03795	0.376465
3	0.038312	0.446533
3.01	0.03816	0.4265
3.02	0.038067	0.375411
3.03	0.038178	0.414046
3.04	0.03751	0.330249
3.05	0.038418	0.435182
3.06	0.037835	0.46322
3.07	0.037762	0.495203
3.08	0.03741	0.53026
3.09	0.037755	0.507336
3.1	0.037233	0.397304
3.11	0.03777	0.377468
3.12	0.036963	0.347738
3.13	0.037115	0.384185
3.14	0.036615	0.362074
3.15	0.036588	0.400713
3.16	0.036815	0.363032
3.17	0.037117	0.483884
3.18	0.037225	0.485458
3.19	0.037542	0.512331
3.2	0.03714	0.489872
3.21	0.036597	0.456862
3.22	0.036145	0.35186
3.23	0.036897	0.360983

3.24	0.03726	0.441294
3.25	0.035967	0.306987
3.26	0.03579	0.357647
3.27	0.036068	0.365463
3.28	0.036395	0.475325
3.29	0.036013	0.403845
3.3	0.037082	0.492863
3.31	0.035937	0.365812
3.32	0.035603	0.37527
3.33	0.035403	0.397541
3.34	0.035135	0.376078
3.35	0.036147	0.381376
3.36	0.035037	0.365462
3.37	0.035408	0.38524
3.38	0.03576	0.428575
3.39	0.035335	0.327691
3.4	0.036057	0.356336
3.41	0.035228	0.40516
3.42	0.035287	0.430261
3.43	0.034598	0.381262
3.44	0.03469	0.398046
3.45	0.034435	0.483866
3.46	0.03476	0.386114
3.47	0.034463	0.353698
3.48	0.03459	0.341664
3.49	0.03492	0.344895
3.5	0.034963	0.431006
3.51	0.033325	0.267622
3.52	0.034365	0.393667
3.53	0.03501	0.397082
3.54	0.034188	0.391153
3.55	0.034732	0.263218
3.56	0.03434	0.313606
3.57	0.034502	0.350665
3.58	0.034188	0.301451
3.59	0.034658	0.37387
3.6	0.03485	0.31644

3.61	0.034763	0.296575
3.62	0.035365	0.437257
3.63	0.035237	0.43982
3.64	0.034397	0.388027
3.65	0.034263	0.438007
3.66	0.03358	0.352716
3.67	0.032857	0.322916
3.68	0.032842	0.313482
3.69	0.033247	0.317079
3.7	0.033723	0.291774
3.71	0.032773	0.284359
3.72	0.03256	0.283623
3.73	0.031997	0.243334
3.74	0.032762	0.26831
3.75	0.032745	0.281389
3.76	0.032915	0.365121
3.77	0.03279	0.436374
3.78	0.03189	0.529521
3.79	0.031503	0.418358
3.8	0.031762	0.339492
3.81	0.031962	0.288938
3.82	0.031988	0.310388
3.83	0.032775	0.372484
3.84	0.032125	0.429024
3.85	0.032532	0.403119
3.86	0.032058	0.378051
3.87	0.032125	0.335898
3.88	0.03235	0.342186
3.89	0.03304	0.433504
3.9	0.032093	0.439038
3.91	0.032128	0.456423
3.92	0.030985	0.367103
3.93	0.03126	0.428535
3.94	0.031585	0.367745
3.95	0.031255	0.459447
3.96	0.031575	0.376101
3.97	0.031422	0.396095

3.98	0.031107	0.328279
3.99	0.03105	0.428729
4	0.030707	0.350861
4.01	0.031085	0.342277
4.02	0.030537	0.309691
4.03	0.030767	0.429676
4.04	0.030695	0.474735
4.05	0.031092	0.503443
4.06	0.031475	0.449919
4.07	0.03182	0.477258
4.08	0.030965	0.480299
4.09	0.030877	0.389881
4.1	0.030415	0.436065
4.11	0.030292	0.414528
4.12	0.03032	0.450775
4.13	0.030732	0.442382
4.14	0.030485	0.445402
4.15	0.03027	0.517859
4.16	0.029212	0.356708
4.17	0.030305	0.407309
4.18	0.029882	0.303346
4.19	0.03033	0.38847
4.2	0.029468	0.315332
4.21	0.030605	0.427048
4.22	0.03047	0.421479
4.23	0.03028	0.368882
4.24	0.030373	0.374273
4.25	0.030485	0.378242
4.26	0.03023	0.327078
4.27	0.03013	0.400913
4.28	0.029562	0.366185
4.29	0.029675	0.44744
4.3	0.029225	0.408974
4.31	0.03008	0.453522
4.32	0.030122	0.370576
4.33	0.029935	0.404706
4.34	0.029362	0.335118

4.35	0.029415	0.340467
4.36	0.029763	0.370262
4.37	0.029845	0.401846
4.38	0.029423	0.408051
4.39	0.029853	0.334345
4.4	0.029982	0.294409
4.41	0.03013	0.404436
4.42	0.029568	0.352702
4.43	0.02941	0.336797
4.44	0.029515	0.353499
4.45	0.02925	0.391587
4.46	0.029462	0.489817

Appendix B

Perturbation analysis of liquid phase cyclohexadienyl kinetics

```
> restart;
> with(linalg):
```

Warning, the protected names norm and trace have been redefined and unprotected

```
> A :=matrix(3,3,[-(k1a+k1b+k3)*x, k_1a, k_1b, k1a*x, -(k_1a+k4a),
0,
> k1b*x, 0, -k_1b]);
```

$$A := \begin{bmatrix} -(k1a + k1b + k3)\,x & k\_1a & k\_1b \\ k1a\,x & -k\_1a - k4a & 0 \\ k1b\,x & 0 & -k\_1b \end{bmatrix}$$

```
> B :=matrix(3,3,[-(3+epsilon)-lambda, gamma, gamma, 2,
> -(gamma+delta)-lambda, 0, 1, 0, -(gamma+lambda)]);
```

$$B := \begin{bmatrix} -3 - \varepsilon - \lambda & \gamma & \gamma \\ 2 & -\gamma - \delta - \lambda & 0 \\ 1 & 0 & -\gamma - \lambda \end{bmatrix}$$

```
> f1:=det(B);
```

$$f1 := -3\,\lambda\gamma - 2\,\delta\gamma - 3\,\lambda\delta - 3\,\lambda^2 - \varepsilon\,\gamma^2 - 2\,\varepsilon\gamma\lambda - \varepsilon\delta\gamma - \varepsilon\delta\lambda - \varepsilon\,\lambda^2 - \lambda\gamma^2 - 2\,\lambda^2\gamma$$
$$- \lambda\delta\gamma - \lambda^2\delta - \lambda^3$$

```
> lambda := a0+a1*epsilon+a2*delta;
```

$$\lambda := a0 + a1\,\varepsilon + a2\,\delta$$

```
> f2:=collect(f1,epsilon);
```

$$f2 := (-a1^2 - a1^3)\,\varepsilon^3 +$$
$$(-3\,(a0 + a2\,\delta)\,a1^2 - a1\,\delta - 3\,a1^2 - 2\,a1^2\gamma - a1^2\delta - 2\,a1\,\gamma - 2\,(a0 + a2\,\delta)\,a1)\,\varepsilon^2$$
$$+ (-\gamma^2 - a1\,\delta\gamma - 4\,(a0 + a2\,\delta)\,a1\,\gamma - (a0 + a2\,\delta)\,\delta - 3\,a1\,\delta - 3\,a1\,\gamma$$
$$- 3\,(a0 + a2\,\delta)^2\,a1 - \delta\gamma - 2\,(a0 + a2\,\delta)\,a1\,\delta - a1\,\gamma^2 - 6\,(a0 + a2\,\delta)\,a1$$
$$- 2\,(a0 + a2\,\delta)\,\gamma - (a0 + a2\,\delta)^2)\varepsilon - 3\,(a0 + a2\,\delta)\,\gamma - (a0 + a2\,\delta)^3 - 2\,\delta\gamma$$
$$- 3\,(a0 + a2\,\delta)\,\delta - (a0 + a2\,\delta)\,\gamma^2 - 3\,(a0 + a2\,\delta)^2 - 2\,(a0 + a2\,\delta)^2\,\gamma$$
$$- (a0 + a2\,\delta)^2\,\delta - (a0 + a2\,\delta)\,\delta\gamma$$

```
> f3:=coeff(f2,epsilon,0);
```

$$f3 := -3\,(a0 + a2\,\delta)\,\gamma - (a0 + a2\,\delta)^3 - 2\,\delta\gamma - 3\,(a0 + a2\,\delta)\,\delta - (a0 + a2\,\delta)\,\gamma^2$$
$$- 3\,(a0 + a2\,\delta)^2 - 2\,(a0 + a2\,\delta)^2\,\gamma - (a0 + a2\,\delta)^2\,\delta - (a0 + a2\,\delta)\,\delta\gamma$$

```
> f4:=collect(f3,delta);
```

$$f4 := (-a2^3 - a2^2)\,\delta^3 + (-2\,a0\,a2 - 3\,a2^2 - 3\,a2 - 3\,a0\,a2^2 - 2\,a2^2\gamma - a2\,\gamma)\,\delta^2$$
$$+ (-a0^2 - 2\,\gamma - 3\,a0^2\,a2 - 6\,a0\,a2 - a2\,\gamma^2 - 3\,a0 - a0\,\gamma - 3\,a2\,\gamma - 4\,a0\,a2\,\gamma)\,\delta$$
$$- 3\,a0\,\gamma - 2\,a0^2\,\gamma - a0^3 - 3\,a0^2 - a0\,\gamma^2$$

```
> f5:=coeff(f4,delta,0);
```

$$f5 := -3\,a0\,\gamma - 2\,a0^2\,\gamma - a0^3 - 3\,a0^2 - a0\,\gamma^2$$

```
> l0:=solve(f5=0,a0);
```

Figure B-2:

$$l0 := 0, -\gamma, -\gamma - 3$$

```
>  f6:=collect(f1,epsilon);
```

$$f6 := (-a1^2 - a1^3)\,\varepsilon^3 +$$

$$(-3\,(a0 + a2\,\delta)\,a1^2 - a1\,\delta - 3\,a1^2 - 2\,a1^2\,\gamma - a1^2\,\delta - 2\,a1\,\gamma - 2\,(a0 + a2\,\delta)\,a1)\,\varepsilon^2$$

$$+ (-\gamma^2 - a1\,\delta\,\gamma - 4\,(a0 + a2\,\delta)\,a1\,\gamma - (a0 + a2\,\delta)\,\delta - 3\,a1\,\delta - 3\,a1\,\gamma$$

$$- 3\,(a0 + a2\,\delta)^2\,a1 - \delta\,\gamma - 2\,(a0 + a2\,\delta)\,a1\,\delta - a1\,\gamma^2 - 6\,(a0 + a2\,\delta)\,a1$$

$$- 2\,(a0 + a2\,\delta)\,\gamma - (a0 + a2\,\delta)^2)\varepsilon - 3\,(a0 + a2\,\delta)\,\gamma - (a0 + a2\,\delta)^3 - 2\,\delta\,\gamma$$

$$- 3\,(a0 + a2\,\delta)\,\delta - (a0 + a2\,\delta)\,\gamma^2 - 3\,(a0 + a2\,\delta)^2 - 2\,(a0 + a2\,\delta)^2\,\gamma$$

$$- (a0 + a2\,\delta)^2\,\delta - (a0 + a2\,\delta)\,\delta\,\gamma$$

```
>  f7:=coeff(f6,epsilon,1);
```

$$f7 := -\gamma^2 - a1\,\delta\,\gamma - 4\,(a0 + a2\,\delta)\,a1\,\gamma - (a0 + a2\,\delta)\,\delta - 3\,a1\,\delta - 3\,a1\,\gamma$$

$$- 3\,(a0 + a2\,\delta)^2\,a1 - \delta\,\gamma - 2\,(a0 + a2\,\delta)\,a1\,\delta - a1\,\gamma^2 - 6\,(a0 + a2\,\delta)\,a1$$

$$- 2\,(a0 + a2\,\delta)\,\gamma - (a0 + a2\,\delta)^2$$

```
>  f8:=collect(f7,delta);
```

$$f8 := (-3\,a2^2\,a1 - 2\,a2\,a1 - a2 - a2^2)\,\delta^2 + (-2\,a2\,\gamma - 6\,a0\,a2\,a1 - a1\,\gamma - 4\,a2\,a1\,\gamma$$

$$- 2\,a0\,a1 - a0 - \gamma - 6\,a2\,a1 - 3\,a1 - 2\,a0\,a2)\delta - \gamma^2 - a1\,\gamma^2 - 4\,a0\,a1\,\gamma - 3\,a1\,\gamma$$

$$- 2\,a0\,\gamma - a0^2 - 6\,a0\,a1 - 3\,a0^2\,a1$$

```
>  f9:=coeff(f8,delta,0);
```

$$f9 := -\gamma^2 - a1\,\gamma^2 - 4\,a0\,a1\,\gamma - 3\,a1\,\gamma - 2\,a0\,\gamma - a0^2 - 6\,a0\,a1 - 3\,a0^2\,a1$$

```
>  f10:=subs(a0=l0[1],f9);
```

$$f10 := -\gamma^2 - a1\,\gamma^2 - 3\,a1\,\gamma$$

```
>  l1[1]:=solve(f10=0,a1);
```

$$l1_1 := -\frac{\gamma}{\gamma + 3}$$

```
>  f11:=subs(a0=l0[2],f9);
```

$$f11 := 3\,a1\,\gamma$$

```
>  l1[2]:=solve(f11,a1);
```

$$l1_2 := 0$$

```
>  f12:=subs(a0=l0[3],f9);
```

$$f12 := -\gamma^2 - a1\,\gamma^2 - 4\,(-\gamma - 3)\,a1\,\gamma - 3\,a1\,\gamma - 2\,(-\gamma - 3)\,\gamma - (-\gamma - 3)^2 - 6\,(-\gamma - 3)\,a1$$

$$- 3\,(-\gamma - 3)^2\,a1$$

```
>  l1[3]:=solve(f12,a1);
```

$$l1_3 := -\frac{3}{\gamma + 3}$$

```
>  f13:=collect(f1,delta);
```

143

Figure B-3:

$f13 := (-a2^3 - a2^2)\,\delta^3 + ($

$-\varepsilon\,a2 - 3\,a2 - 2\,a2^2\,\gamma - \varepsilon\,a2^2 - 2\,(a0 + a1\,\varepsilon)\,a2 - a2\,\gamma - 3\,a2^2 - 3\,(a0 + a1\,\varepsilon)\,a2^2$

$)\delta^2 + (-3\,a0 - 3\,a1\,\varepsilon - 4\,(a0 + a1\,\varepsilon)\,a2\,\gamma - 2\,\gamma - \varepsilon\,\gamma - \varepsilon\,(a0 + a1\,\varepsilon) - 2\,\varepsilon\,\gamma\,a2$

$\quad - 2\,\varepsilon\,(a0 + a1\,\varepsilon)\,a2 - \%1 - a2\,\gamma^2 - 6\,(a0 + a1\,\varepsilon)\,a2 - 3\,\%1\,a2 - (a0 + a1\,\varepsilon)\,\gamma$

$\quad - 3\,a2\,\gamma)\delta - 3\,(a0 + a1\,\varepsilon)\,\gamma - \varepsilon\,\%1 - 2\,\%1\,\gamma - (a0 + a1\,\varepsilon)\,\gamma^2 - 3\,\%1$

$\quad - (a0 + a1\,\varepsilon)^3 - \varepsilon\,\gamma^2 - 2\,\varepsilon\,\gamma\,(a0 + a1\,\varepsilon)$

$\%1 := (a0 + a1\,\varepsilon)^2$

```
> f14:=coeff(f13,delta,1);
```

$f14 := -3\,a0 - 3\,a1\,\varepsilon - 4\,(a0 + a1\,\varepsilon)\,a2\,\gamma - 2\,\gamma - \varepsilon\,\gamma - \varepsilon\,(a0 + a1\,\varepsilon) - 2\,\varepsilon\,\gamma\,a2$

$\quad - 2\,\varepsilon\,(a0 + a1\,\varepsilon)\,a2 - (a0 + a1\,\varepsilon)^2 - a2\,\gamma^2 - 6\,(a0 + a1\,\varepsilon)\,a2 - 3\,(a0 + a1\,\varepsilon)^2\,a2$

$\quad - (a0 + a1\,\varepsilon)\,\gamma - 3\,a2\,\gamma$

```
> f15:=collect(f14,epsilon);
```

$f15 := (-3\,a1^2\,a2 - a1 - a1^2 - 2\,a2\,a1)\varepsilon^2 + (-2\,a2\,\gamma - 6\,a0\,a2\,a1 - a1\,\gamma - 4\,a2\,a1\,\gamma$

$\quad - 2\,a0\,a1 - a0 - \gamma - 6\,a2\,a1 - 3\,a1 - 2\,a0\,a2)\varepsilon - a0^2 - 2\,\gamma - 3\,a0^2\,a2 - 6\,a0\,a2$

$\quad - a2\,\gamma^2 - 3\,a0 - a0\,\gamma - 3\,a2\,\gamma - 4\,a0\,a2\,\gamma$

```
> f16:=coeff(f15,epsilon,0);
```

$f16 := -a0^2 - 2\,\gamma - 3\,a0^2\,a2 - 6\,a0\,a2 - a2\,\gamma^2 - 3\,a0 - a0\,\gamma - 3\,a2\,\gamma - 4\,a0\,a2\,\gamma$

```
> f17:=subs(a0=l0[1],f16);
```

$$f17 := -2\,\gamma - a2\,\gamma^2 - 3\,a2\,\gamma$$

```
> l2[1]:=solve(f17=0,a2);
```

$$l2_1 := -\frac{2}{\gamma + 3}$$

```
> f18:=subs(a0=l0[2],f16);
```

$$f18 := \gamma + 3\,a2\,\gamma$$

```
> l2[2]:=solve(f18=0,a2);
```

$$l2_2 := \frac{-1}{3}$$

```
> f19:=subs(a0=l0[3],f16);
```

$f19 := -(-\gamma - 3)^2 + \gamma - 3\,(-\gamma - 3)^2\,a2 - 6\,(-\gamma - 3)\,a2 - a2\,\gamma^2 + 9 - (-\gamma - 3)\,\gamma - 3\,a2\,\gamma$

$\quad - 4\,(-\gamma - 3)\,a2\,\gamma$

```
> l2[3]:=solve(f19=0,a2);
```

$$l2_3 := -\frac{2\,\gamma}{3\,(\gamma + 3)}$$

```
> e1:=l0[1]+l1[1]*epsilon+l2[1]*delta;
```

$$e1 := -\frac{\gamma\,\varepsilon}{\gamma + 3} - \frac{2\,\delta}{\gamma + 3}$$

```
> e2:=l0[2]+l1[2]*epsilon+l2[2]*delta;
```

Figure B-4:

$$e2 := -\gamma - \frac{\delta}{3}$$

```
>   e3:=10[3]+11[3]*epsilon+12[3]*delta;
```

$$e3 := -\gamma - 3 - \frac{3\,\varepsilon}{\gamma + 3} - \frac{2\,\gamma\,\delta}{3\,(\gamma + 3)}$$

```
>   subs({gamma = k_1a/k1b/x, epsilon = k3/k1b, delta = k4a/k1b/x},
>   e3);
```

$$-\frac{k_{\_}1a}{k1b\,x} - 3 - \frac{3\,k3}{(\frac{k_{\_}1a}{k1b\,x} + 3)\,k1b} - \frac{2\,k_{\_}1a\,k4a}{3\,k1b^2\,x^2\,(\frac{k_{\_}1a}{k1b\,x} + 3)}$$

```
>   expand(k1b*x*%);
```

$$-k_{\_}1a - 3\,k1b\,x - \frac{3\,x\,k3}{\frac{k_{\_}1a}{k1b\,x} + 3} - \frac{2\,k_{\_}1a\,k4a}{3\,k1b\,x\,(\frac{k_{\_}1a}{k1b\,x} + 3)}$$

145

Appendix C

GC/MS results

Figure C-1:

File   : C:\HPCHEM\1\DATA\KTJT420B.D
Operator   : FOL1/James
Acquired   : 20 Apr 2005 14:23   using AcqMethod KTJT0405
Instrument :   GC/MS Ins
Sample Name : Uv9 240 nm)1,4 cyclohexadiene
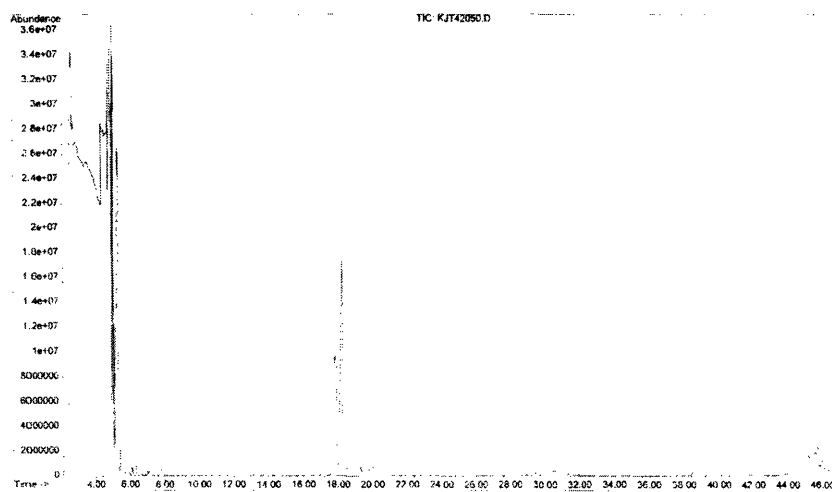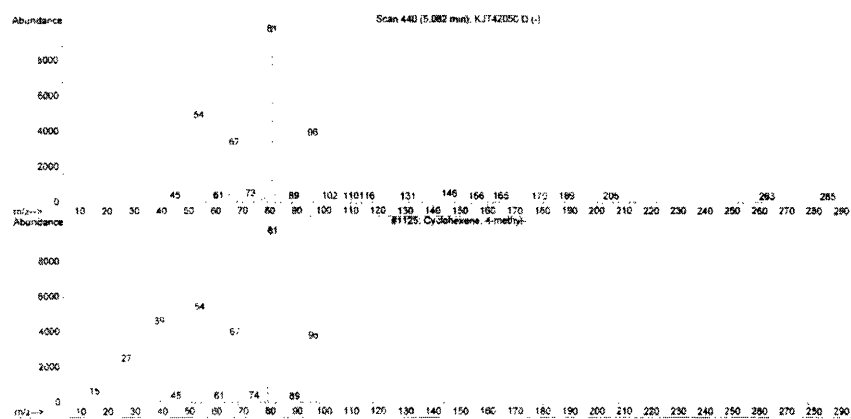Misc Info   : HP-17 MS, 30 M
Vial Number : 1
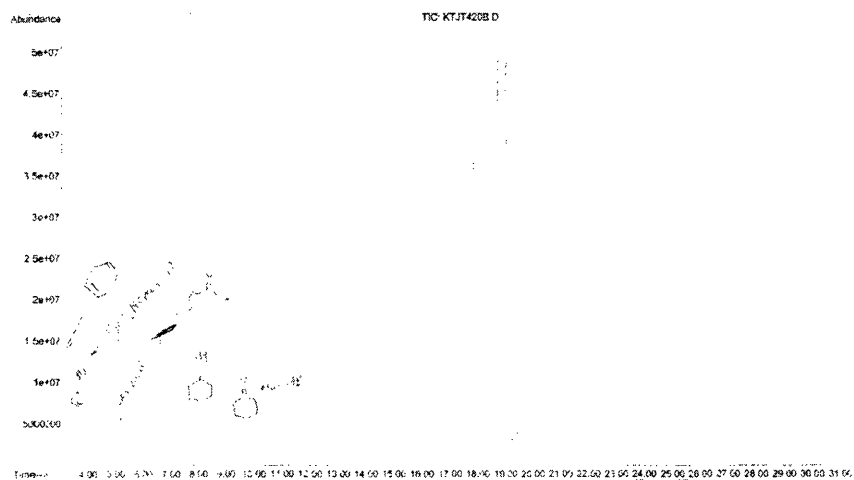
Figure C-2:
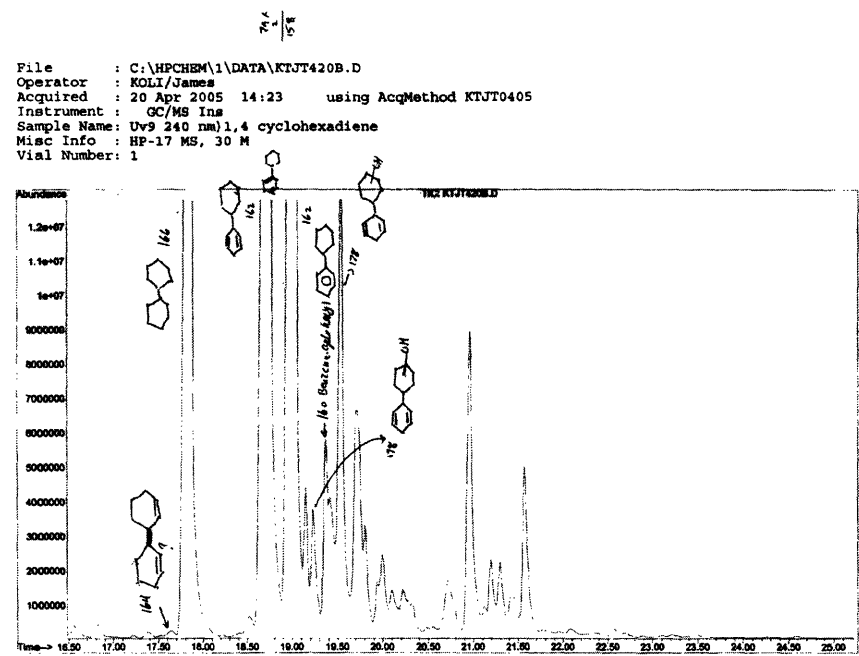
Figure C-3:

File   : C:\HPCHEM\1\DATA\KJT42050.D
Operator   : Koli/James
Acquired   : 20 Apr 05   10:43 am using AcqMethod KTJT
Instrument :   GC/MS Ins
Sample Name: UV(240 nm) Radition of 1,4-cycohexadiene
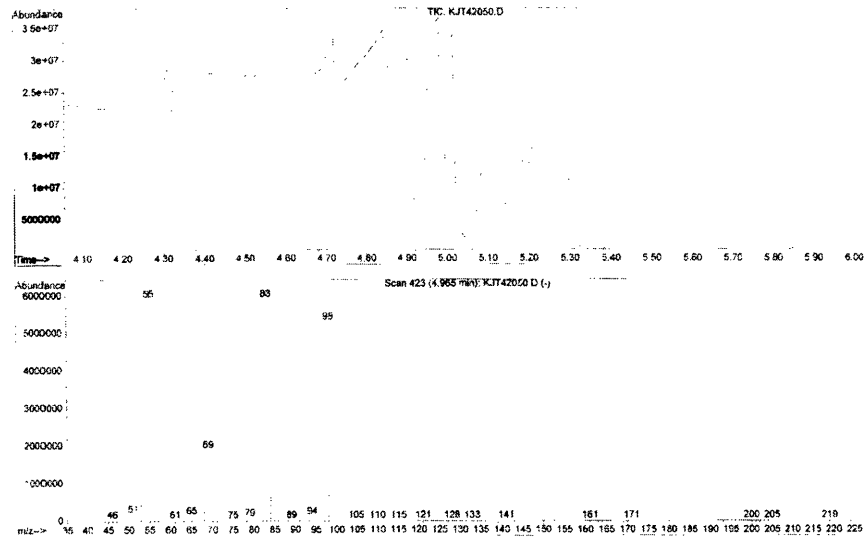Misc Info   : HP_5MS 30 m
Vial Number: 1

149
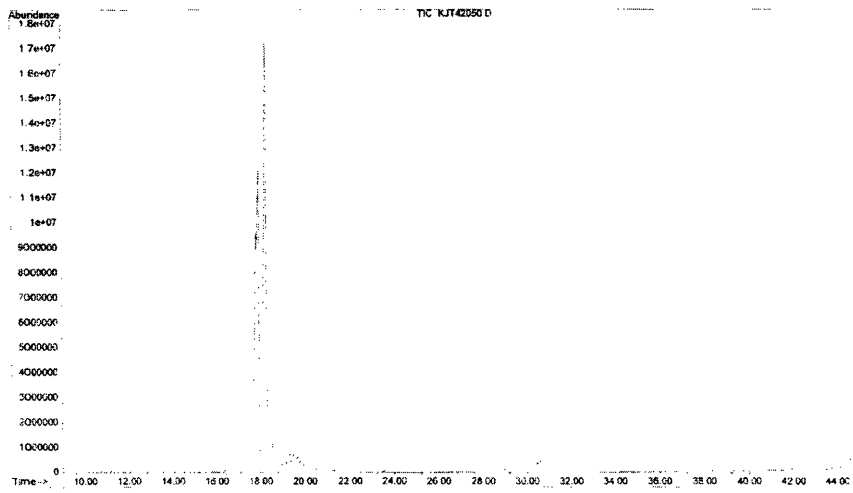
Figure C-4:

File   : C:\HPCHEM\1\DATA\KJT42050.D
Operator   : Koli/James
Acquired   : 20 Apr 05   10:43 am using AcqMethod KTJT
Instrument :   GC/MS Ins
Sample Name: UV(240 nm) Radition of 1,4-cycohexadiene
Misc Info : HP_5MS 30 m
Vial Number: 1

150
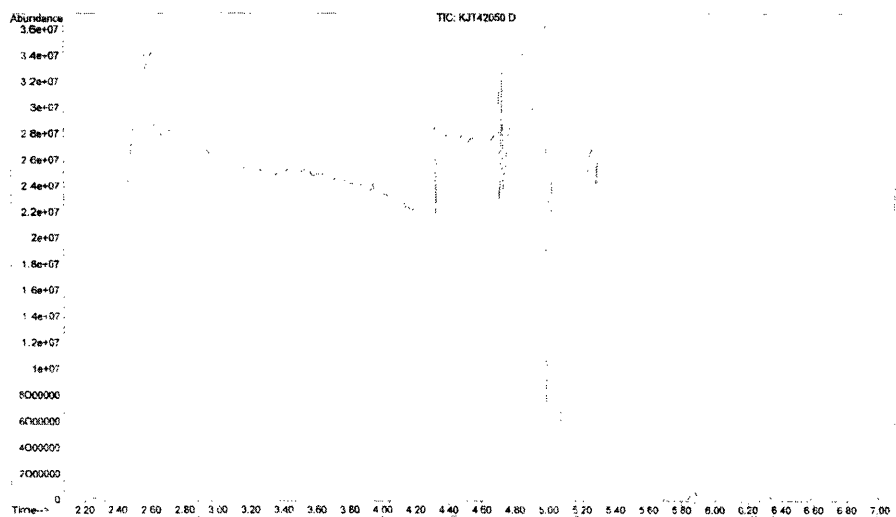
Figure C-5:

File   : C:\HPCHEM\1\DATA\KJT42050.D
Operator   : Koli/James
Acquired   : 20 Apr 05   10:43 am using AcqMethod KTJT
Instrument :   GC/MS Ins
Sample Name: UV(240 nm) Radition of 1,4-cycohexadiene
Misc Info : HP_5MS 30 m
Vial Number: 1

151

Figure C-6:

Library Searched : C:\DATABASE\NBS75K.L
Quality   : 97
ID   : Cyclohexene, 4-methyl-

Scan 440 (5.082 min), KJT4205C.D (-)

#1125: Cyclohexene, 4-methyl-

Figure C-7:

Figure C-8:

154

Figure C-9:

Abundance

Scan 730 (7.069 min): KJT42050 D (-)

58

8000

6000

4000

2000

53
49   62 67   71   77 81   85   91 95 99 105109 114   124 129   142   159 165 170   186
0
m/z--> 5 10 15 20 25 30 35 40 45 50 55 60 65 70 75 80 85 90 95 100 105 110 115 120 125 130 135 140 145 150 155 160 165 170 175 180 185 190

Abundance

#64177 Pentanal, 2,3-dimethyl-

58

8000

43

6000

4000

29

39

2000

85

15   49 53   65 69 73 77 81   97   114
0
m/z--> 5 10 15 20 25 30 35 40 45 50 55 60 65 70 75 80 85 90 95 100 105 110 115 120 125 130 135 140 145 150 155 160 165 170 175 180 185 190

155
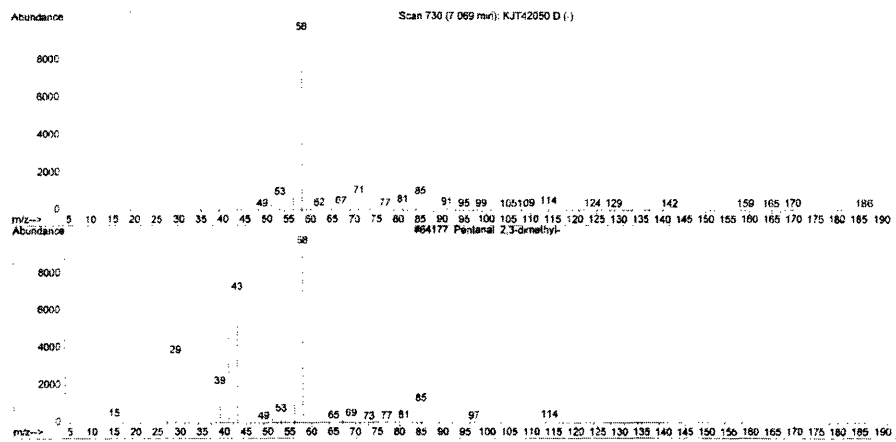
Figure C-10:

Library Searched : C:\DATABASE\NBS75K.L
Quality   : 94
ID   : 1,4-Cyclohexadiene, 1,2-dimethyl-

156

Figure C-11:

Scan 583 (8.061 min). KJT42050.D (-)
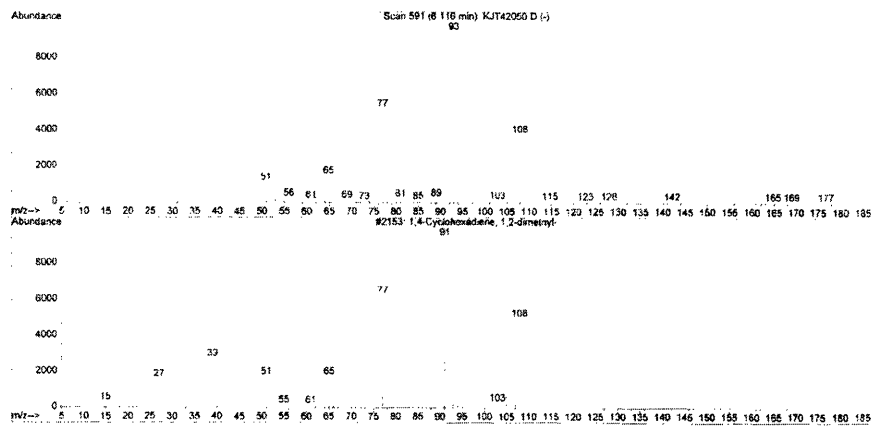
#2362- Cyclohexene, 1,2-dimethyl-

157

Figure C-12:

```
Library Searched     C:\DATABASE\NBS75K.L
Quality              93
ID                   4-Methyl-1,3-heptadiene (c,t)
```

Figure C-13:

Library Searched   C:\DATABASE\NBS75K.L
Quality   91
ID   Cyclohexane

Figure C-14:

160
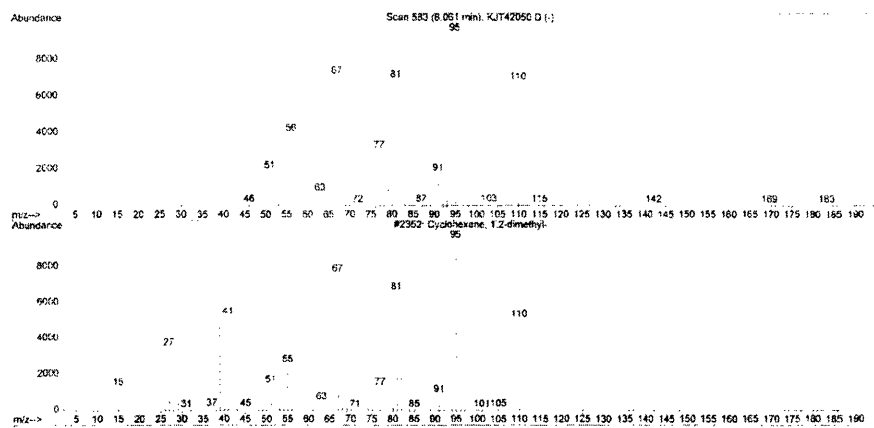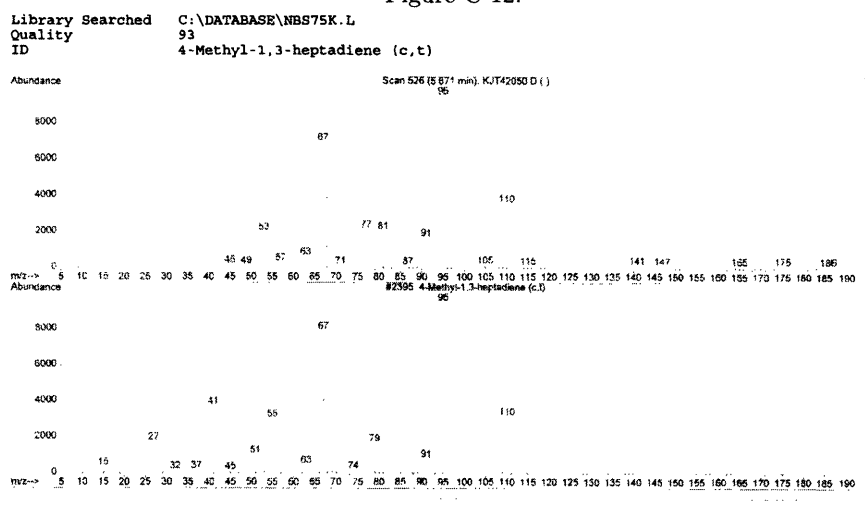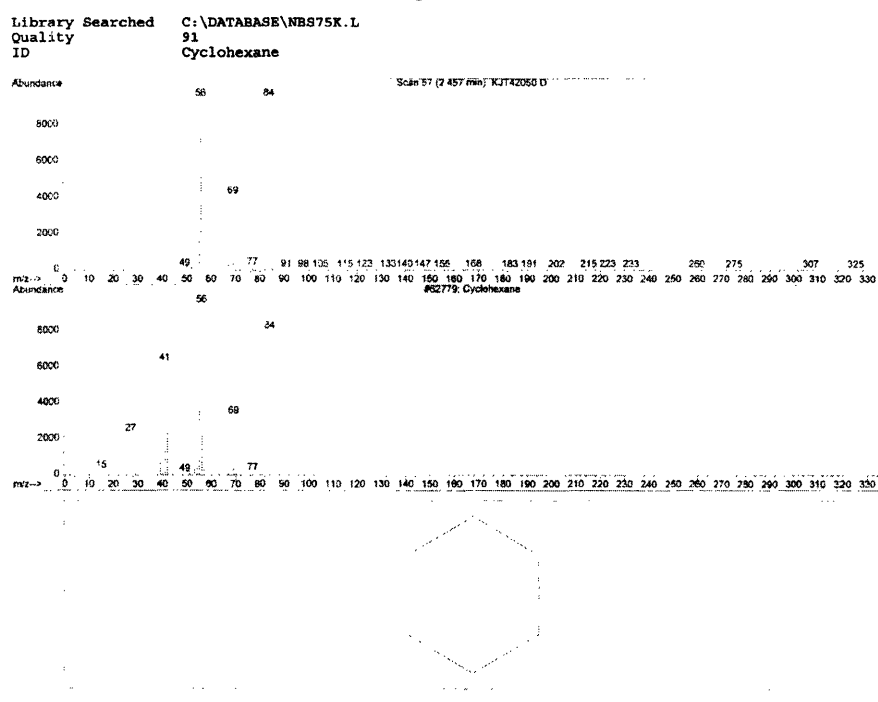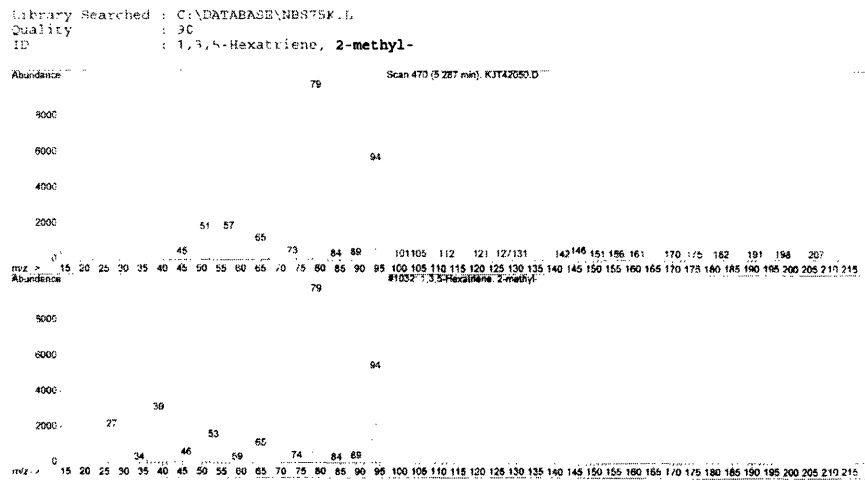
Figure C-15:

```
Library Searched    C:\DATABASE\NBS75K.L
Quality             89
ID                  1,4-Cyclohexadiene, 1-methyl-
```
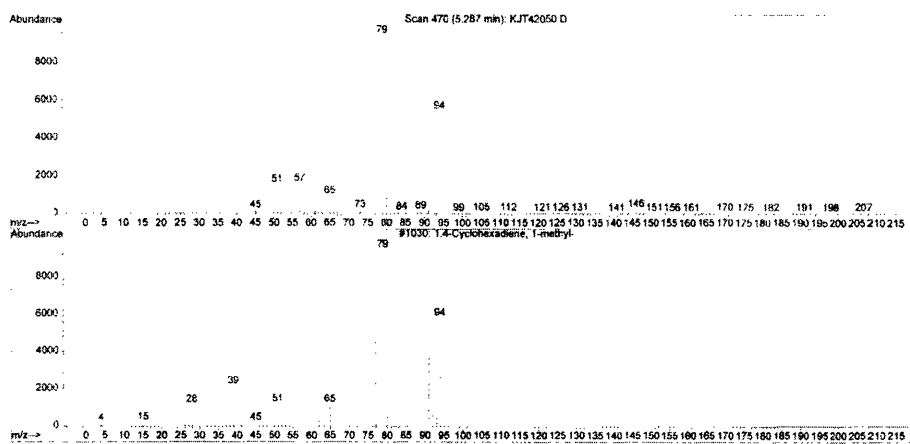
Figure C-16:

```
Library Searched : C:\DATABASE\NBS75K.L
Quality          : 90
ID               : 1,3,5-Hexatriene, 3-methyl-, (Z)-
```
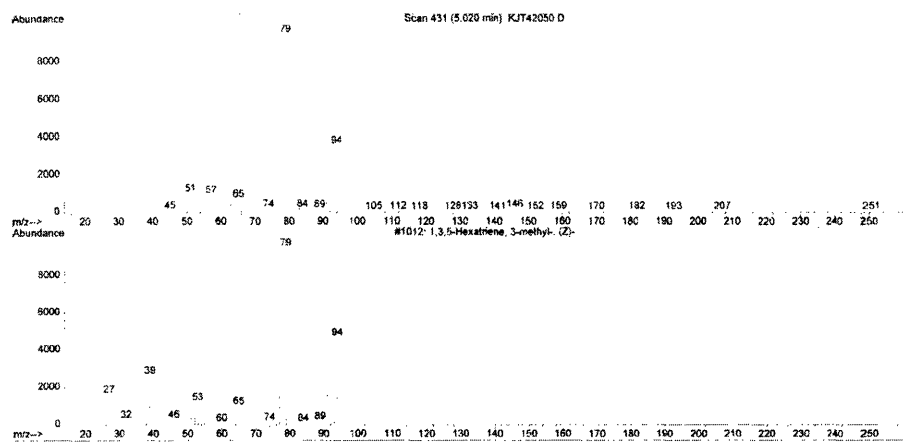
Figure C-17:

```
Library Searched    C:\DATABASE\NBS75K.L
Quality             92
ID                  Cyclohexane, methyl-
```
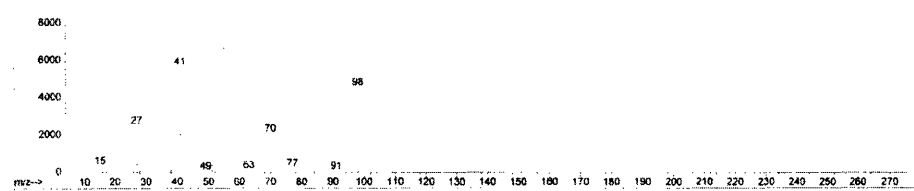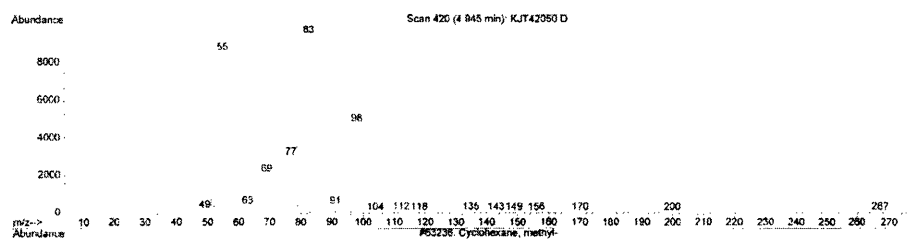
Figure C-18:

Abundance   Scan 661 (6.596 min): KJT42050.D ( )
                                               93

8000

6000   77

                                                   108
4000

2000   67
                      51

             46   57 62   82 87   97 103   141   169   186   213
   0   ...
m/z--> 5 10 15 20 25 30 35 40 45 50 55 60 65 70 75 80 85 90 95 100 105 110 115 120 125 130 135 140 145 150 155 160 165 170 175 180 185 190 195 200 205 210 215 220
Abundance   #2149: 1,5-Dimethyl-1,4-cyclohexadiene
                                               91

8000

6000   77

                                                   108
4000

                      39
2000
         27   51   65

      15   32   45   103
   0
m/z--> 5 10 15 20 25 30 35 40 45 50 55 60 65 70 75 80 85 90 95 100 105 110 115 120 125 130 135 140 145 150 155 160 165 170 175 180 185 190 195 200 205 210 215 220

164

Figure C-19:

Figure C-20:

Abundance

Scan 2362 (18.251 min): KJT42050 D (-)
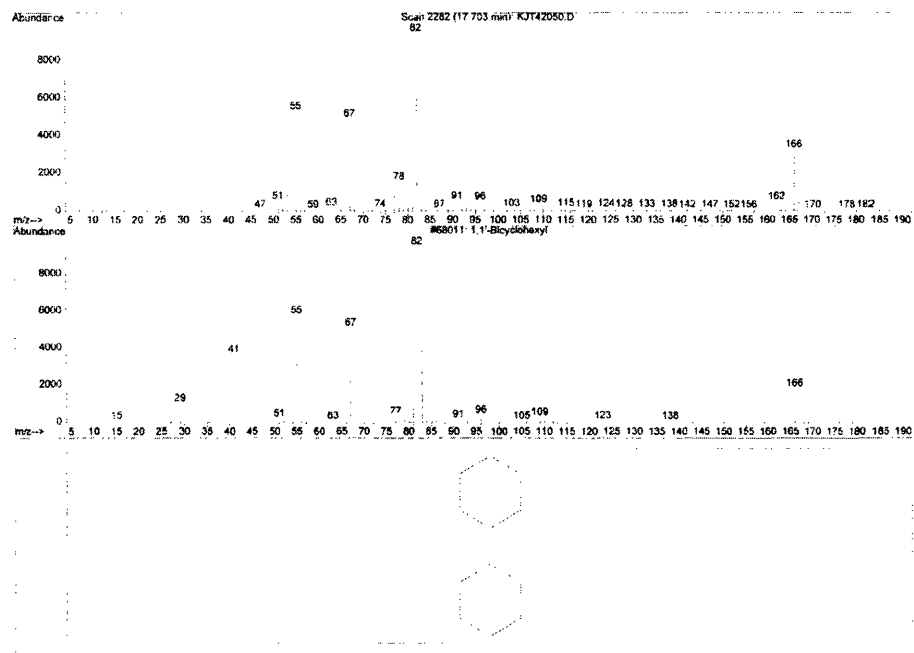
Figure C-21:

Library Searched   C:\DATABASE\NBS75K.L
Quality   62
ID   Cyclohexene, 3,3,5-trimethyl-

Figure C-22:

Abundance

Scan 455 (5 184 min): KJT42053 D

8000

6000

4000

2000

146

73

57

45

65   80 87 94 101 112119 131 139   154 165 173 186   205 215   229 238   265   332

0

m/z-->   10 20 30 40 50 60 70 80 90 100 110 120 130 140 150 160 170 180 190 200 210 220 230 240 250 260 270 280 290 300 310 320 330

Abundance   #8881. Di-tert-butyl peroxide

57

8000

6000   43

4000

2000

146

73

15   29   90   131   207

38

0

m/z -->   1C 20 30 40 50 60 70 80 90 100 110 120 130 140 150 160 170 180 190 200 210 220 230 240 250 260 270 280 290 300 310 320 330

Figure C-23:

Library Searched   C:\DATABASE\NBS75K.L
Quality   86
ID   Hexanal, 2-methyl-
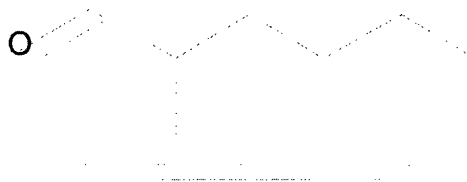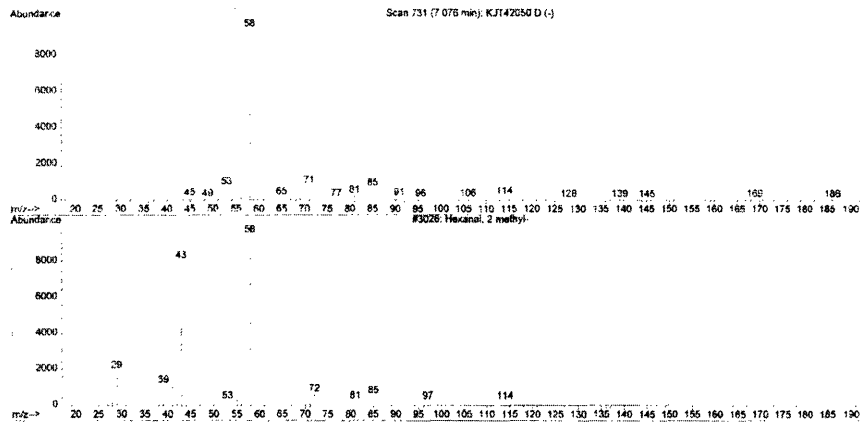
Figure C-24:

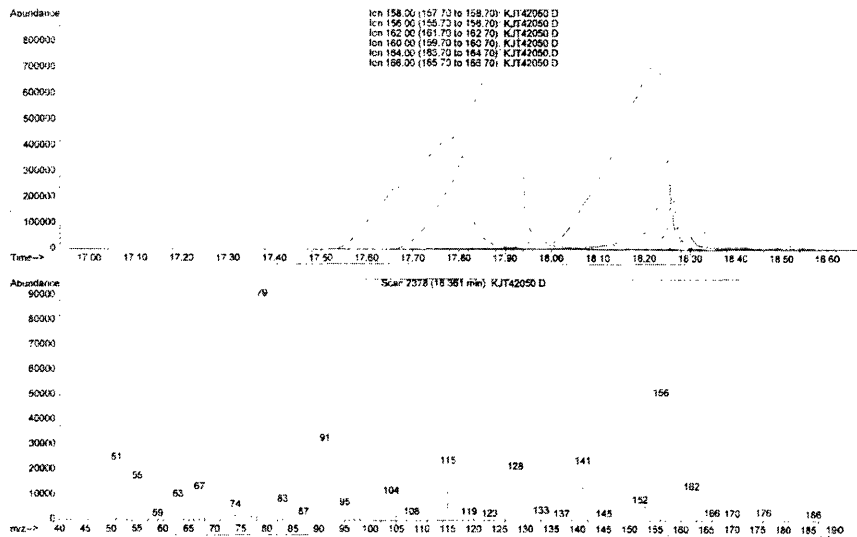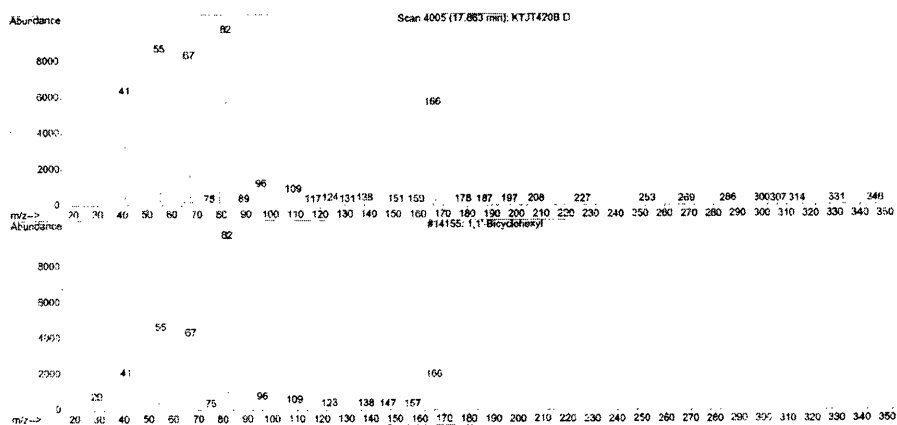## Figure C-25:
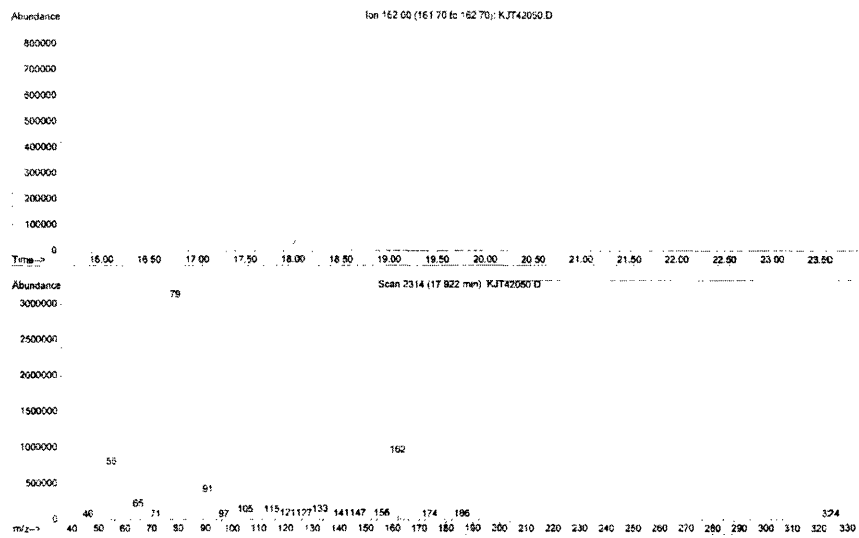
Figure C-26:

```
Library Searched : C:\DATABASE\NBS75K.L
Quality          : 90
ID               : 1,1'-Bicyclohexyl
```


171

Bibliography

[1] Claire S. Adjiman and Christodoulos A. Floudas. Rigorous convex underestimators for general twice-differentiable problems. *Journal of Global Optimization*, 9(1):23–40, July 1996.

[2] J.M. Andino, J.N. Smith, R.C. Flagan, W.A. Goddard, and J.H. Seinfeld. Mechanism of atmospheric photooxidation of aromatics: A theoretical study. *Journal of Physical Chemistry*, 100(26):10967–10980, June 1996.

[3] I. W. C. E Arends, P. Mulder, K. B. Clark, and D. D. M. Wayner. Rate constants for termination and tempo trapping of some resonance stabilized hydroaromatic radicals in the liquid-phase. *Journal of Physical Chemistry*, 99(20):8182–8189, 1995.

[4] John R. Barker. Multiple-Well, multiple-path unimolecular reaction systems. I. Multi-Well computer program suite. *International Journal of Chemical Kinetics*, 33(4):232–45, 2001.

[5] John R. Barker. Multiwell-1.3.1 software. http://aoss.engin.umich.edu/multiwell/: Ann Arbor, MI, 2003.

[6] E. R. Bell, F. F. Rust, and W. E. Vaughan. Decompositions of di-t-alkyl peroxides. iv. decomposition of pure liquid peroxide. *Journal of the American Chemical Society*, 72(1):337–38, January 1950.

[7] Sidney W. Benson. Effects of resonance and structure on the thermochemistry of organic peroxy radicals and the kinetics of combustion reactions. *Journal of the American Chemical Society*, 87(5):972–79, March 1965.

[8] Florence Berho and Robert Lesclaux. Gas phase reactivity of the cyclohexadienyl radical with O_2 and NO and thermochemistry of the association reaction with NO. *Physical Chemistry Chemical Physics*, 3(6):970–979, 2001.

[9] Torsten Berndt and Olag Böge. Gas-phase reaction of OH radicals with benzene: products and mechanism. *Physical Chemistry Chemical Physics*, 3:4946–4956, 2001.

[10] Binita Bhattacharjee, Douglas A. Schwer, Paul I. Barton, and Jr. William H. Green. Optimally-reduced kinetic models: reaction elimination in large-scale kinetic mechanisms. *Combustion and Flame*, 135(3):191–208, November 2003.

[11] Erling Bjergbakke, Alfred Sillesen, and Palle Pagsberg. UV spectrum and kinetics of hydroxycyclohexadienyl radicals. *Journal of Physical Chemistry*, 100(14):5729–5736, April 1996.

[12] B. Bohn and C. Zetzsch. Gas-phase reaction of the OH-benzene adduct with O_2: reversibility and secondary formation of HO_2. *Physical Chemistry Chemical Physics*, 1(22):5097–5107, 1999.

[13] William E. Boyce and Richard C. DiPrima. *Elementary Differential Equations*. John Wiley and Sons, Inc., New York, 5 edition, 1992.

[14] P. Dagaut and M. Cathonnet. The oxidation of 1,3-butadiene: Experimental results and kinetic modeling. *Combustion Science and Technology*, 140(1–6):225–257, 1998.

[15] John D. Desain, Craig A. Taatjes, James A. Miller, Stephen J. Klippenstein, and David K. Hahn. Infrared frequency-modulation probing of product formation in alkyl + O_2 reactions. *Faraday Discussions*, 119:101–120, 2001.

[16] A. Effio, D. Griller, K.U. Ingold, J.C. Scaiano, and S.J. Sheng. Studies on the spiro[2.5]octadienyl radical and the 2-phenylethyl rearrangement. *Journal of the American Chemical Society*, 102(19):6063–6068, 1980.

[17] E. Estupiñán, E. Villenave, S. Raoult, J. C. Rayez, M. T. Rayez, and R. Lesclaux. Kinetics and mechanism of the gas-phase reaction of the cyclohexadienyl radical (c-C_6H_7) with O_2. *Physical Chemistry Chemical Physics*, 5:4840–4845, October 2003.

[18] James E. Falk and Richard M. Soland. An algorithm for separable nonconvex programming problems. *Management Science*, 15(9):550–569, 1969.

[19] Xingwang Fang, Xianming Pan, Anja Rahmann, Heinz-Peter Schuchmann, and Clemens von Sonntag. Reversibility in the reaction of cyclohexadienyl radicals with oxygen in aqueous solution. *Journal of European Chemistry*, 1(7):423–429, 1995.

[20] C. A. Floudas and V. Visweswaran. A global optimization algorithm (GOP) for certain classes of nonconvex nlps - i. theory. *Computers and Chemical Engineering*, 14(12):1397–1417, December 1990.

[21] J. B. Foresman, T. A. Keith, K. B. Wiberg, J. Snoonian, and M. J. Frisch. Solvent effects 5. influence of cavity shape, truncation of electrostatics, and electron correlation ab initio reaction field calculations. *Journal of Physical Chemistry*, 100(40):16098–16104, October 1996.

[22] Michael Frenklach, Andrew Packard, Pete Seiler, and Ryan Feeley. Collaborative data processing in developing predictive models of complex reaction systems. *International Journal of Chemical Kinetics*, 36(1):57–66, November 2004.

[23] Michael Frenklach, H. A. I. Wang, and Martin J. Rabinowitz. Optimization and analysis of large chemical kinetic mechanisms using the solution mapping method - combustion of methane. *Progress in Energy and Combustion Science*, 18(1):47–73, 1992.

175

[24] M. J. Frisch, G. W. Trucks, H. B. Schlegel, G. E. Scuseria, M. A. Robb, J. R. Cheeseman, V. G. Zakrzewski, J. A. Montgomery, Jr., R. E. Stratmann, J. C. Burant, S. Dapprich, J. M. Millam, A. D. Daniels, K. N. Kudin, M. C. Strain, O. Farkas, J. Tomasi, V. Barone, M. Cossi, R. Cammi, B. Mennucci, C. Pomelli, C. Adamo, S. Clifford, J. Ochterski, G. A. Petersson, P. Y. Ayala, Q. Cui, K. Morokuma, D. K. Malick, A. D. Rabuck, K. Raghavachari, J. B. Foresman, J. Cioslowski, J. V. Ortiz, B. B. Stefanov, G. Liu, A. Liashenko, P. Piskorz, I. Komaromi, R. Gomperts, R. L. Martin, D. J. Fox, T. Keith, M. A. Al-Laham, C. Y. Peng, A. Nanayakkara, C. Gonzalez, M. Challacombe, P. M. W. Gill, B. Johnson, W. Chen, M. W. Wong, J. L. Andres, C. Gonzalez, M. Head-Gordon, E. S. Replogle, , and J. A. Pople. *Gaussian 98, Revision A.9*. Gaussian, Inc., Pittsburgh, PA, 1998.

[25] G. Ghigo and G. Tonachini. Benzene oxidation in the troposphere. theoretical investigation on the possible competition of three postulated reaction channels. *Journal of the American Chemical Society*, 120(27):6753–6757, July 1998.

[26] Philip E. Gill, Walter Murray, Michael A. Saunders, and Margaret H. Wright. User's guide for NPSOL 5.0: A fortran package for nonlinear programming. Technical report, Stanford University, July 1998.

[27] Sergey Y. Grebenkin and Lev N. Krasnaperov. Kinetics and thermochemistry of the hydroxycyclohexadienyl radical reaction with O_2: C_6H_6OH + $\rightleftharpoons$ $C_6H_6(OH)OO$. *The Journal of Physical Chemistry A*, 108:1953–1963, 2004.

[28] D.G. Hendry and D. Schuetzle. Reactions of hydroperoxy radicals - liquid-phase oxidation of 1,4-cyclohexadiene. *Journal of the American Chemical Society*, 97(24):7123–7127, 1975.

[29] Jan P. Hessler. The use of monte carlo simulations to evaluate kinetic data and analytic approximations. *International Journal Of Chemical Kinetics*, 29(11):803–817, November 1997.

[30] Alan C. Hindmarsh and Radu Serban. User documentation for CVODES, an ODE solver with sensitivity analysis capabilities. Technical report, Lawrence Livermore National Laboratory, July 2002.

[31] Reiner Horst and Hoang Tuy. *Global Optimization.* Springer-Verlag, Berlin, 1993.

[32] Takashi Imamura and Weijun Zhang. Laser-induced fluorescence of cyclohexadienyl (c-C_6H_7) radical in the gas phase. *Journal of Chemical Physics,* 121(14):6861–6867, October 2004.

[33] M. E. Jenkin, T. P. Murrells, S. J. Shalliker, and G. D. Hayman. Kinetics and product study of the self-reactions of allyl and allyl peroxy radicals at 296 K. *The Journal of the Chemical Society, Faraday Transactions,* 89:433–446, 1993.

[34] David Johnson, Severine Raoult, Marie-Thérèse Rayez, Jean-Claude Rayez, and Robert Lesclaux. An experimental and theoretical investigation of the gas-phase benzene-OH radical adduct + O_2 reaction. *Physical Chemistry Chemical Physics,* 4:4678–4686, 2002.

[35] Jimmy E. Jordan, David W. Pratt, and David E. Wood. Direct observation of the optical absorption spectra of reactive free radicals at room temperature. *Journal of the American Chemical Society,* 96(17):5588–5590, 1974.

[36] E. W. Kaiser. Mechanism of the reaction $C_2H_5 + O_2$ from 298 to 680 K. *Journal of Physical Chemistry A,* 106(7):1256–1265, February 2002.

[37] A. H. G. Rinooy Kan and G. T. Timmer. Stochastic global optimization methods; part ii: multi-level methods. *Mathematical Programming,* 39:57–78, 1987.

[38] P.J. King. Pro-k: global analysis and simulation software for acorn risc based computer. Applied Photophysics, Leatherhead (UK), 1996.

[39] Marieke Kranenburg, Maria Victoria Ciriano, Artem Cherkasov, and Peter Mulder. Carbon-oxygen bond dissociation enthalpies in peroxyl radicals. *Journal of Physical Chemistry A,* 104(5):915–921, February 2000.

[40] Awadhesh Kumar, P. D. Naik, R. D. Saini, and J. P. Mittal. Direct evidence of a radical channel in photodissociation of 1,4-cyclohexadiene with an ArF laser at 193 nm. *Chemical Physics Letters*, 309(3):191–197, August 1999.

[41] T.H. Lay, J.W. Bozzelli, and J.H. Seinfeld. Atmospheric photochemical oxidation of benzene: Benzene plus OH and the benzene-OH adduct (hydroxyl-2,4-cyclohexadienyl) plus O_2. *Journal of Physical Chemistry*, 100(16):6543–6554, April 1996.

[42] K. Levenberg. A method for the solution of certain problems in least squares. *Quarterly of Applied Mathematics*, 2:164–168, 1944.

[43] B. Maillard, K. U. Ingold, and J. C. Scaiano. Rate constants for the reactions of free radicals with oxygen in solution. *Journal of the American Chemical Society*, 105(15):5095–5099, 1983.

[44] D. Marquardt. An algorithm for least-squares estimation of nonlinear parameters. *SIAM Journal on Applied Mathematics*, 11:431–441, 1963.

[45] Garth P. McCormick. Computability of global solutions to factorable nonconvex programs: Part 1 – convex underestimating problems. *Mathematical Programming*, 10:147–175, 1976.

[46] E.F. Meyer. Thermodynamics of solution by gas-liquid chromatography. *Journal of Chemical Education*, 50(3):191–194, 1973.

[47] E.F. Meyer, K.S. Stec, and R.D. Hotz. Thermodynamic study of solute-solvent interactions using gas-liquid chromatography. *Journal of Physical Chemistry*, 77(17):2140–2145, 1973.

[48] J.A. Miller, S.J. Klippenstein, and S.H. Robertson. A theoretical analysis of the reaction between ethyl and molecular oxygen. *Proceedings of the Combustion Institute*, 28(2):1479–1486, 2000.

[49] Press release: The 1998 nobel prize in physiology or medicine.

[50] Babatunde A. Ogunnaike and W. Harmon Ray. *Process dynamics, modeling, and control.* Oxford University Press, New York, 1994.

[51] Xian-Ming Pan, Man Nien Schuchmann, and Clemens von Sonntag. Hydroxyl-radical induced oxidation of cyclohexa-1,4-diene by O_2 in aqueous solution. a pulse radiolysis and product study. *Journal of the Chemical Society, Perkins Transactions,* 2:1021–1028, 1993.

[52] X.M. Pan, E. Bastian, and C. von Sonntag. The reactions of hydroxyl radicals with 1,4-cyclohexadiene and 1,3-cyclohexadiene in aqueous-solution - a pulse-radiolysis and product study. *Zeitschrift Fur Naturforschung Section B-a Journal of Chemical Sciences,* 43(9):1201–1205, September 1988.

[53] M.J. Pilling and P.W. Seakins. *Reaction Kinetics.* Oxford University Press, Oxford, 1995.

[54] W. H. Powell. Revised nomenclature for radicals, ions, radical ions and related species. *Pure and Applied Chemistry,* 65(6):1357–1455, 1993.

[55] William H. Press, Brian P. Flannery, Saul A. Teukolsky, and William T. Vetterling. *Numerical Recipes in C: The Art of Scientific Computing.* Cambridge University Press, Cambridge (UK) and New York, 2nd edition, 1992.

[56] Séverine Raoult, Marie-Thérèse Rayez, Jean-Claude Rayez, and Robert Lesclaux. Gas phase oxidation of benzene: Kinetics, thermochemistry and mechanism of initial steps. *Physical Chemistry Chemical Physics,* 6:2245–2253, 2004.

[57] J. C. Rienstra-Kiracofe, W. D. Allen, and H. F. Schaefer. The $C_2H_5 + O_2$ reaction mechanism: High-level *ab initio* characterizations. *Journal of Physical Chemistry A,* 104(44):9823–9840, November 2000.

[58] Edward R. Ritter and Joseph W. Bozelli. THERM: Thermodynamic Property Estimation for Gas Phase Radicals and Molecules. *International Journal of Chemical Kinetics,* 23:767–778, 1991.

[59] Myran C. Sauer, Jr and Barry Ward. The reactions of hydrogen atoms with benzene and toluene studied by pulsed radiolysis: Reaction rate constants and transient spectra in the gas phase and aqueous solution. *Journal of Physical Chemistry*, 71(12):3971–3983, November 1967.

[60] Chad Y. Sheng, Joseph W. Bozelli, Anthony M. Dean, and Albert Y. Chang. Detailed kinetics and thermochemistry of $C_2H_5 + O_2$: Reaction kinetics of the chemically-activated and stabilized $CH_3CH_2OO\cdot$. *The Journal of Physical Chemistry A*, 106(32):7276–7293, 2002.

[61] M. Simic and E. Hayon. Spectroscopic investigation of cyclohexanol and cyclohexyl radicals and their corresponding peroxy radicals. *Journal of Physical Chemistry A*, 75(11):1677–1680, 1971.

[62] Adam B. Singer. *Global Dynamic Optimization*. PhD thesis, Massachusetts Institute of Technology, 2004.

[63] Adam B. Singer. Libbandb.a version 3.2 manual. Technical report, Massachusetts Institute of Technology, January 2004.

[64] Adam B. Singer and Paul I. Barton. Global solution of linear dynamic embedded optimization problems. *Journal of Optimization Theory and Applications*, 121(3):613–646, 2004.

[65] Adam B. Singer and Paul I. Barton. Bounding the solutions of parameter dependent nonlinear ordinary differential equations. SIAM Journal on Scientific Computing, In Press, 2005.

[66] Adam B. Singer and Paul I. Barton. Global optimization with nonlinear ordinary differential equations. *Journal of Global Optimization*, May 2005. In Press.

[67] Irene R. Slagle, Emil Ratajczak, Michael C. Heaven, David Gutman, and Albert F. Wagner. Kinetics of Polyatomic Free-Radicals Produced by Laser Photolysis 4. Study

of the Equilibrium i-C$_3$H$_7$ + O$_2$ $\rightleftharpoons$ i-C$_3$H$_7$O$_2$ between 592 K and 692 K. *Journal of the American Chemical Society*, 107(7):1838–1845, 1985.

[68] S.E. Stein and B.S. Rabinovitch. Accurate evaluation of internal energy-level sums and densities including anharmonic oscillators and hindered rotors. *Journal of Chemical Physics*, 58(6):2438–2445, 1973.

[69] A. K. Suresh, T. Sridhar, and O. E. Potter. Mass transfer and solubility in autocatalytic oxidation of cyclohexane. *AIChE Journal*, 34(1):55–68, January 1988.

[70] C.A. Taatjes and S.J. Klippenstein. Kinetic isotope effects and variable reaction coordinates in barrierless recombination reactions. *Journal of Physical Chemistry A*, 105(37):8567–8578, September 2001.

[71] James W. Taylor. *Direct Measurement and Analysis of Cyclohexadienyl Oxidation*. PhD thesis, Massachusetts Institute of Technology, 2005.

[72] James W. Taylor, Gerhard Ehlker, Hans-Heinrich Carstensen, Leah Ruslen, Robert W. Field, and William H. Green. Direct measurement of the fast, reversible reaction of cyclohexadienyl radicals with oxygen in nonpolar solvents. *Journal of Physical Chemistry A*, 108(35):7193–7203, 2004.

[73] Yuri P. Tsentalovich, Leonid V Kulik, Nina P. Gritsan, and Alexandra V. Yurkovskaya. Solvent effect on the rate of β-scission of the *tert*-butoxyl radical. *Journal of Physical Chemistry A*, 102:7975–7980, 1998.

[74] Prasana K. Venkatesh, Morrel H. Cohen, Robert W. Carr, and Anthony M. Dean. Bayesian method for global optimization. *Physical Review E*, 55(5):6219–6232, May 1997.

[75] Clemens von Sonntag and Heinz-Peter Schuchmann. The elucidation of peroxyl radical reactions in aqueous solution with the help of radiation-chemical methods. *Angewandte Chemie - International Edition*, 30:1229–1253, 1991.

[76] C. D. Wijaya, R. Sumathi, and W. H. Green. Thermodynamic and kinetic parameters for cyclic ether formation from hydroperoxyalkyl radicals. *Journal of Physical Chemistry A*, 107(24):4908–4920, 2003.

[77] E. Wilhelm and R. Battino. Solubility of gases in liquids. 5. Solubility of molecular nitrogen, molecular oxygen, carbon monoxide, and carbon dioxide in cyclohexane at 283 to 313 K. *Journal of Chemical Thermodynamics*, 5(1):117–120, 1973.

[78] C. L. Yaws, editor. *Chemical Properties Handbook*. McGraw-Hill, 1999.

[79] Genshi Zhao, Tianhui Xia, Randy S. Fischer, and Roy A. Jensen. Cyclohexadienyl dehydratase from *pseudomona aeruginosa*: Molecular cloning of the gene and characterization of the gene product. *The Journal of Biological Chemistry*, 267(4):2487–2493, February 1992.

[80] Régis Zils, Satoshi Inomata, Takashi Imamura, Akira Miyoshi, and Nobuaki Washida. Determination of the equilibrium constant and thermodynamic parameters for the reaction of pentadienyl radicals with O_2. *Journal of Physical Chemistry A*, 105:1277–1282, 2001.